

TR-DA1569

ESTIMATION OF INERTIAL
PLATFORM ERRORS

Contract No. NAS8-20358

21 October 1967

Prepared by
John V. Brown
and
James S. Tyler, Jr.

PHILCO-FORD CORPORATION
Space & Re-Entry Systems Division
Palo Alto, California

for
National Aeronautics and Space Administration
Marshall Space Flight Center
Huntsville, Alabama

TABLE OF CONTENTS

<u>Section</u>		<u>Page</u>
1	INTRODUCTION	
2	DERIVATION OF EQUATIONS	2-1
	2.1 Inertial Platform Error Model	2-1
	2.2 Dynamic Equation of the Vehicle	2-4
	2.3 Tracking Equations	2-7
	2.4 Minimum Variance Estimation Equations	2-8
3	POWERED FLIGHT ERROR PROPAGATION PROGRAM	3-1
4	THE ASCENT TRAJECTORY	4-1
5	SELECTION OF COMBINED PLATFORM-TRACKING	5-1
	5.1 Dispersions from the Platform Errors Without Tracking	5-1
	5.2 The Tracking Model	5-18
6	THE ESTIMATION OF INERTIAL PLATFORM ERRORS	6-1
	6.1 Estimation of Platform Errors With Nominal Tracking	6-2
	6.2 Estimation of Guidance Errors With Additional Knowledge of Platform	6-5
	6.3 Estimation of Guidance Errors With Improved Tracking	6-7
	6.4 Estimation of Guidance Errors With Perfect Knowledge of the Trajectory End Point	6-8
	6.5 Estimation of Guidance Error with Large Initial Uncertainties	6-9
	6.6 Estimation of Guidance Errors With Increased Observation Rate	6-11
	6.7 Estimation of Guidance Errors With Different Kinds of Tracking	6-13
7	CONCLUSIONS	7-1
APPENDIX A	COVARIANCE MATRIX DESCRIPTION	A-1
REFERENCES		

LIST OF ILLUSTRATIONS

<u>Figure</u>		<u>Page</u>
2-1	Platform Orientation	2-2
2-2	Effect of Equivalent Observations	2-16
3-1	Functional Diagram of Powered Flight Error Analysis Program	3-2
4-1	Trajectory Altitude vs Time	4-2
4-2	Trajectory and Tracking Station Location	4-3
4-3	Acceleration Levels for Nominal Trajectory	4-4
5-1	RMS Uncertainty in Position State from the 30 Platform Error Sources (No Tracking)	5-2
5-2	RMS Uncertainty in Velocity State from the 30 Platform Error Sources	5-3
5-3	3 σ Standard Deviation of Error in Estimate of the State in Cross Range Direction	5-4
5-4	3 σ Standard Deviation of Error in Estimate of the State in the Up Direction	5-5
5-5	3 σ Standard Deviation of Error in Estimate of the State in the Down-Range Direction	5-6
5-6	3 σ Standard Deviation of Error in Estimate of the Velocity State in the Up Direction	5-7
5-7	3 σ Standard Deviation of Error in Estimate of the Velocity State in the Down-Range Direction	5-8
5-8	3 σ Standard Deviation of Error in Estimate of the Velocity State in Cross Range Direction	5-9
5-9	Variations in Final RMSPE for Changes in Initial Standard Deviation of Initial Misalignment About Y Axis	5-13
5-10	Variations in Final RMSPE for Changes in Initial Standard Deviation of Initial Platform Misalignment About Z Axis	5-14
5-11	Variations in Final RMSPE for Changes in Initial Standard Deviation of Y Accelerometer Into X Axis	5-15
5-12	Variations in Final RMSPE for Changes in Initial Standard Deviation of Z Accelerometer Into X Axis	5-16
5-13	Variations in Final RMSPE for Changes in Initial Standard Deviation of Initial Platform Misalignment About X Axis	5-17

LIST OF ILLUSTRATIONS (Cont)

<u>Figure</u>		<u>Page</u>
6-1	Variation in Position Uncertainties - Nominal Case	6-15
6-2	Variation in Velocity Uncertainties - Nominal Case	6-16
6-3	Position and Velocity Uncertainties with Tracking Only (No Telemetry Data)	6-17
6-4	3σ Uncertainty in Y-Accelerometer Misalignment into X-Axis	6-18
6-5	3σ Uncertainty in Z-Accelerometer Misalignment into X-Axis	6-19
6-6	3σ Uncertainty in Z-Accelerometer Misalignment into Y-Axis	6-20
6-7	3σ Uncertainty in X-Accelerometer Misalignment into Y-Axis	6-21
6-8	3σ Uncertainty in Initial Platform Misalignment about X-Axis	6-22
6-9	3σ Uncertainty in Initial Platform Misalignment about Y-Axis	6-23
6-10	3σ Uncertainty in Initial Platform Misalignment about Z-Axis	6-24
6-11	3σ Uncertainty in X-Axis Gyro Drift Rate	6-25
6-12	3σ Uncertainty in Y-Axis Gyro Drift Rate	6-26
6-13	3σ Uncertainty in Z-Axis Gyro Drift Rate	6-27
6-14	3σ Uncertainty in X-Accelerometer Bias	6-28
6-15	3σ Uncertainty in Y-Accelerometer Bias	6-29
6-16	3σ Uncertainty in Z-Accelerometer Bias	6-30
6-17	3σ Uncertainty in X-Accelerometer Scale Factor	6-31
6-18	3σ Uncertainty in Y-Accelerometer Scale Factor	6-32
6-19	3σ Uncertainty in Z-Gyro Spin Axis Mass Unbalance	6-33
6-20	3σ Uncertainty in Z-Gyro Anisoelastic Drift	6-34
6-21	3σ Uncertainty in X-Accelerometer Misalignment into Y-Axis for High Initial Uncertainties	6-35

LIST OF ILLUSTRATIONS (Cont)

<u>Figure</u>		<u>Page</u>
6-22	3 σ Uncertainty in Initial Platform Misalignment about X-Axis for High Initial Uncertainties	6-36
6-23	3 σ Uncertainty in Initial Platform Misalignment about Y-Axis for High Initial Uncertainties	6-37
6-24	3 σ Uncertainty in Initial Platform Misalignment about Z-Axis for High Initial Uncertainties	6-38
6-25	3 σ Uncertainty in X-Axis Gyro Drift Rate for High Initial Uncertainties	6-39
6-26	3 σ Uncertainty in Y-Axis Gyro Drift Rate for High Initial Uncertainties	6-40
6-27	3 σ Uncertainty in Z-Axis Gyro Drift Rate for High Initial Uncertainties	6-41
6-28	3 σ Uncertainty in X-Accelerometer Bias for High Initial Uncertainties	6-42
6-29	3 σ Uncertainty in Y-Accelerometer Bias for High Initial Uncertainties	6-43
6-30	3 σ Uncertainty in Z-Accelerometer Bias for High Initial Uncertainties	6-44
6-31	3 σ Uncertainty in X-Accelerometer Scale Factor for High Initial Uncertainties	6-45
6-32	3 σ Uncertainty in X-Accelerometer Scale Factor for High Initial Uncertainties	6-46
6-33	Variation in Position Uncertainty for Different Kinds of Tracking	6-47
6-34	Variation in Velocity Uncertainty for Different Kinds of Tracking	6-48

SECTION 1

INTRODUCTION

This report presents the results of one of the three parts of Contract NAS8-20358, entitled Advanced Spaceborne Tracking, Detection, and Navigation Study. The objective of this part of the contract was to evaluate the feasibility of estimating the inertial guidance platform errors from data obtained during a powered flight ascent.

One method of estimating the inertial platform errors is to combine the telemetry data, which contains information on the vehicle position-velocity state plus deviations in the trajectory caused by the platform errors, with the tracking data, which also contains information on the vehicle state, but includes errors from the tracking system.

There are three potential uses for the information contained in this combined platform-tracking system. If it is possible to estimate the platform errors during a flight, then the guidance system could be updated. Also the ability to determine platform errors would be useful in a postflight analysis where the objective is to determine whether the guidance components performed according to specification. Although the primary interest in this study is to evaluate the ability to estimate the guidance errors, a third use of this data would be to obtain a better estimate of the vehicle than could be obtained with tracking data alone.

The feasibility of estimating the platform errors has been evaluated in this study by simulating an orbit determination process that would combine the telemetry and tracking data. It is the ensemble behavior of this combined system and in particular the behavior of the covariance matrix of the errors in estimate of the position-velocity state plus the platform and tracking errors, that has been investigated. A Kalman or minimum variance filter has been assumed for the estimation process.

Platform errors as well as a nominal trajectory that are similar to a Saturn V mission have been used in the study. The equations for the platform model, the tracking model, and the minimum variance estimation are presented in Section 2. A discussion of the computer program used to generate the covariance matrix of errors, and the nominal ascent trajectory along which the covariance matrix is propagated, are included in Section 3 and Section 4, respectively. Section 5 discusses the effect of individual error sources in the platform and tracking systems on the trajectory. These results are used to define the significant error sources which should be included in the combined platform-tracking system model.

The principal results of the study are presented in Section 6. In this section the feasibility of estimating the platform errors is evaluated as a parametric function of the system error sources and tracking parameters.

SECTION 2

DERIVATION OF EQUATIONS

2.1 INERTIAL PLATFORM ERROR MODEL

The inertial platform model that has been used for this study consists of up to 30 error sources and is similar to that used by Daniels, Neighbors, and Cole, in Reference 1. The four types of accelerometer errors and the four types of gyro errors considered are:

α_i the i^{th} accelerometer bias, km/sec^2

β_{ij} the misalignment of the i^{th} accelerometer into the j^{th} axis, radians

ϵ_i the scale factor error of the i^{th} accelerometer, parts/part

s_i the threshold of the i^{th} accelerometer, km/sec^2

θ_{oi} the initial platform misalignment about the i^{th} axis, radians

$\dot{\theta}_{oi}$ the steady-state drift rate of the i^{th} gyro, rad/sec

μ_{Ii} } the mass unbalance drift about the input and spin
 μ_{Si} } axes, $(\text{rad/sec})/(\text{km/sec}^2)$

c_i the anisoelastic drift of the i^{th} gyro, $(\text{rad/sec})/(\text{km/sec}^2)^2$

The platform is oriented in an inertial frame fixed at launch as shown in Figure 2-1.

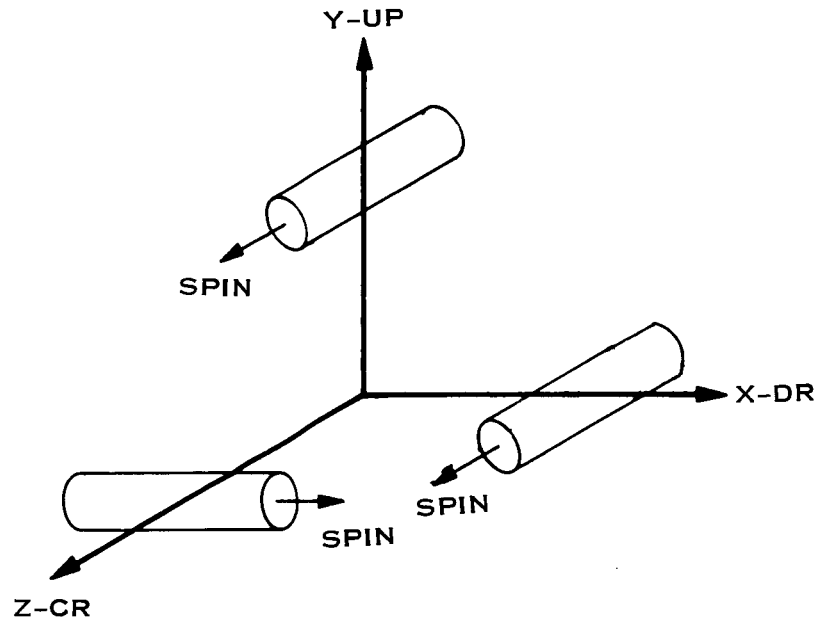


Figure 2-1 Platform Orientation

The gyro input axes are along the X, Y, and Z axes and the three accelerometers are also assumed to be mounted along these axes.

The platform error model used in this study includes the total error in acceleration caused by (1) the misalignment of the platform axes resulting from the gyro drifts and initial misalignment, and (2) the errors in the accelerometers themselves which are mounted on the drifting platform axes, for a given nominal acceleration time history. The drift rate for the i^{th} gyro is given by

$$\dot{\phi}_i = \dot{\phi}_{oi} + \begin{bmatrix} \mu_{si} & \mu_{Ii} & 0 \end{bmatrix} \begin{bmatrix} a_{Gis} \\ a_{GiI} \\ a_{Gio} \end{bmatrix} + c_i (a_{Gis})^2, \quad (2-1)$$

where a_{Gis} , a_{GiI} , and a_{Gio} are the accelerations along the spin, input, and output axes of the i^{th} gyro, respectively. The total platform drift, which is found by integrating (2-1), is

$$\begin{aligned} \phi_i = & \phi_{oi} + \dot{\phi}_{oi} t + \begin{bmatrix} \mu_{si} & \mu_{Ii} & 0 \end{bmatrix} T_{PI2Gi} \int_0^t a_{PIi}(\tau) d\tau \\ & + c_i \int_0^t (q_i a_{PIi}(\tau))^2 d\tau, \end{aligned} \quad (2-2)$$

where a_{PIi} is the acceleration along the i^{th} ideal platform axis, T_{PI2Gi} is the transformation from the ideal platform axes to the i^{th} gyro axis, and q_i is the first row of T_{PI2Gi} . For the gyro orientation in Figure 2-1, T_{PI2G1} , the transformation from the ideal platform axes to the X gyro axes, is

$$T_{PI2G1} = \begin{bmatrix} 0 & 0 & 1 \\ 1 & 0 & 0 \\ 0 & 1 & 0 \end{bmatrix}, \quad (2-3)$$

where the order of the gyro axes is $\begin{bmatrix} s \\ I \\ o \end{bmatrix}$.

The accelerometer errors are found from the sensed acceleration along the accelerometer axes, a_{si}' , which is

$$a_{si}' = \begin{bmatrix} \alpha_x + s_x \\ \alpha_y + s_y \\ \alpha_z + s_z \end{bmatrix} + \left\{ I + \begin{bmatrix} \epsilon_x & \beta_{xy} & \beta_{xz} \\ \beta_{yx} & \epsilon_y & \beta_{yz} \\ \beta_{zx} & \beta_{zy} & \epsilon_z \end{bmatrix} \right\} \begin{bmatrix} a_{PIx} \\ a_{PIy} \\ a_{PIz} \end{bmatrix} \quad (2-4)$$

The total error in acceleration is given by the sum of the accelerometer errors plus the error in acceleration caused by the platform misalignment. The total sensed acceleration can be written as the sum of the acceleration in (2-4) plus the cross product of the platform orientation angles, Φ_1 in (2-2), and the true acceleration along the ideal platform axes. This expression is

$$a_{si} = \begin{bmatrix} \alpha_x + s_x \\ \alpha_y + s_y \\ \alpha_z + s_z \end{bmatrix} + [I + E] a_{PI} + \begin{bmatrix} \Phi_x \\ \Phi_y \\ \Phi_z \end{bmatrix} \otimes a_{PI}, \quad (2-5)$$

where \otimes denotes the cross product, and E is the matrix of scale factor and misalignment errors in (2-4).

2.2 DYNAMIC EQUATION OF THE VEHICLE

The dynamic equations of the vehicle include the effects of gravity as well as the thrusting accelerations and the acceleration errors. These equations can be expressed in an inertial frame as

$$\ddot{R} = G(R,t) + T_{A2I} a_{PI}(t), \quad (2-6)$$

where $G(R,t)$ is the gravitational acceleration and T_{A2I} is the transformation from accelerometer axes to the inertial axes, and $a_{PI}(t)$ has been defined as the true value of the non-gravitational acceleration. Since $a_{PI}(t)$ can be expressed as the difference between the sensed acceleration and the acceleration errors, equation (2-6) can be written as

$$\ddot{R} = G(R,t) + T_{A2I} [a_s(t) - \delta_a(e,t)], \quad (2-7)$$

where $\delta_a(e,t)$ is a function of the platform errors and from (2-5) is given by

$$\delta_a(e,t) = \begin{bmatrix} \alpha_x + s_x \\ \alpha_y + s_y \\ \alpha_z + s_z \end{bmatrix} + E a_{PI} + \Phi \otimes a_{PI} \quad (2-8)$$

Representing (2-7) as

$$\ddot{R} = G(R,t) + f(e,t), \quad (2-9)$$

and considering perturbations only about the nominal values of R and a , results in the linear equations of motion that are used for the error analysis. These equations are

$$\Delta \ddot{R} = F \Delta R + B \Delta a, \quad (2-10)$$

where

$$F = \left. \frac{\partial G(R,t)}{\partial R} \right|_{R \text{ Nominal}} \quad B = \left. \frac{\partial f(e,t)}{\partial a} \right|_{a \text{ Nominal}}$$

For the purpose of error propagation, the total state vector (z), in general, may consist of the 6 vector of position (R) and velocity (V) plus any number of the sensor error and tracking bias error sources (e), i.e.,

$$z = \begin{bmatrix} R \\ V \\ e \end{bmatrix} = \begin{bmatrix} x \\ e \end{bmatrix} \quad (2-11)$$

The state transition matrix for this expanded state vector is given by

$$\Phi(t, t_0) = \begin{bmatrix} \frac{\partial x}{\partial x_0} & \frac{\partial x}{\partial e} \\ 0 & I \end{bmatrix} = \begin{bmatrix} \emptyset & \emptyset_u \\ 0 & I \end{bmatrix} \quad (2-12)$$

The expression $\frac{\partial x}{\partial x_0}$ is found by solving the following equation for

$$\frac{\partial R}{\partial x_0} :$$

$$\frac{\partial R}{\partial x_0}'' = \frac{d^2}{dt^2} \frac{\partial R}{\partial x_0} = \frac{\partial G}{\partial R} \frac{\partial R}{\partial x_0}, \quad (2-13)$$

where $\frac{\partial R}{\partial x_0}$ is a 3x6 matrix and

$$\frac{\partial G}{\partial R} = F$$

The sensitivities of the position and velocity state to the i^{th} platform error source are found by integrating the equation

$$\frac{d^2}{dt^2} \frac{\partial R}{\partial e_i} = \frac{\partial R}{\partial e_i}'' = \frac{\partial G}{\partial R} \frac{\partial R}{\partial e_i} - \frac{\partial \delta a}{\partial e_i} \quad (2-14)$$

The velocity partial $\frac{\partial V}{\partial e_i}$ in (2-12) is found by differentiating the solution for $\frac{\partial R}{\partial e_i}$ in (2-14). Detailed descriptions of the error source sensitivities $\left(\frac{\partial \delta a}{\partial e_i}\right)$ are given in Reference 2.

2.3 TRACKING EQUATIONS

The tracking model is obtained by assuming that the radar observations are of the form

$$y = f(X, W, T) + q$$

where $X = 6$ state of position and velocity (2-15)

$W =$ tracking bias errors

Linearization of this equation about a nominal trajectory results in the following equations for the measurement y :

$$y = \frac{\partial f}{\partial X} x + \frac{\partial f}{\partial W} W + q(t) \quad (2-16)$$

The tracking model consists of the partials of the observation with respect to the state (H) and the partial of the observation with respect to the measurement bias parameters (G), and the random measurement error vector $q(t)$. For each observation the model is given by

$$y = Hx + Gw + q(t), \quad (2-17)$$

where H and G are row vectors.

The tracking that can be simulated includes range, range-rate, azimuth, elevation, right ascension, declination, and direction cosines and their rates. Each of these measurements may contain a random and a bias error, in addition to the station-location errors for the station and a station clock error.

2.4 MINIMUM VARIANCE ESTIMATION EQUATIONS

Since the equations for the minimum-variance estimator are an essential part of the error analysis of the inertial platform and tracking systems, these equations are summarized here. It is the ensemble type behavior of the inertial platform-tracking system that is to be studied and therefore the variance-covariance matrix of the error in estimate of the state (P) is processed by the filter. The nominal trajectory is used throughout to evaluate the measurement, platform, and state sensitivities, H , ϕ_u , and ϕ , respectively. Residuals are not determined in this analysis. The following equations summarize the minimum variance or Kalman estimation process.

Propagating in Time

$$x(t) = \phi(t, t_0) x(t_0) \quad (2-18)$$

$$P(t) = \phi(t, t_0) P(t_0) \phi(t, t_0)^T \quad (2-19)$$

After an Observation

$$\hat{x}_n = \hat{x}(t) + P_n H^T (HP_n H^T + Q)^{-1} (y - \hat{y}) \quad (2-20)$$

or

$$\hat{x}_n = \hat{x}(t) + K(y - \hat{y}) \quad (2-21)$$

$$P_n = P(t) - P(t) H^T (HP(t)H^T + Q)^{-1} HP(t) \quad (2-22)$$

where

\hat{x}_n = new estimate of the state after an observation

$\hat{x}(t)$ = estimate of the state at time t before an observation

H = the gradient of the observation with respect to the state

y = measurement

K = filter gain

Q = $E[qq^T]$ - the covariance matrix of the random measurement error q

\tilde{x} = $x - \hat{x}$ - the error in estimate of the state

P_n = $E[\tilde{x}\tilde{x}^T]$ - variance-covariance matrix of the error in estimate of the state

Since the measurements are assumed to be processed sequentially, H = h is a 1 x m vector and Q = q is a scalar. Also, if no bias errors are estimated x is a 6 x 1 vector of the position-velocity state. However, if dynamic bias errors and measurement bias errors are estimated, then the total state vector x_e is given by

$$x_e = \begin{bmatrix} x \\ u \\ w \end{bmatrix}, \quad (2-23)$$

where

$u = d \times 1$ vector of dynamic bias errors

$w = m \times 1$ vector of measurement bias errors

For this study u may include the inertial platform bias error sources and w may include (1) range, range-rate, azimuth, elevation, or direction cosine, etc., measurement bias errors, (2) station location errors in latitude, longitude, and elevation, and (3) the clock or measurement timing error. The transition matrix for the expanded state vector x_e is then given by

$$\Phi_e = \begin{pmatrix} 6 \times 6 & 6 \times d & 6 \times m \\ \emptyset & \emptyset_u & 0 \\ & d \times d & \\ 0 & I & 0 \\ & & m \times m \\ 0 & 0 & I \end{pmatrix} \quad (2-24)$$

The covariance matrix of the error in estimate of the expanded state (P_e) will have the dimensions of Φ_e and is again propagated in time according to Section 2.4 with the Φ_e of (2-24), and updated at an observation according to (2-20) with an expanded H vector that is given by

$$H_z = \begin{bmatrix} H \\ 0 \\ G \end{bmatrix}, \quad (2-25)$$

and an expanded covariance matrix given by

$$P_e = \begin{bmatrix} 6 \times 6 & & \\ P & C_{de} & C_{me} \\ C_{de}^T & D & C_1 \\ C_{me}^T & C_1^T & W \end{bmatrix}, \quad (2-26)$$

where

$D = E[uu^T]$ - the covariance matrix of the dynamic bias errors (including the inertial guidance errors)

$W = E[ww^T]$ - the covariance matrix of the measurement bias errors and station location errors.

A more detailed description of these equations is given in Reference 3.

2.4.1 Equations for Determining the Effect of Neglecting Error Sources

The standard equations for the Kalman filter, which have been summarized in the previous section, are applicable when all the elements in the state vector are to be estimated. A variation on this basic estimation process has been developed which enables one to determine the effect of neglecting error sources.

The problem of determining which error sources are significant arises because of the large number of errors that may exist in the combined inertial platform-tracking system. Since it is unlikely that in an actual orbit determination, all the known error sources would be estimated, it becomes necessary to determine in advance, which sources contribute significantly

to the error in estimate of the state, and therefore should be modeled. Determining which error sources are significant can be accomplished by simulating the mission with the error sources of questionable importance neglected from the model, and determining the effect of neglecting these sources at the end of the simulation.

The general form of the total state covariance matrix (P_{ne}), when some parameters are estimated and other parameters are neglected, is shown in (2-27). The equations for updating the estimated parameters whose covariance matrices are P , D and W , have been given in the previous section. The variances of the neglected dynamic parameters D_o and the neglected measurement parameters W_o , are constant, and therefore not updated in time or after one observation. However, the correlations between the neglected parameters and the estimated state, C_{dn} and C_{mn} , are updated, and it is through these correlations that the effect of neglecting parameters is determined.

$$P_{ne} = \begin{array}{|c|c|c|c|c|} \hline \text{exs} & & & & \\ \hline P & C_{de} & C_{me} & & \\ \hline C_{de}^T & D & C_l & C_{dn} & C_{mn} \\ \hline C_{me}^T & C_l^T & W & & \\ \hline & & & D_o & 0 \\ \hline & & & 0 & W_o \\ \hline \end{array} \quad (2-27)$$

The correlation between the state and the measurement biases (C_{mn}) and the correlation between the state and the dynamic biases (C_{dn}) are computed as follows:

$$C_{dn}(t) = \phi(t, t_0) C_{dn}(t_0) + \phi_u D \quad (2-28)$$

$$C_{mn}(t) = \phi(t, t_0) C_{mn}(t_0) \quad (2-29)$$

$$C_{dn}^+ = [I - KH] C_{dn}^- \quad (2-30)$$

$$C_{mn}^+ = [I - KH] C_{mn}^- - KGW_o, \quad (2-31)$$

where (-) and (+) denote time before and after an observation, respectively.

The total covariance matrix P_T which gives the uncertainty of having neglected measurement and dynamic bias errors, in addition to the uncertainties given by P_n and $P(t)$ in (2-19) and (2-22), is

$$P_T = P_e + C_{dn} D_o^{-1} C_{dn}^T + C_{mn} W_o^{-1} C_{mn}^T \quad (2-32)$$

where P_e is the $m \times n$ matrix in (2-26) which includes P , D and W . Since the last two terms in (2-32) can be written with C_{dn} and C_{mn} as column vectors and D and W as scalars, or with C_{dn} , C_{mn} , D , and W as matrices, equation (2-32) may be used to obtain the effect of neglecting individual error sources or groups of error sources.

2.4.2 The Concept of an Equivalent Observation

One of the implications of this study is that a parametric analysis of the error sources be made in order to determine the effect of different numerical values of the error sources. A parametric study of these error sources requires that the initial standard deviations of each error parameter be changed through a wide range of values, and the effect of these changes on the uncertainty in the other error sources as well as the state, noted at the trajectory. The technique presented in this section enables the initial

standard deviations of any of the estimated bias parameters, to be changed in one simulation of the mission, i.e., one computer run.

A special case of what has been defined as an equivalent observation, is where there is no random measurement error. In this case a perfect observation of the position-velocity state or of other parameters can be made. The perfect observation is useful for determining the effect of an uncertainty in one parameter on the uncertainty in another parameter, or the uncertainty in the position or velocity state.

2.4.2.1 Equations For an Equivalent Observation. In a conventional error analysis, where for example one element of P may be the variance of an inertial guidance error and a number of observations are made of the vehicle (range, range-rate, etc.), the effect of changing the initial variance on the final uncertainty of the vehicle state, would be determined by simulating the mission with a new value of this particular variance. This would correspond to changing the initial variance of the parameter (P_0) by a factor of k, i.e.,

$$P'_0 = kP_0 \quad (2-33)$$

However, this same value of the initial variance (P'_0) can be found by taking a direct observation of the parameter whose variance is to be changed ($h = 1$), with a measurement error variance (q) that is specified such that the state variance after the observation is P'_0 . For the scalar case the equation for an observation is

$$P = \frac{P_0 q}{h^2 P_0 + q} \quad (2-34)$$

Since the value of P after the observation (P'_0) is given by (2-33), equating (2-33) to (2-34) and solving for q gives the result

$$q = P_0 \frac{k}{1-k} \quad (2-35)$$

The second part of this derivation is to show that the order of the observations does not matter, i.e. the direct observation can be made at the end of the run as well as at the beginning. The fact that the order of the observations can be interchanged without changing the final state uncertainty can easily be seen from the least squares form of P . The identity between the Kalman and least squares form of the observation equation is

$$\begin{aligned} P &= P_0 - P_0 H^T [H P_0 H^T + Q]^{-1} H P_0 \\ &= [P_0^{-1} - H^T Q^{-1} H]^{-1} \end{aligned} \quad (2-36)$$

After a number of observations it can be seen that the state uncertainty P is given by

$$\begin{aligned} P_n &= [P_0^{-1} + H_1^T Q_1^{-1} H_1 + H_2^T Q_2^{-1} H_2 + \dots \\ &\quad H_n^T Q_n^{-1} H_n]^{-1} \end{aligned} \quad (2-37)$$

Clearly the order in which the terms in (2-37) are added, does not affect the result. Therefore it is possible to change the initial variance of a parameter by a direct observation of this parameter at the end of a run.

The use of an equivalent observation to change the initial variance can be summarized with the aid of Figure 2-2.

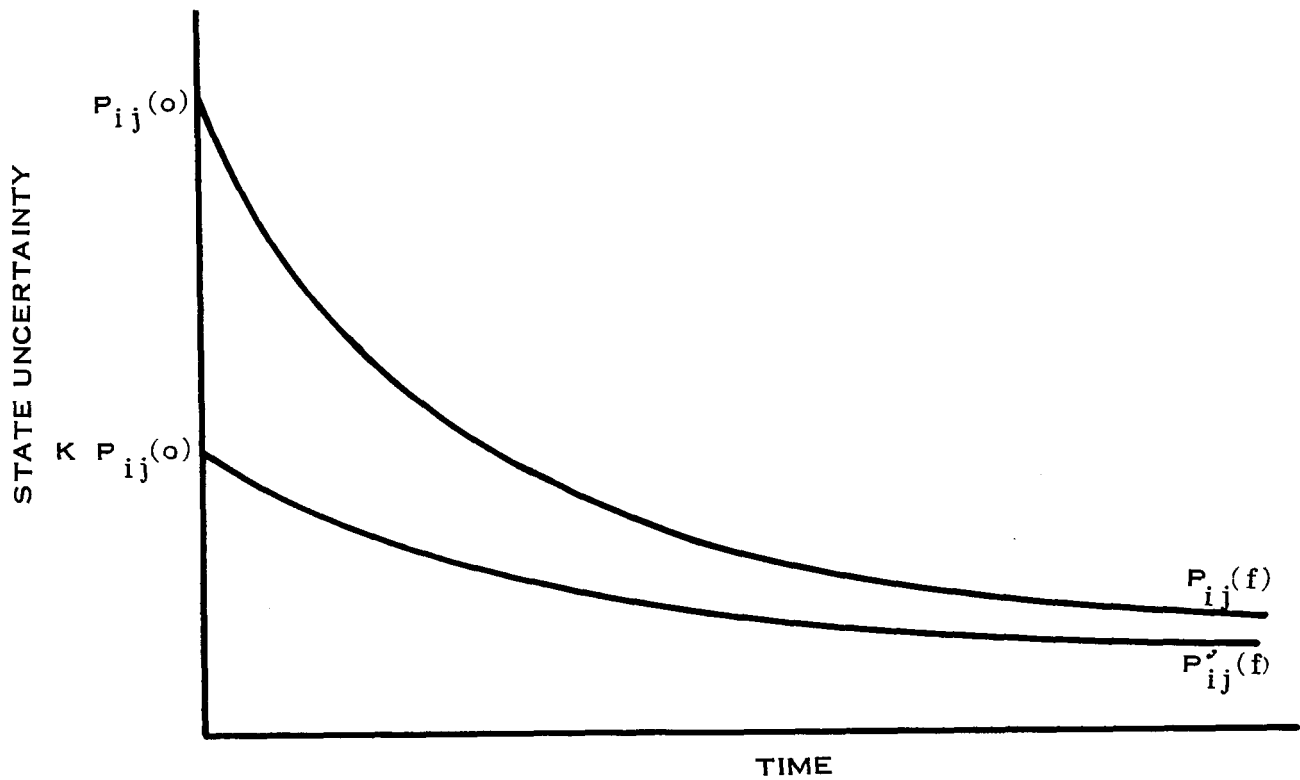


Figure 2-2 Effect of an Equivalent Observation

The standard method of studying a parameter P_{ij} is to first make a run where the initial value is $P_{ij}(0)$ and the final value is $P_{ij}(f)$. A second run is then made where the initial uncertainty is changed by a factor of $k P_{ij}(0)$ to $P'_{ij}(0)$. The uncertainty at the end of the run is $P'_{ij}(f)$. With the equivalent observation concept, the final value $P'_{ij}(f)$, as well as effect on other elements of the state, is obtained by the equation

$$P'(f) = P(f) - P(f) H^T \left[H P(f) H^T + P_{ij}^{(0)} \frac{k}{1-k} \right]^{-1} H P(f) \quad (2-38)$$

where

$$H = [0 \cdots 1 \cdots 0], \quad (2-39)$$

and the location of the 1 in (2-39) corresponds to the parameter that is being observed.

In this manner any number of changes can be made in one or more of the initial variances by adding equivalent observations at the end of a run. Thus the results of a number of computer runs can be obtained in one run.

2.4.2.2 The Equations For a Perfect Observation. A special case of the equivalent observation concept is where a perfect observation is made of a parameter. An observation of this type has the H of (2-39), where the element in H which is 1 corresponds to the element of the state which is being observed, but there is no measurement error variance Q. The effect of a perfect observation of a measurement bias error on the covariance matrix P is given by

$$P' = P - C_m W^{-1} C_m^T \quad (2-40)$$

where C_m is the column vector of correlations between the state and the measurement bias which is being observed. The effect on P of a perfect observation of a dynamic bias error is given by

$$P' = P - C_d D^{-1} C_d^T \quad (2-41)$$

A perfect observation of a parameter may be useful for determining some of the interrelationships between the parameter uncertainties. For example, by comparing the uncertainty in a platform error source at the end of a run with the same uncertainty after a perfect observation of a measurement bias error, the effect of the uncertainty in the measurement bias error on the uncertainty in the platform error source can be determined. A more detailed discussion of these concepts are included in Reference 4.

SECTION 3

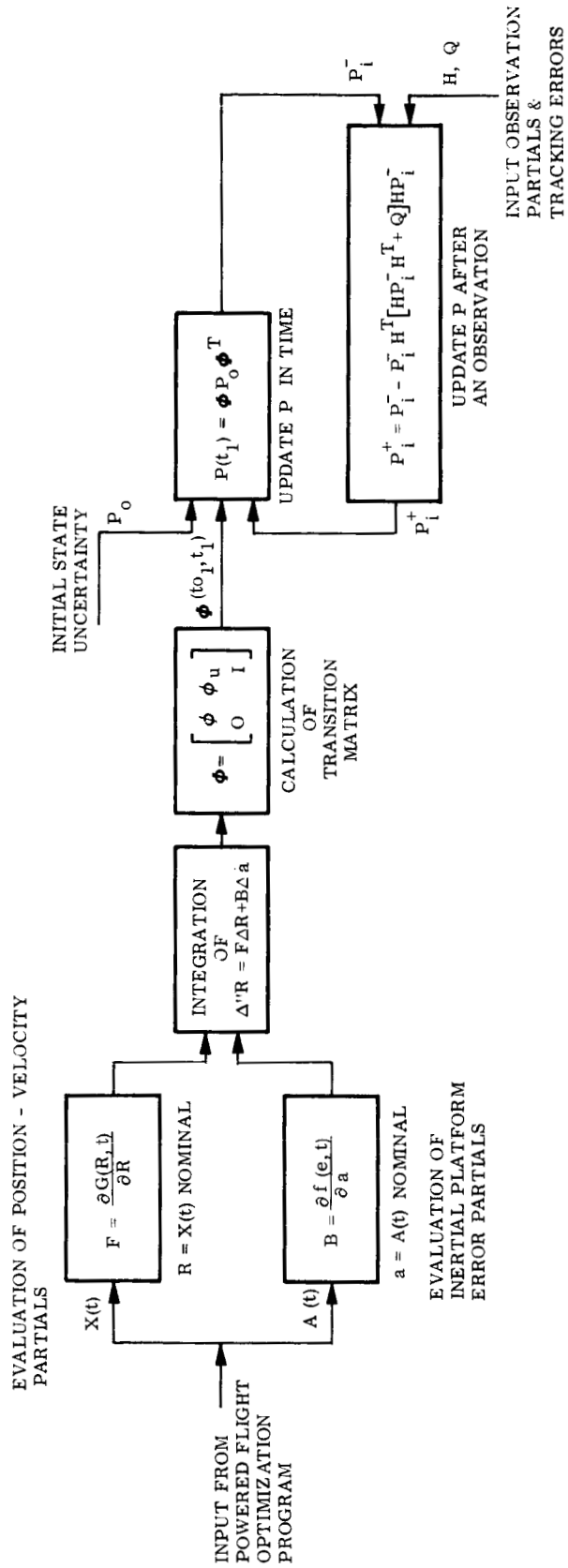
POWERED FLIGHT ERROR PROPAGATION PROGRAM

The computer program that has been used to obtain the numerical results for this study is the Powered Flight Error Propagation Program. The original version of this program was written by Philco-Ford for NASA Goddard under Contract NAS-5-9700, and is described in Reference 2.

The program simulates an actual orbit determination that would combine the tracking data from the ETR radars with the telemetry data from the vehicle, and would be used to estimate the position and velocity of the vehicle plus any additional parameters such as the inertial platform errors or the tracking bias errors. As a result, it is a useful tool for studying the ensemble behavior of the combined inertial platform-tracking system under a wide variety of conditions.

The essential output from the program is a variance-covariance matrix of errors in estimate of the position and velocity state, and the estimated error parameters. The covariance matrix is propagated along a nominal powered flight trajectory. A general flow diagram of the program functions are shown in Figure 3-1.

The program reads an input tape of the nominal trajectory position $X(t)$ and acceleration $A(t)$ that is generated by the Philco Ford Powered Flight Optimization Program. (Ref. 2) The gravity partials (F) are evaluated for the nominal values of $X(t)$ and the platform error partials are evaluated for the nominal values of acceleration $A(t)$. These partials define the differential equations for the deviations about the nominal trajectory. These equations are integrated for short time intervals in order to obtain the transition matrices Φ and Φ_u . The matrix Φ_u defines the perturbation of the trajectory resulting from the guidance errors.



3-2

Figure 3-1 Functional Diagram of Powered Flight Error Analysis Program

The transition matrices are used to update the covariance matrix (P) in time. There is no modification made to the trajectory in the sense that the actual perturbed trajectory is calculated.

The essential part of the estimation process which simulates an orbit determination is the updating of the covariance matrix P. As shown in Figure 3-1 P is propagated between two points in time based in the previous value of P and the total transition matrix Φ . This propagation in time accounts for the fact that the guidance errors will in general increase the state uncertainty P as the time along the trajectory increases.

The data from the trackers is incorporated into the estimation by updating the state uncertainty at each observation. Observations are processed one at a time, that is the partial of the observation with respect to the state (H) is a vector and the random tracking error q is a scalar.

The program has a capability of handling a 60 x 60 covariance matrix. It's elements include the uncertainty in the three coordinates of position and the three coordinates of velocity, which are initially zero, plus the uncertainty in any inertial guidance error, or tracking bias error. Up to 30 guidance errors may be included in the guidance model. The 30 guidance errors that may be included in the program are summarized below. The numbers associated with them are used in the program for "bookkeeping" purposes.

<u>ERROR SOURCE</u>	<u>PROGRAM NUMBER</u>
Accelerometer scale factor ~ x, y, z axes	1,5,9 respectively
Accelerometer misalignment y to x, y to z axes	2,8
Accelerometer misalignment z to x, z to y axes	3,6
Accelerometer misalignment x to y, x to z axes	4,7
Accelerometer bias x, y, z axes	10,11,12
Accelerometer thresholds x, y, z axes	13,14,15
Initial platform misalignment x, y, z axes	16,17,18
Steady state drift rate Roll,Yaw,Pitch Gyros	19,20,21

<u>ERROR SOURCE</u>		<u>PROGRAM NUMBER</u>
Input axis mass unbalance drift	Roll, Yaw, Pitch Gyros	22,23,24
Spin axis mass unbalance drift	Roll, Yaw, Pitch Gyros	25,26,27
Anisoelastic drift of	Roll, Yaw, Pitch Gyros	28,29,30

These numbers will appear in the covariance matrix output shown in Appendix A. In addition, tracking bias errors such as range, range-rate, azimuth, elevation, latitude, longitude, and altitude can be included in the covariance matrix.

The program has a number of options which have been developed for this study. There are two basic options for treating bias error sources. The standard option is where all the bias errors are estimated. In this option an initial variance is assigned to a bias error source such as a platform error or tracking bias error, and the estimation process attempts to reduce this initial uncertainty in the bias error. The bias error is part of the total covariance matrix P and the applicable equations for updating P are those discussed in Section 2.4.

The second option that can be used for bias errors is the neglect option. For this option the variance of the error source remains constant throughout the run; however, the correlations between the neglected parameters and the estimated parameters are updated according to (2-28) through (2-31). The effect on the total state uncertainty (the position-velocity state plus any estimated error sources) of neglecting the error sources is calculated at each output time according to (2-32).

Two additional options exist in the Powered Flight Error Propagation Program that enable equivalent observations to be made. The first option has been described in Section 2.4.2 and provides a way of studying bias errors parametrically in one computer run. The effect on the final covariance matrix of varying the initial value of one or more bias error sources through a wide range of values is obtained by adding equivalent observations at the end of a run.

The second equivalent observation, a direct observation of a specific parameter ($h = 1$) with zero error variance (q), can be used to determine the uncertainty in the position, velocity, or other error parameter, that results from another error source. The use of this option provides a means of separating the total uncertainty in one error source according to the contribution from other error sources.

SECTION 4

THE ASCENT TRAJECTORY

The ascent trajectory which has been used as the nominal trajectory for this study is similar to a Saturn V trajectory. This trajectory was generated by the Philco-Ford Powered Flight Optimization Program. The output of the program is a trajectory tape which contains the vehicle position and acceleration at discrete time points. An altitude profile of the nominal trajectory is shown in Figure 4-1. The ground track for this trajectory (latitude vs. longitude) is shown in Figure 4-2. The locations of the tracking stations are also shown in this figure.

Variations of this basic trajectory have also been used. However, it was determined the results presented in the succeeding sections are not sensitive to small variations in the trajectory. In particular, one trajectory whose final altitude was about twice the value in Figure 4-1 caused no significant changes in the ability to estimate the guidance errors. Acceleration levels in the DR, CR, UP coordinate system are shown in Figure 4-3.

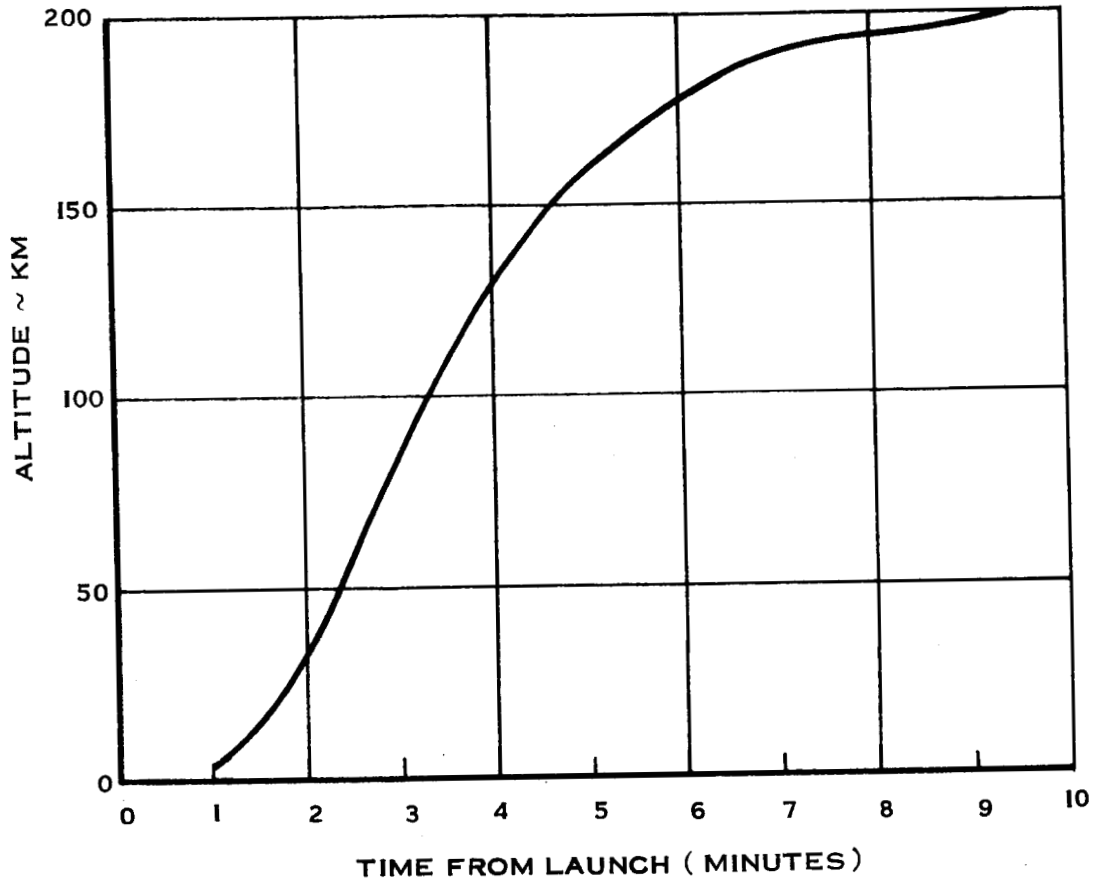


Figure 4-1 Trajectory Altitude vs Time

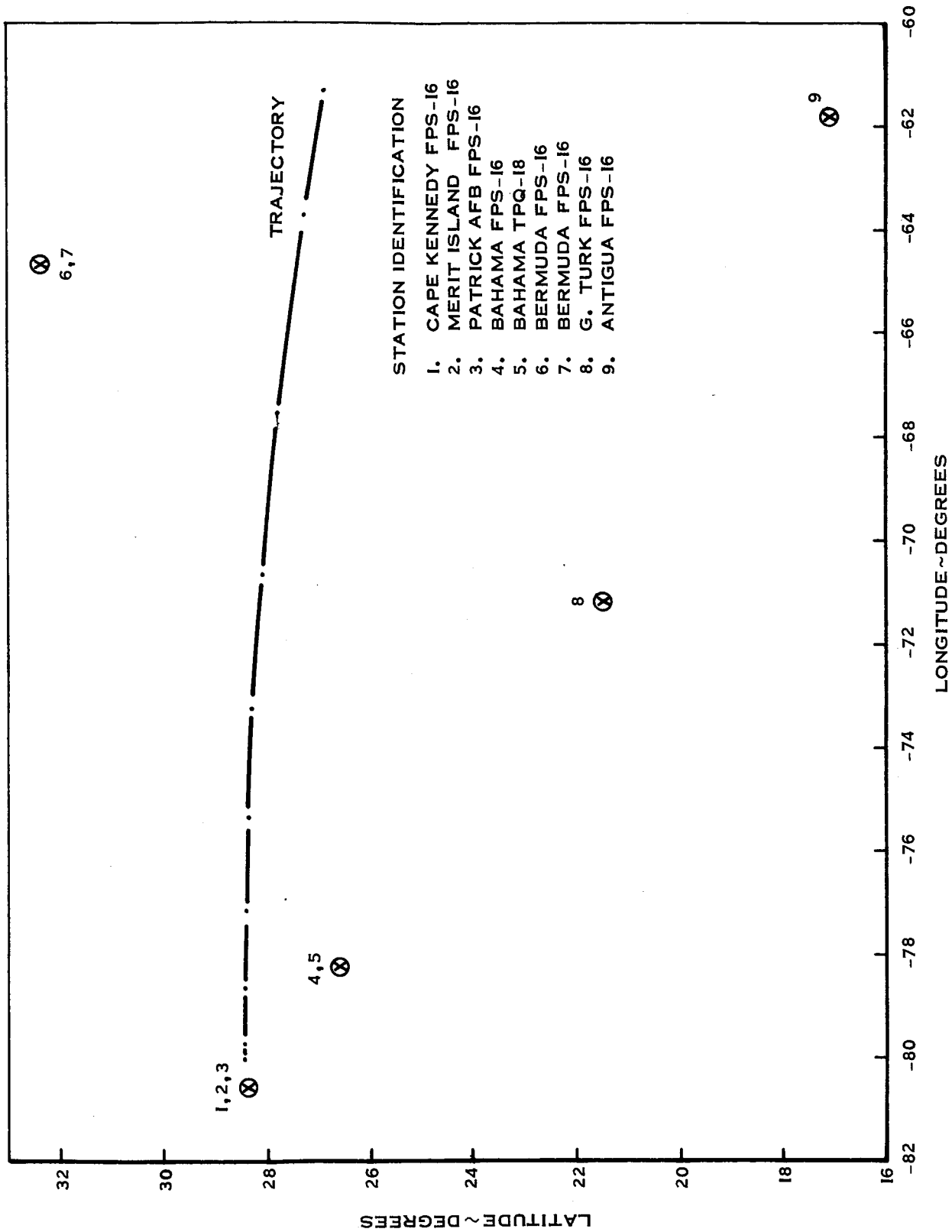


Figure 4-2 Trajectory and Tracking Station Location

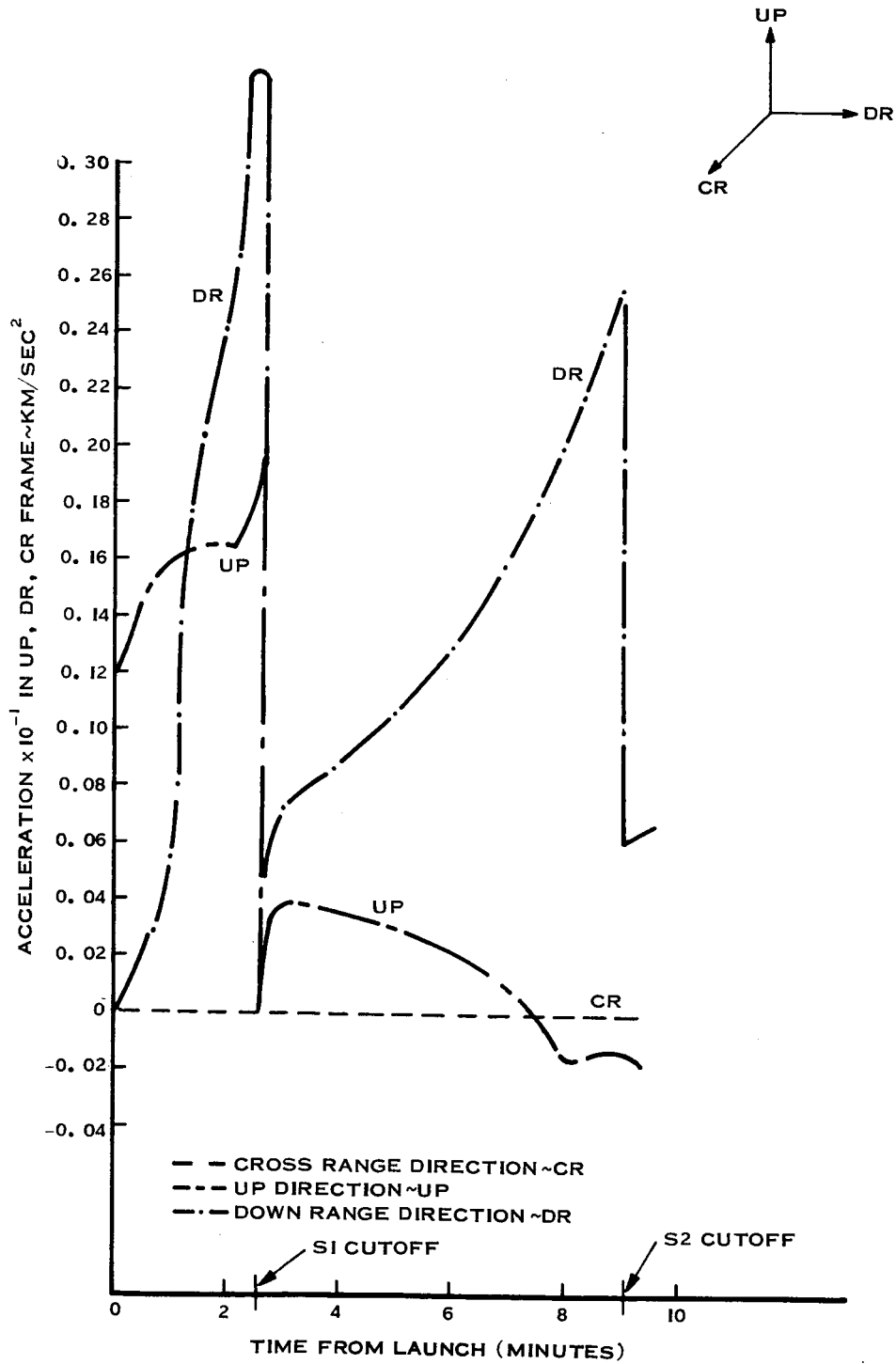


Figure 4-3 Acceleration Levels for Nominal Trajectory

SECTION 5

SELECTION OF COMBINED PLATFORM-TRACKING

Prior to determining the feasibility of estimating the inertial platform errors, an analysis was made to evaluate the effect of individual errors, both from the tracking and the inertial platform. This analysis shows (1) the effect of the inertial platform errors on the trajectory dispersions, (2) the effect of varying the numerical values of the platform errors, and (3) the effect of the tracking bias errors.

5.1 DISPERSIONS FROM THE PLATFORM ERRORS WITHOUT TRACKING

The dispersions resulting from the inertial platform errors have been determined by propagating an initial covariance matrix (P_0), consisting of the 30 platform errors, along the nominal trajectory according to (2-19). The RMSV and the RMSV of these errors are shown in Figures 5-1 and 5-2 where the RMSV and RMSV are defined as

$$\text{RMSV} = \sqrt{P_{11} + P_{22} + P_{33}}$$

$$\text{RMSV} = \sqrt{P_{44} + P_{55} + P_{66}}$$

The total uncertainty in position and velocity at the end of the trajectory is seen to be 0.5 km and 2 m/sec, respectively. A breakdown of these errors in the local tangent plane (DR, CR, UP) is shown in Figures 5-3 through 5-8. Although the three components of errors do not differ significantly, the largest error in both position and velocity is an altitude, and the smallest is in the down range direction.

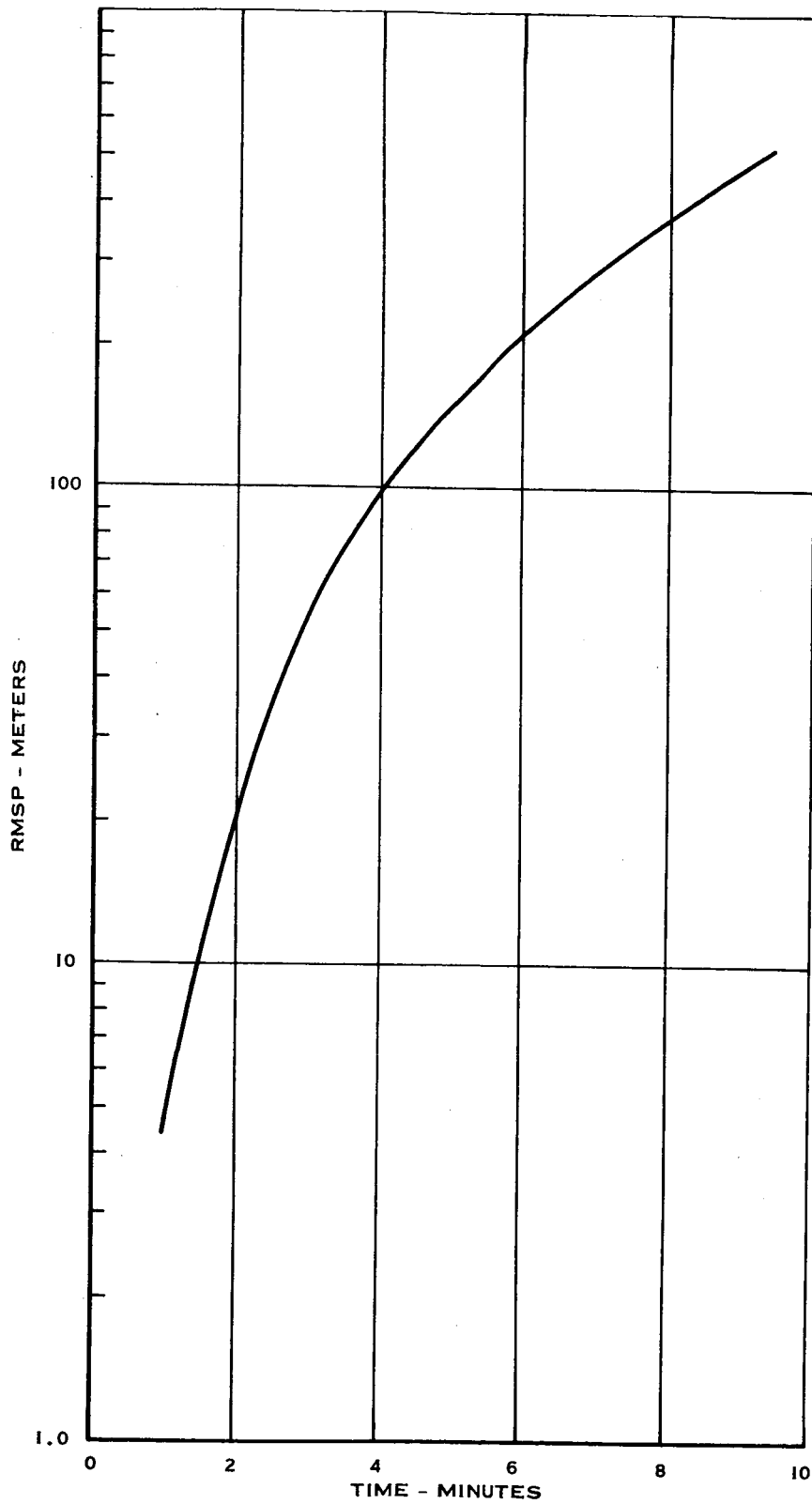


Figure 5-1 RMS Uncertainty in Position State From the 30 Platform Error Sources (No Tracking)

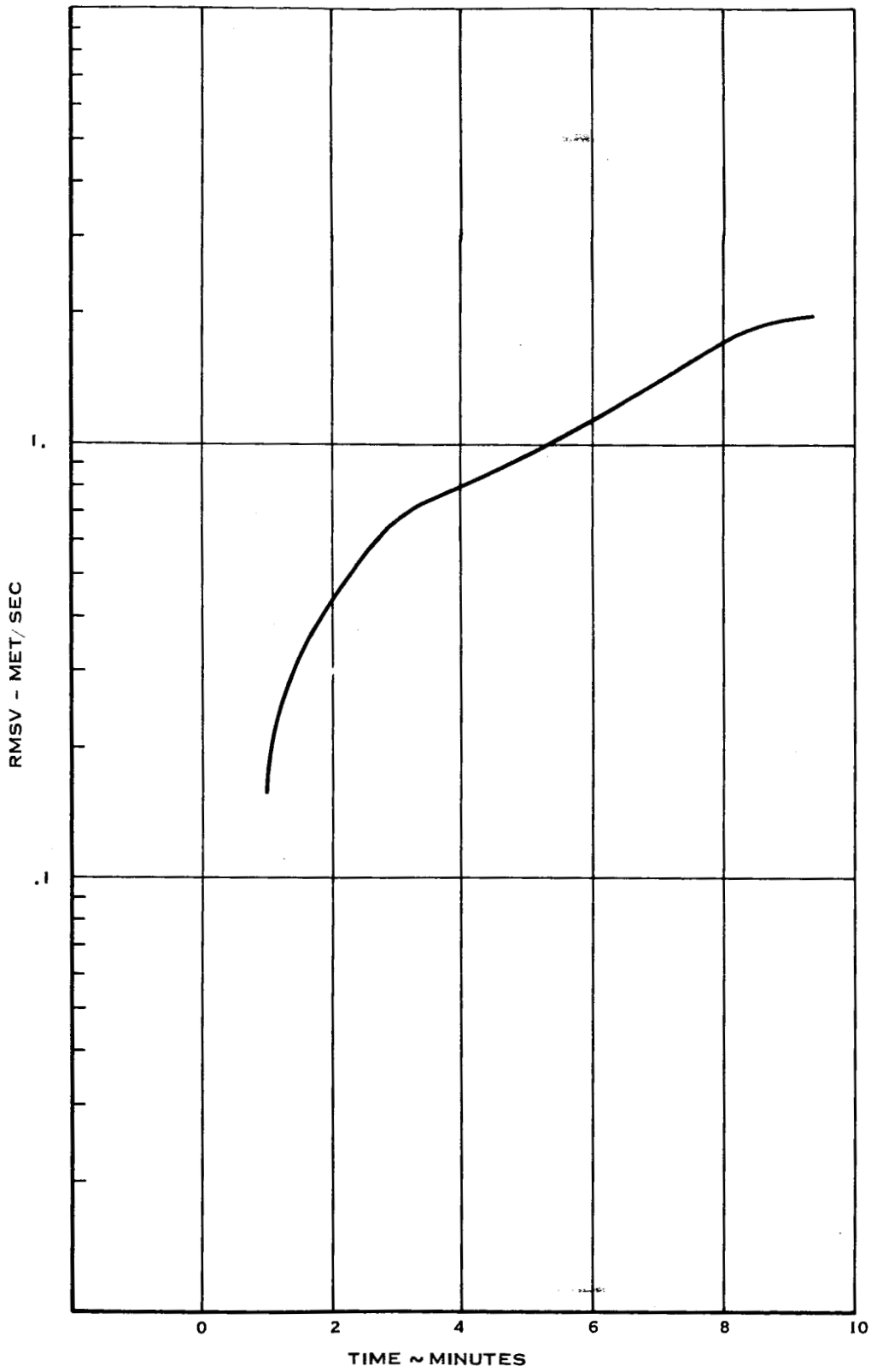


Figure 5-2 RMS Uncertainty in Velocity State from the 30 Platform Error Sources

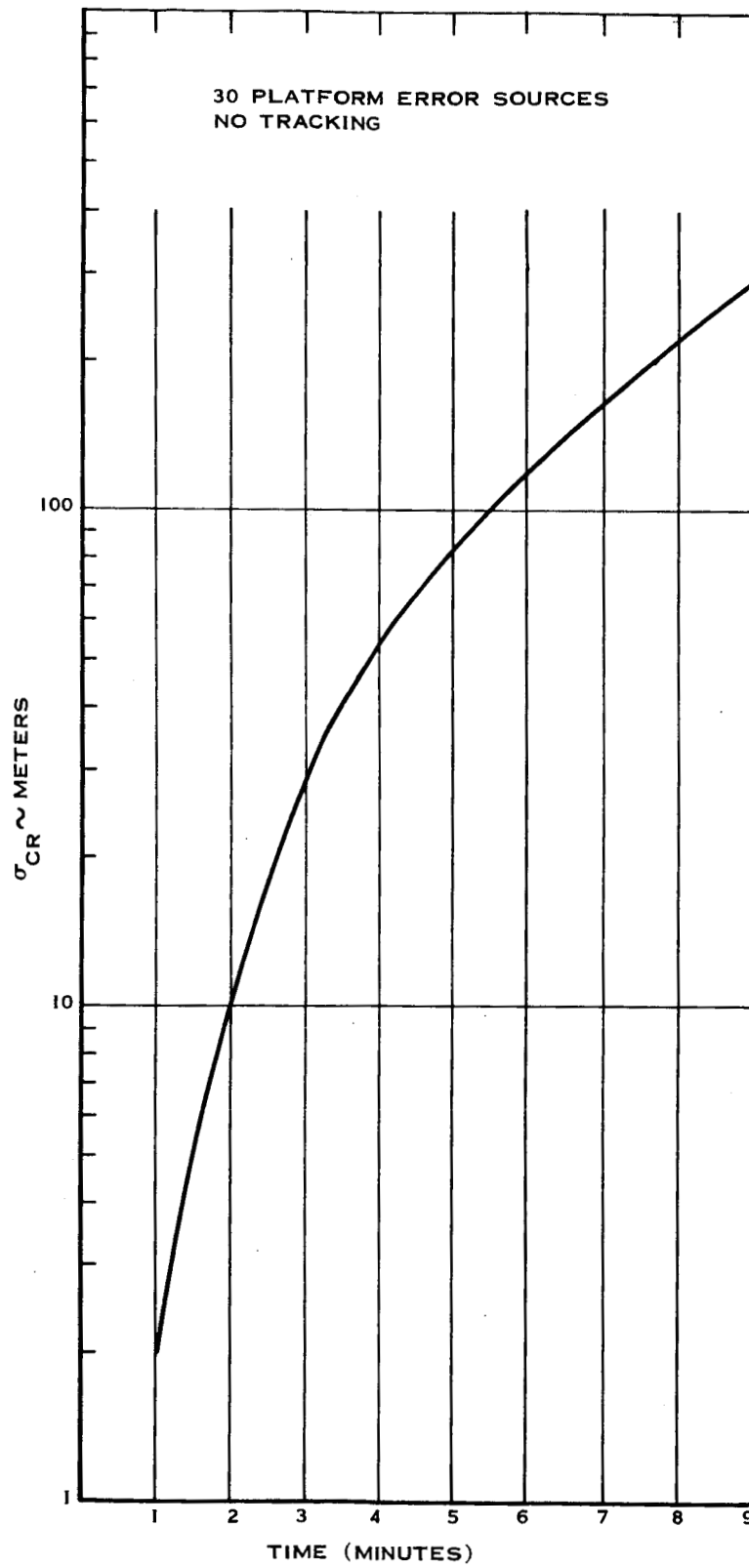


Figure 5-3 3 σ Standard Deviation of Error in Estimate of the State in Cross Range Direction

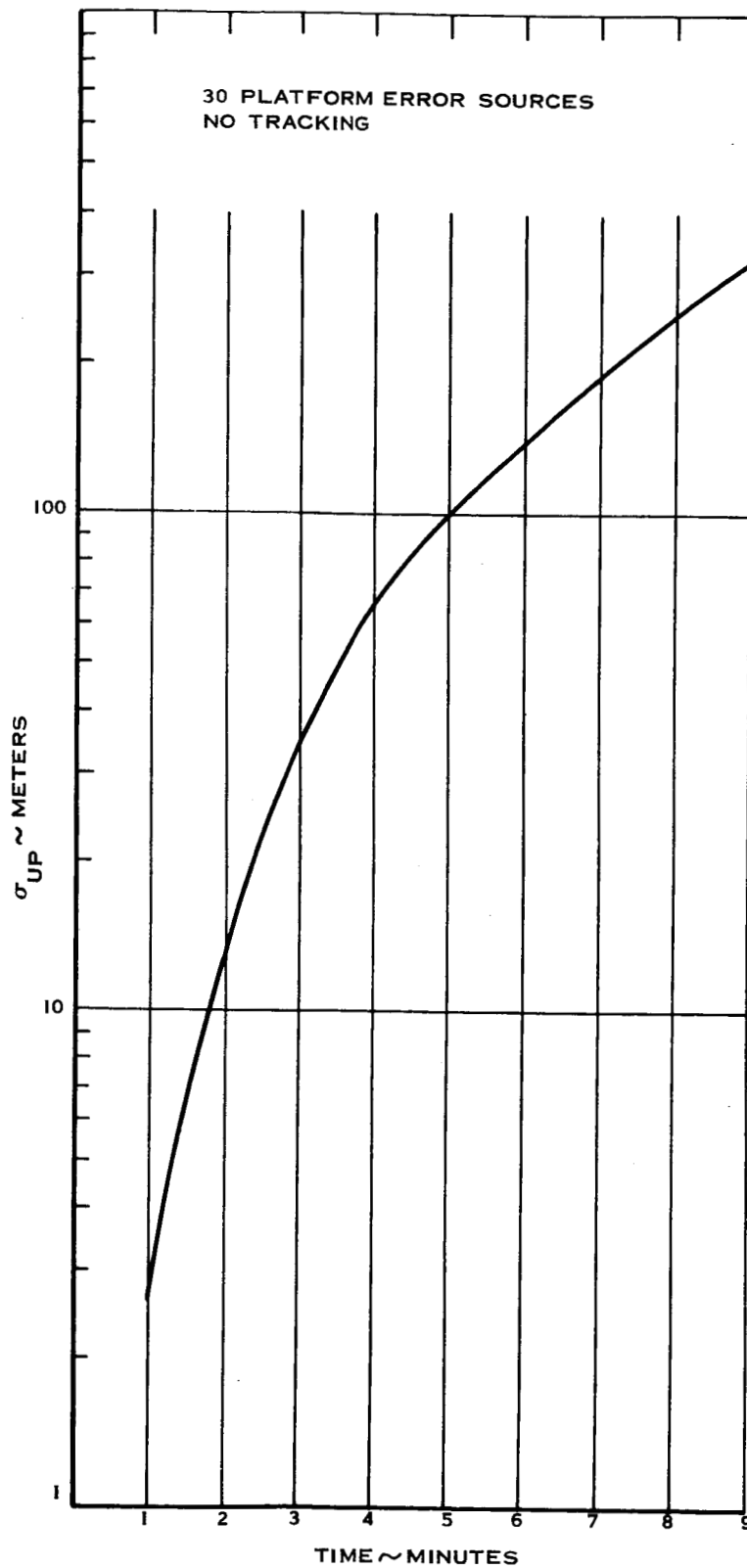


Figure 5-4 3σ Standard Deviation of Error in Estimate of the State in the Up Direction

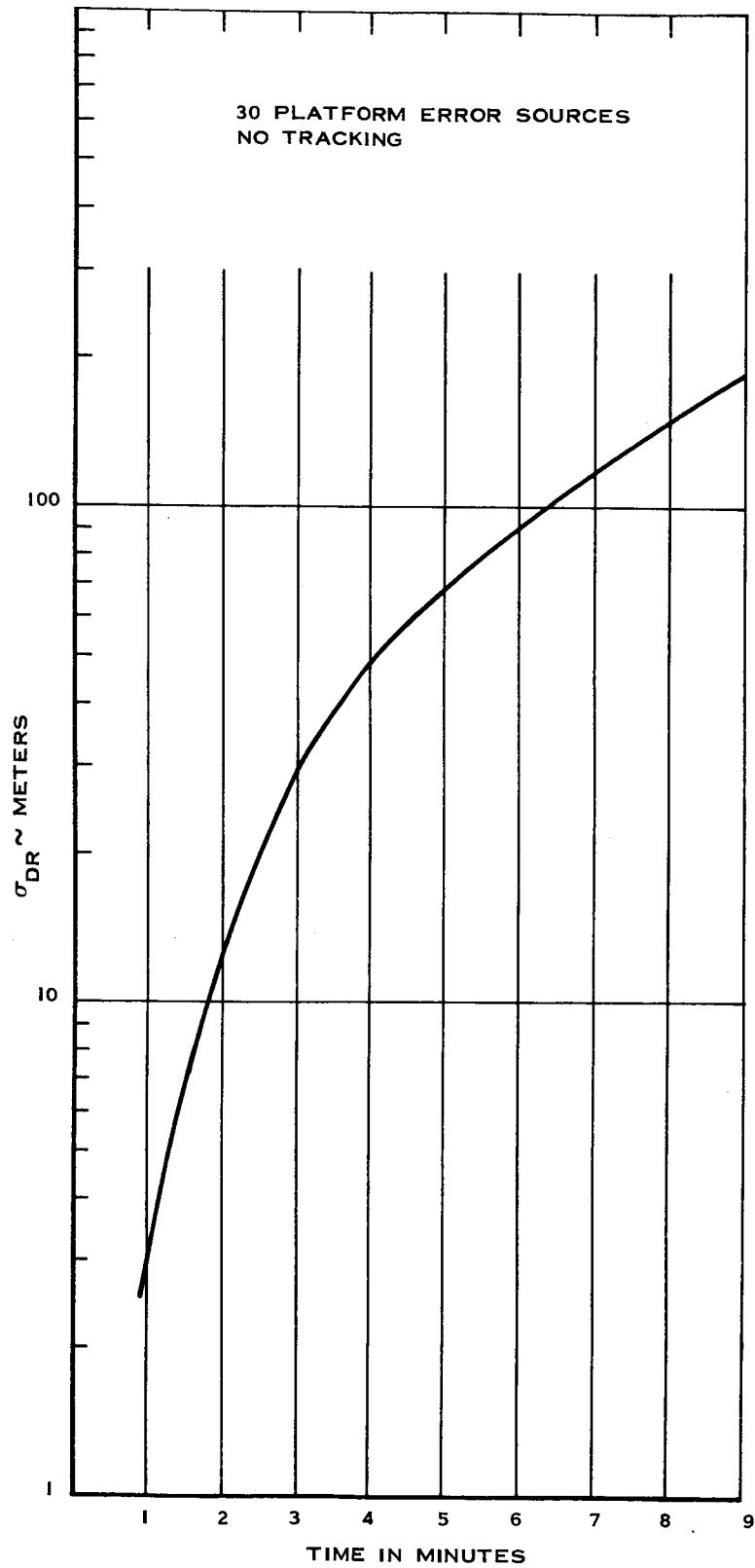


Figure 5-5 30 Standard Deviation of Error in Estimate of the State in the Down-Range Direction

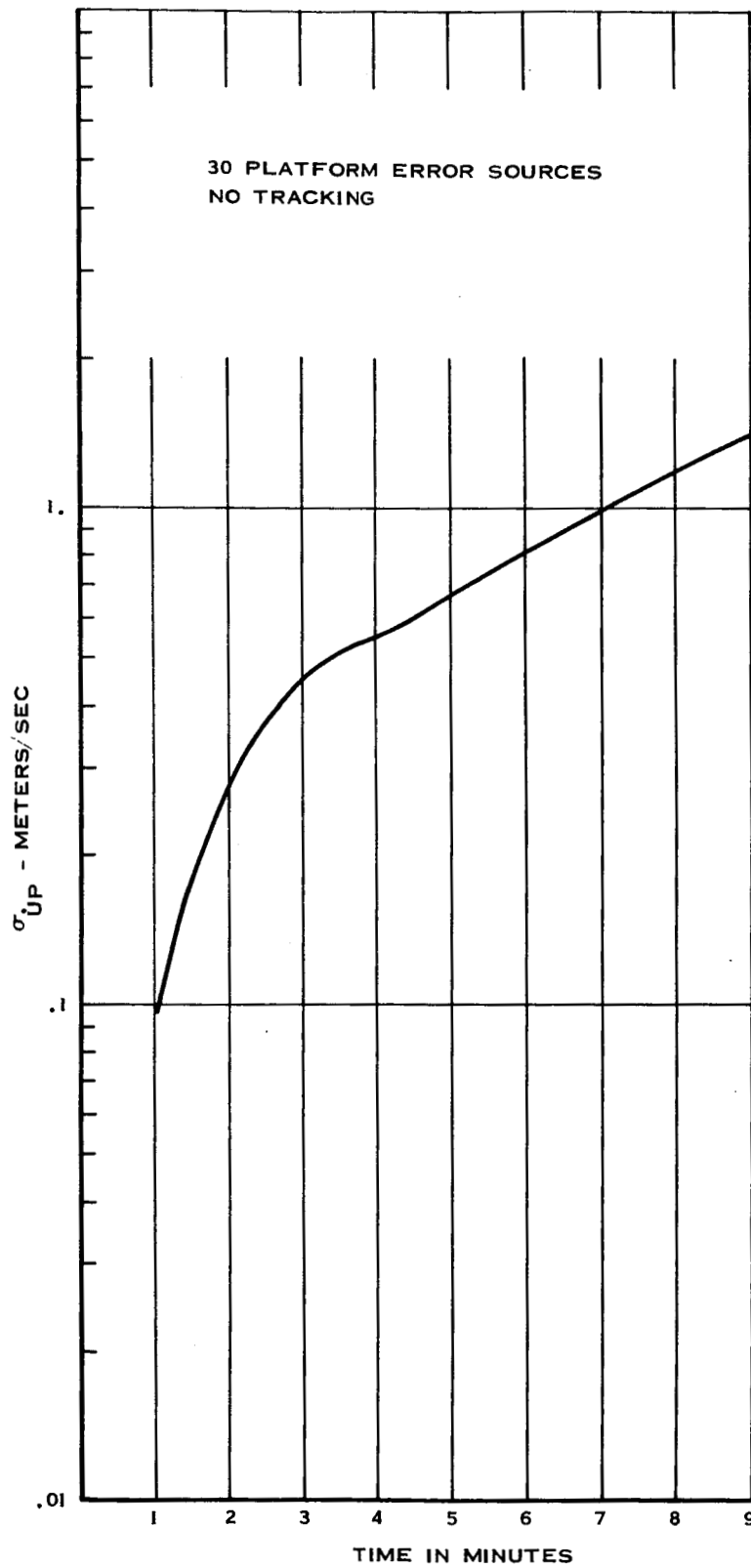


Figure 5-6 30 Standard Deviation of Error in Estimate of the Velocity State in the Up Direction

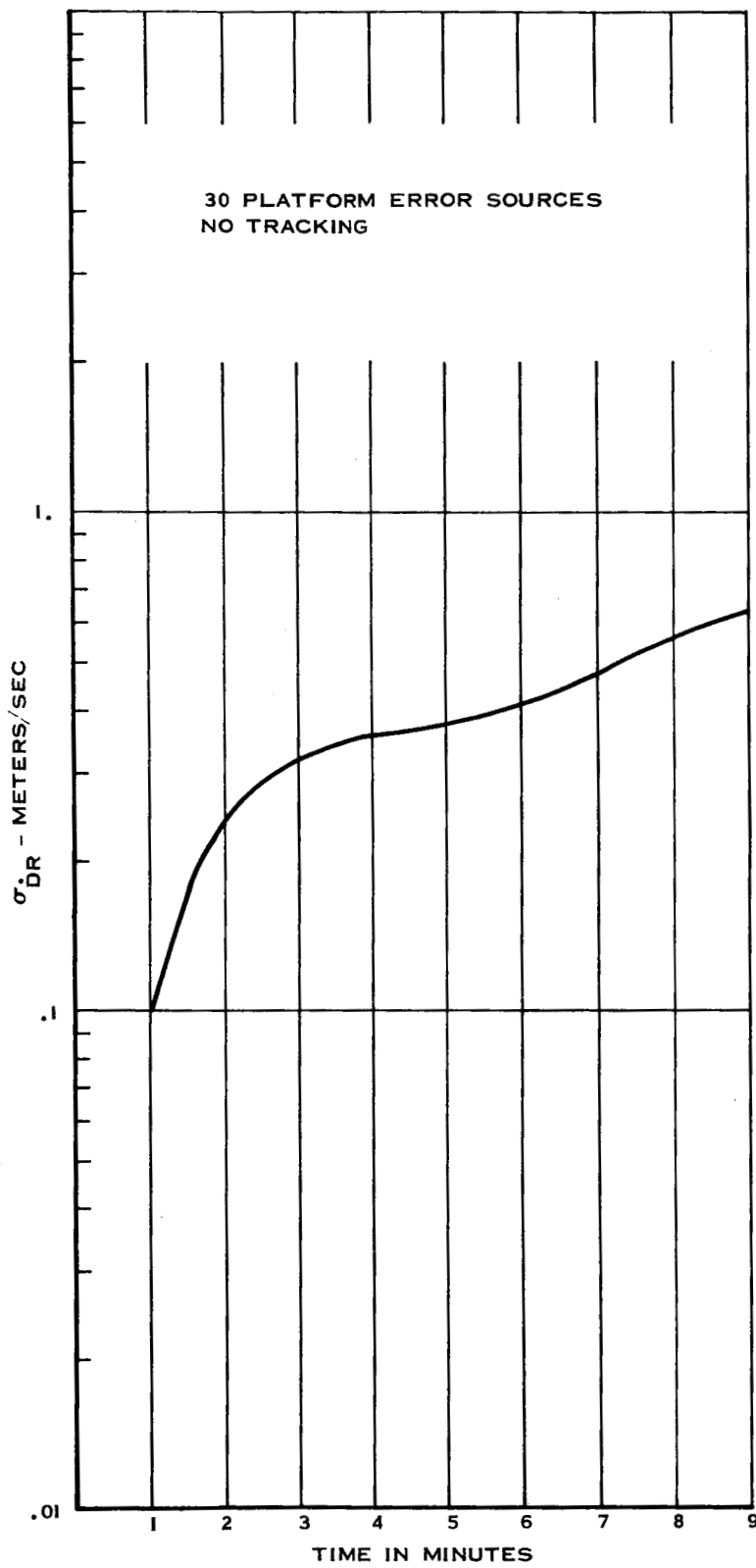


Figure 5-7 3σ Standard Deviation of Error in Estimate of the Velocity State in the Down-Range Direction

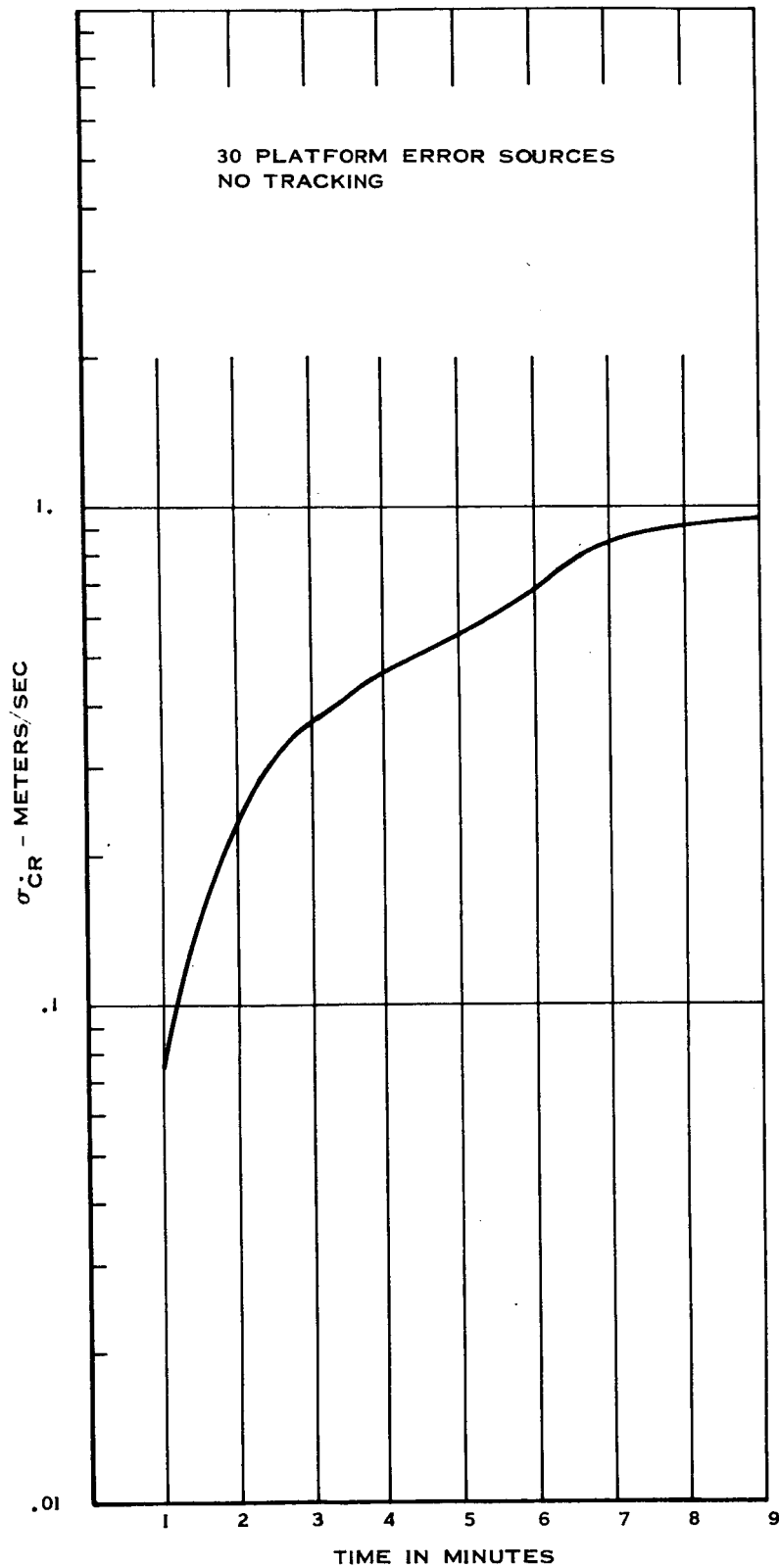


Figure 5-8 3 σ Standard Deviation of Error in Estimate of the Velocity State in Cross Range Direction

In order to determine the relative effect of individual error sources on the total position and velocity dispersions, the effect of neglecting each of the 30 error sources has been evaluated. The effect of each error source on the position uncertainty is given by

$$\text{RMSPP} = \sqrt{\sum_{i=1}^3 C_i \frac{1}{d} C_i^T},$$

where each C_i is the correlation between one inertial error source and one of the three coordinates of position. Since the total position uncertainty is only from the platform error sources, the square root of the sum of the RMSPP's squared from all the error sources is equal to the 0.5 km in Figure 5-1. The relative importance of the individual error sources is shown in Table 5-1. The most significant error sources are seen to be the initial platform misalignments. The first 20 error sources listed in Table 5-1 were selected for the final error model of the inertial platform. The last 10 error sources in this table clearly have a negligible effect on the trajectory, and therefore were omitted from the final model.

If the same platform error sources are propagated by considering each source as an element of the state vector, i.e., by (2.19), then the effect of parametric changes in the platform error sources can be obtained. This is done by making an equivalent observation of the particular error source of interest, for each parametric change. The effect of changing the initial variance for each source, through a range of 10^{-2} to 10^2 around the nominal value, has been obtained. Changes in the final RMSP for changes in the initial variances of the five most significant error sources, are shown in Figures 5-9 through 5-13. As might be expected, it takes a significant change in any one source to improve the RMSP at injection, however, a slight increase in one of the sensor variances will cause a significant change in the RMSP.

TABLE 5-1 ORDER OF IMPORTANCE OF THE INERTIAL PLATFORM ERRORS

PROGRAM NO.	RANK	SOURCE	RMSFP IN METERS
17	1.	θ_{oy} Initial platform misalignment about Y-axis	316
18	2.	θ_{oz} Initial platform misalignment about Z-axis	213
2	3.	β_{yx} Y Accelerometer misalignment into X-axis	146
3	4.	β_{zx} Z Accelerometer misalignment into X-axis	134
16	5.	θ_{ox} Initial platform misalignment about X-axis	129
21	6.	$\dot{\theta}_z$ Steady-state drift of Z gyro	112
4	7.	β_{xy} X Accelerometer misalignment into Y-axis	110
6	8.	β_{zy} Z Accelerometer misalignment into Y-axis	110
20	9.	$\dot{\theta}_y$ Steady-state drift of Y gyro	100
11	10.	α_y Y Accelerometer bias	85
10	11.	α_x X Accelerometer bias	77
12	12.	α_z Z Accelerometer bias	77
1	13.	ϵ_x X Accelerometer scale factor	65
5	14.	ϵ_y Y Accelerometer scale factor	62
19	15.	$\dot{\theta}_x$ Steady-state drift of X gyro	38
27	16.	μ_{sz} Spin axis mass unbalance of Z gyro	33
30	17.	C_z Anisoelastic drift of Z gyro	32
23	18.	μ_{ly} Input axis mass unbalance of Y gyro	7.9

TABLE 5-1 ORDER OF IMPORTANCE OF THE INERTIAL PLATFORM ERRORS (Cont)

PROGRAM NO.	RANK	SOURCE	RMSPP IN METERS
22	19.	μ_{Ix} Input axis mass unbalance of X gyro	6.1
15	20.	S_z Z Accelerometer threshold	1.7
13	21.	S_x X Accelerometer threshold	.009
8	22.	β_{yz} Y Accelerometer misalignment into Z axis	.006
7	23.	β_{xz} X Accelerometer misalignment into Z axis	.005
9	24.	ϵ_z Z Accelerometer scale factor	.003
25	25.	μ_{sx} Spin axis mass unbalance of X gyro	.002
26	26.	μ_{sy} Spin axis mass unbalance of Y gyro	.001
24	27.	μ_{Iz} Input axis mass unbalance of Z gyro	.0008
29	28.	E_y Anisoelastic drift of Y gyro	$.2 \times 10^{-9}$
28	29.	C_x Anisoelastic drift of X gyro	$.2 \times 10^{-9}$
14	30.	S_y Y Accelerometer threshold	0

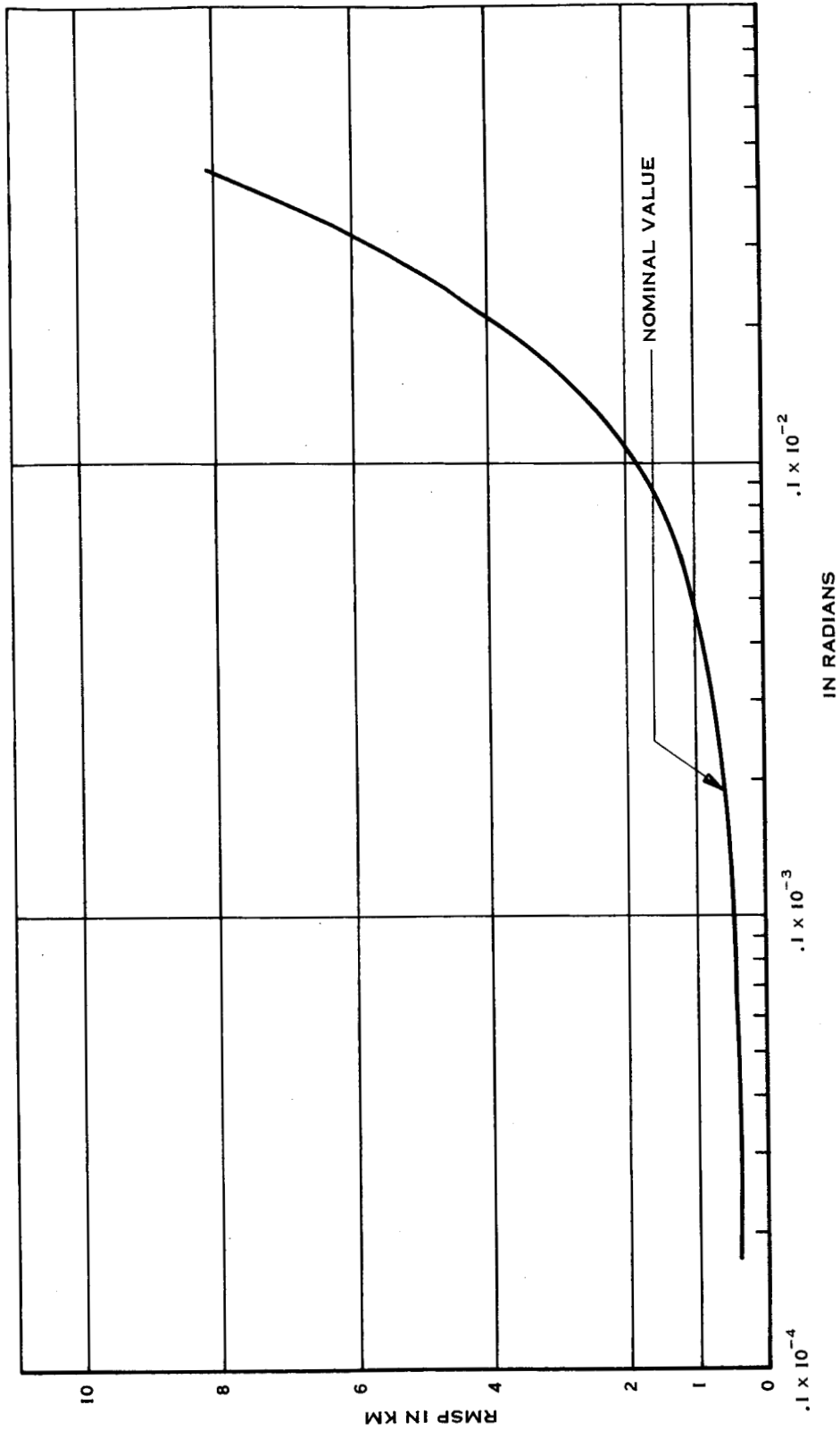


Figure 5-9 Variations in Final RMSP for Changes in Initial Standard Deviation of Initial Misalignment About Y Axis

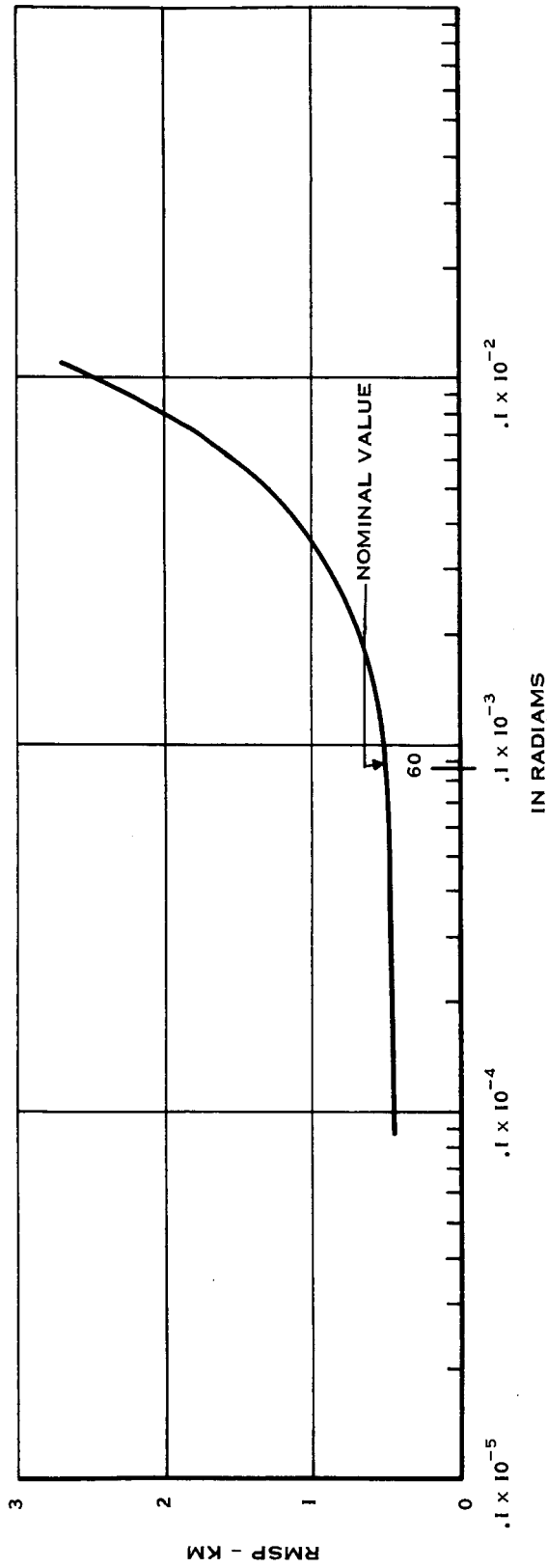


Figure 5-10 Variations in Final RMS for Changes in Initial Standard Deviation of Initial Platform Misalignment About Z Axis

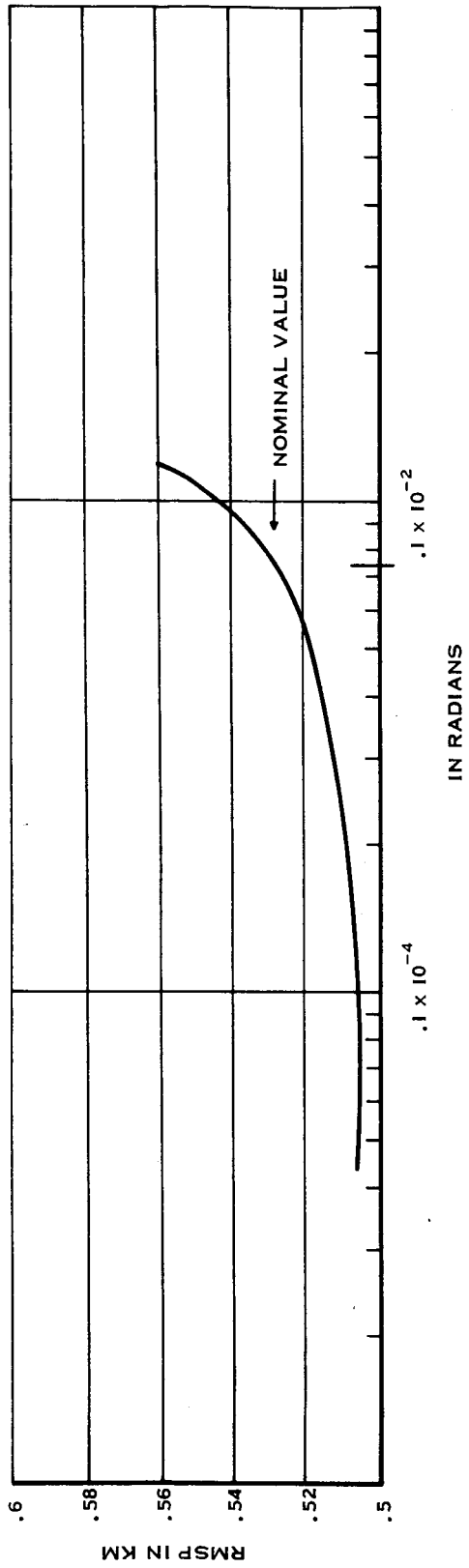


Figure 5-11 Variations in Final RMSP for Changes in Initial Standard Deviation of Y Accelerometer Into X Axis

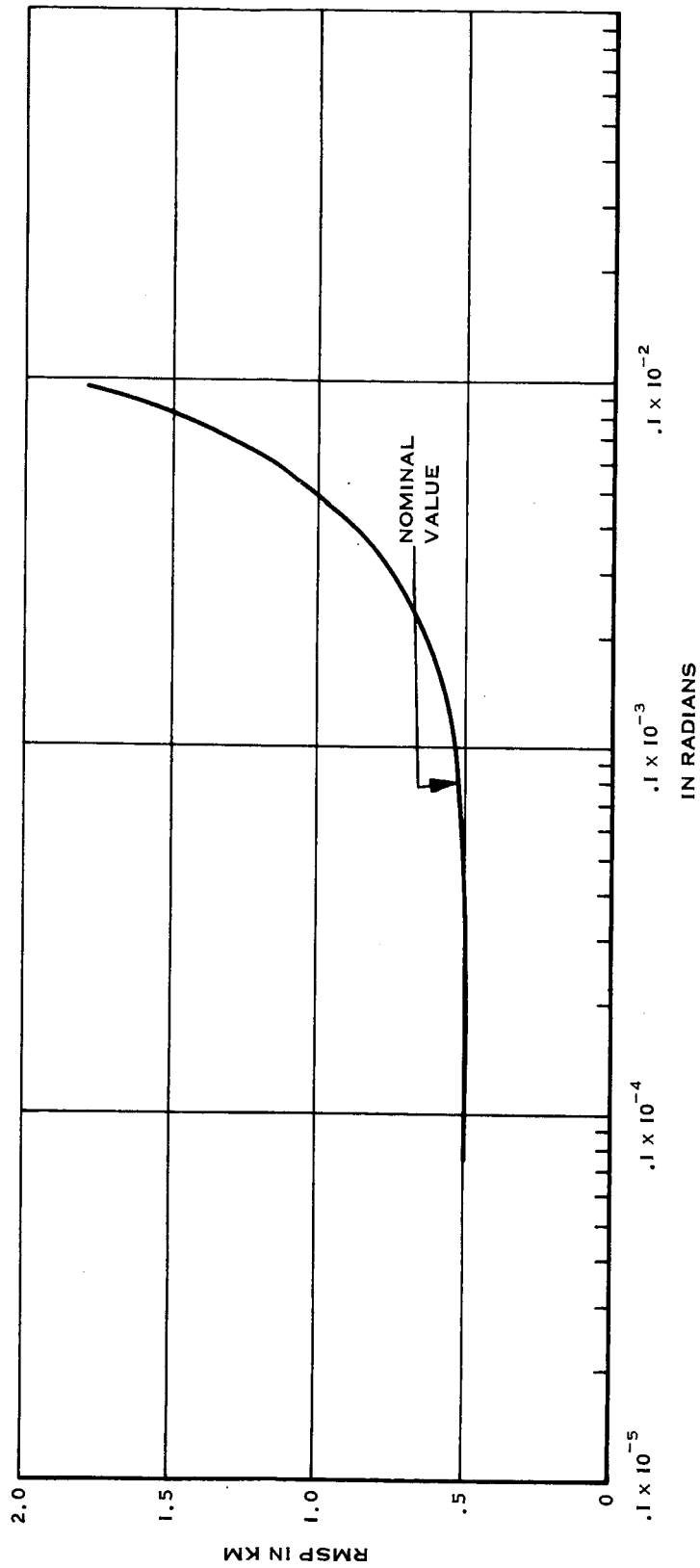


Figure 5-12 Variations in Final RMSP for Changes in Initial Standard Deviation of Z Accelerometer Into X Axis

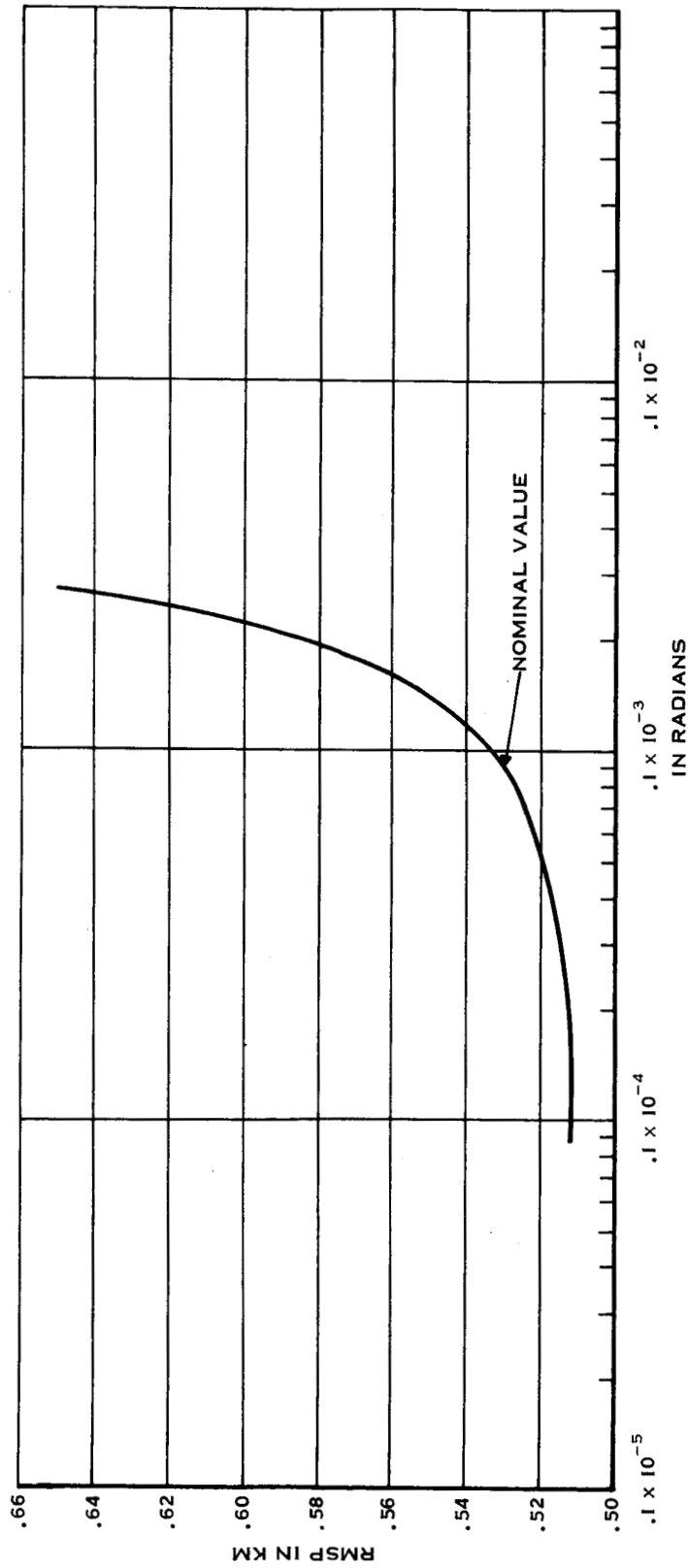


Figure 5-13 Variations in Final RMSP for Changes in Initial Standard Deviation of Initial Platform Misalignment About X Axis

5.2 THE TRACKING MODEL

The tracking model that was used for this study consisted of significant error sources from the C-band radars. Up to nine trackers were considered. Ascension Island could not observe the vehicle until near the very end of the trajectory, and therefore the two radars at this site were not considered. The error sources at each radar consisted of random and bias errors in range, azimuth and elevation. Station location errors (latitude, longitude, and altitude) were also considered.

The numerical values of the tracking errors as well as the location of the C-band radars are listed in Table 5-2. These values were obtained from Reference 5, with the exception of the station location errors and the accuracy of the NASA tracker at Bermuda.

Since the total number of bias errors from the nine trackers could be as many as 54, a study was first made to determine the importance of these errors in order to eliminate any errors that do not significantly affect the system. This was accomplished by making two runs; first, with the measurement biases neglected, and second, with the station location errors neglected from the model. In both cases the combined inertial platform-tracking system was simulated with 20 guidance errors included in the model. The effect of neglecting the station location and measurement bias is shown in Table 5-3.

The values shown represent the effect of neglecting the individual tracking errors on both the position uncertainty and the velocity uncertainty. Since the total size of the covariance matrix (P) could be up to 60 x 60, and this number must include the 20 guidance errors and the six coordinates of position and velocity, up to 34 tracking biases could be included in the model. The tracking bias errors that were omitted from the final model are indicated in Table 5-3.

TABLE 5-2 C-BAND RADAR ACCURACIES

STATION NUMBER	STATION NAME	LAT (Deg)	LON (Deg)	ALT (ft)	RANDOM ERRORS				STATION LOCATION ERRORS*			BIAS ERRORS					
					3 σ _R (ft)	3 σ _A (mr)	3 σ _E (mr)	3 σ _{LAT} (ft)	3 σ _{LON} (ft)	3 σ _{ALT} (ft)	3 σ _R (ft)	3 σ _A (mr)	3 σ _A (mr)				
	TPQ-18 RADARS																
19.18	MERRITT IS.	28.417	80.667	36.9	60	0.45	0.45	4.46	4.46	0	150	0.3	0.3				
3.18	GRAND BAHAMA	26.633	78.267	39.0	60	0.45	0.45	22.3	22.3	13.4	150	0.3	0.3				
7.18	GRAND TURK	21.467	71.133	118.9	60	0.45	0.45	325	325	107	150	0.3	0.3				
	FPQ-6 RADARS																
91.18	ANTIQUA	17.15	61.8	138.8	60	0.45	0.45	475	475	147	150	0.3	0.3				
0.18	PATRICK	28.233	80.6	48.9	60	0.45	0.45	18	18	0	150	0.3	0.3				
NASA**	BERMUDA	32.348	64.654	0.0984	60	0.45	0.45	1050	1050	151	150	0.3	0.3				
	FPS-16 RADARS																
1.16	CAPE KENNEDY	28.483	80.583	44.8	60	0.6	0.6	8.92	8.92	0	150	0.3	0.3				
3.16	GRAND BAHAMA	26.617	78.35	45.5	60	0.6	0.6	22.3	22.3	13.4	150	0.3	0.3				
NASA	BERMUDA	32.348	64.654	0.0984	60	0.6	0.6	1050	1050	151	150	0.3	0.3				

* Station Location Errors, except for Bermuda, obtained from: "The accuracy of AMR instrumentation," H. P. Mann, AD #432034, Systems Analysis RCA Service Co., Patrick Air Force Base, Florida, 13 December 1963.

** NASA Tracking Station Accuracies at Bermuda obtained from: APOLLO Navigation Working Group TR No. AN-1.1.1-NASA Goddard, Greenbelt, Md., April 4, 1966.



TABLE 5-3

STATION	ERROR	POSITION UNCERTAINTY (RMSPP) (km)	VELOCITY UNCERTAINTY (RMSVP) (km/sec)
BERMUDA 1	La	.164	.527 x 10 ⁻³
BERMUDA 2	La	.163	.524 x 10 ⁻³
ANTIGUA	La	.134	.889 x 10 ⁻³
BERMUDA 1	Lo	.548 x 10 ⁻¹	.261 x 10 ⁻²
BERMUDA 2	Lo	.546 x 10 ⁻¹	.261 x 10 ⁻²
ANTIGUA	R	.518 x 10 ⁻¹	.306 x 10 ⁻³
ANTIGUA	Lo	.461 x 10 ⁻¹	.330 x 10 ⁻³
G. TURK	Lo	.451 x 10 ⁻¹	.569 x 10 ⁻³
G. TURK	La	.288 x 10 ⁻¹	.453 x 10 ⁻³
BERMUDA 1	R	.212 x 10 ⁻¹	.146 x 10 ⁻³
BERMUDA 2	R	.212 x 10 ⁻¹	.146 x 10 ⁻³
BAHAMA 1	R	.171 x 10 ⁻¹	.282 x 10 ⁻³
BAHAMA 2	R	.171 x 10 ⁻¹	.282 x 10 ⁻³
G. TURK	R	.163 x 10 ⁻¹	.189 x 10 ⁻³
BERMUDA 2	Al	.155 x 10 ⁻¹	.795 x 10 ⁻⁴
BERMUDA 1	Al	.154 x 10 ⁻²	.793 x 10 ⁻⁴
CAPE 5	R	.993 x 10 ⁻²	.724 x 10 ⁻⁴
MERIT IS.	R	.942 x 10 ⁻²	.770 x 10 ⁻⁴
PATRICK	R	.920 x 10 ⁻²	.108 x 10 ⁻⁴
ANTIGUA	Al	.842 x 10 ⁻²	.728 x 10 ⁻⁴
G. TURK	Al	.527 x 10 ⁻²	.377 x 10 ⁻⁴
BAHAMA 1	Lo	.110 x 10 ⁻²	.259 x 10 ⁻⁴
BAHAMA 2	Lo	.109 x 10 ⁻²	.254 x 10 ⁻⁴
BAHAMA 1	La	.982 x 10 ⁻³	.229 x 10 ⁻⁴
PATRICK	Lo	.973 x 10 ⁻³	.108 x 10 ⁻⁴
BAHAMA 2	La	.961 x 10 ⁻³	.227 x 10 ⁻⁴
PATRICK	E	.925 x 10 ⁻³	.135 x 10 ⁻⁴
MERIT IS	E	.859 x 10 ⁻³	.124 x 10 ⁻⁴
BERMUDA 2	E	.828 x 10 ⁻³	.256 x 10 ⁻⁵

TABLE 5-3 (Cont)

STATION	ERROR	POSITION UNCERTAINTY (RMSPP) (km)	VELOCITY UNCERTAINTY (RMSVP) (km/sec)
MERIT IS	A	$.764 \times 10^{-3}$	$.203 \times 10^{-4}$
PATRICK	A	$.633 \times 10^{-3}$	$.195 \times 10^{-4}$
ANTIGUA	E	$.531 \times 10^{-3}$	$.272 \times 10^{-5}$
CAPE 5	E	$.516 \times 10^{-3}$	$.720 \times 10^{-4}$
G. TURK	E	$.503 \times 10^{-3}$	$.161 \times 10^{-5}$
BERMUDA 2	A	$.498 \times 10^{-3}$	$.555 \times 10^{-5*}$
CAPE 5	A	$.482 \times 10^{-3}$	$.125 \times 10^{-4*}$
CAPE 5	Lo	$.481 \times 10^{-3}$	$.373 \times 10^{-5*}$
BAHAMA 2	A l	$.477 \times 10^{-3}$	$.103 \times 10^{-4} *$
BAHAMA 2	E	$.476 \times 10^{-3}$	$.108 \times 10^{-4} *$
BERMUDA 1	E	$.466 \times 10^{-3}$	$.144 \times 10^{-5} *$
BAHAMA 1	A l	$.462 \times 10^{-3}$	$.101 \times 10^{-4} *$
BAHAMA 2	A	$.445 \times 10^{-3}$	$.117 \times 10^{-4} *$
BERMUDA 1	A	$.280 \times 10^{-3}$	$.312 \times 10^{-5} *$
BAHAMA 1	E	$.268 \times 10^{-3}$	$.611 \times 10^{-5} *$
G. TURK	A	$.265 \times 10^{-3}$	$.154 \times 10^{-5} *$
BAHAMA 1	A	$.250 \times 10^{-3}$	$.656 \times 10^{-5} *$
ANTIGUA	A	$.250 \times 10^{-3}$	$.182 \times 10^{-5} *$
MERIT IS	Lo	$.226 \times 10^{-3}$	$.191 \times 10^{-5} *$
PATRICK	La	$.218 \times 10^{-3}$	$.629 \times 10^{-5} *$
CAPE 5	La	$.320 \times 10^{-4}$	$.131 \times 10^{-5} *$
MERIT IS	La	$.274 \times 10^{-4}$	$.946 \times 10^{-6} *$

* Denotes those error sources eliminated

The tracking model therefore consists of thirty-four tracking station error sources.

Although the selection of the tracking model has been made on the basis of the position and velocity uncertainties, the effect of neglecting tracking biases on the guidance errors has also been evaluated. Table 5-4 shows these results. The initial values of the guidance error uncertainties and the final values for the nominal model are shown. Also the final values of the guidance error standard deviations are shown for the cases where (1) all the measurement biases are neglected and (2) all the station location errors are neglected. Clearly both of these classes of error sources are too important to be neglected from the model, if the guidance errors are to be estimated.

The tracking radars that have been used for this study are in general the same ones that have been used for preliminary Saturn test flights (Reference 6).

TABLE 5-4

EFFECT OF NEGLECTING TRACKING BIASES ON THE ESTIMATION
OF PLATFORM ERRORS

ERROR* SOURCE	INITIAL 3 σ VALUE	FINAL 3 σ VALUES		
		For Nominal Model	With Measurement Biases Neglected	With Station Location Biases Neglected
17	0.174×10^{-3}	0.632×10^{-4}	0.566×10^{-3}	0.309×10^{-3}
18	0.873×10^{-4}	0.394×10^{-4}	0.218×10^{-3}	0.474×10^{-3}
16	0.873×10^{-4}	0.312×10^{-4}	0.191×10^{-3}	0.474×10^{-3}
21	0.242×10^{-6}	0.127×10^{-6}	0.107×10^{-5}	0.351×10^{-5}
4	0.739×10^{-4}	0.352×10^{-4}	0.176×10^{-3}	0.208×10^{-3}
20	0.242×10^{-6}	0.156×10^{-6}	0.139×10^{-5}	0.122×10^{-5}
11	0.5×10^{-6}	0.396×10^{-6}	0.167×10^{-5}	0.240×10^{-5}
10	0.5×10^{-6}	0.333×10^{-6}	0.271×10^{-5}	0.660×10^{-5}
12	0.5×10^{-6}	0.448×10^{-6}	0.310×10^{-5}	0.653×10^{-5}
1	0.36×10^{-4}	0.203×10^{-4}	0.141×10^{-3}	0.310×10^{-3}
5	0.36×10^{-4}	0.197×10^{-4}	0.207×10^{-3}	0.355×10^{-3}
19	0.242×10^{-6}	0.229×10^{-6}	0.560×10^{-6}	0.126×10^{-5}
27	0.371×10^{-4}	0.370×10^{-4}	0.570×10^{-4}	0.429×10^{-4}
30	0.201×10^{-2}	0.201×10^{-4}	0.386×10^{-2}	0.231×10^{-2}
23	0.148×10^{-4}	0.148×10^{-4}	0.151×10^{-4}	0.154×10^{-4}
22	0.148×10^{-4}	0.148×10^{-4}		
15	0.2×10^{-7}	0.200×10^{-7}		

* These numbers refer to program number assigned to each error source in Table 5.1

SECTION 6

THE ESTIMATION OF INERTIAL PLATFORM ERRORS

The principal results of the study are presented in this section. These results show the feasibility of estimating the inertial platform errors during a powered flight ascent by combining the telemetry and tracking data.

The general method that has been used is to examine the behavior of a covariance matrix of error dispersions along the nominal trajectory. In particular, the amount by which the standard deviations of the guidance errors reduced, was used as a criterion. Although no absolute figure of merit has been defined for the amount by which these standard deviations decrease, it has been assumed that a decrease in the 3σ value of an error source by an order of magnitude, would be significant; conversely, if the standard deviation of a particular error was reduced by a small percentage, it has been assumed that this error source could not be estimated very well in an actual fitting process using real telemetry and tracking data.

In addition to the results for the nominal platform-tracking model, the results of a number of parametric variations of the error sources are presented. The objective for studying the error sources parametrically was twofold. First, it was desired to determine whether the ability to estimate each of the error sources depended on the relative accuracies of the guidance error compared to the tracking accuracies, or whether there are certain error sources that cannot be estimated regardless of the relative accuracies. The second reason for presenting parametric data was simply to show how the results changed for changes in significant parameters of the model.

6.1 ESTIMATION OF PLATFORM ERRORS WITH NOMINAL TRACKING

A simulation of the combined platform-tracking system has been made with an error model that includes (1) the first 20 guidance errors in Table 5-1. (2) the first 34 tracking has errors in Table 5-3, and (3) the uncertainties in the six components of position and velocity. Although the primary objective was to evaluate the behavior of the standard deviations of the guidance errors, the uncertainty in the vehicle position (RMSP) and velocity (RMSV) have also been included in the results.

The uncertainties in the vehicle position and velocity are about 30 meters and 0.2 meters/sec as shown in Figures 6-1 and 6-2.* A breakdown of these uncertainties into the DR, CR, and UP directions is also shown in the figures. Although the magnitude of the dispersions has been reduced considerably from the case where there was no tracking (Section 5.1), the largest uncertainty is still in the UP direction and the smallest is in the DR direction.

As a point of interest, the ability to estimate the vehicle position and velocity with the combined platform-tracking model was compared with an estimate of the vehicle state with tracking only. Figure 6-3 shows the position and velocity uncertainties with no platform errors in the model. A large initial uncertainty was assumed in order to evaluate the tracking system alone. A comparison of Figures 6-1 and 6-2 with 6-3 shows that a much better estimate of the vehicle state can be obtained with the guidance errors in the model. (60 meters in position compared to the 30 meters in Figure 6-1, and 0.06 m/sec in velocity compared to the 0.2 m/sec in Figure 6-2.)

* Figures appear at end of Section 6.

The time histories of the first 17 guidance error standard directions are shown in Figures 6-4 through 6-20. Five error sources showed no improvement along the trajectory for the nominal case. These sources are

1. Spin axis mass unbalance of the Z gyro
2. Anisoelastic drift Z gyro
3. Input axis mass unbalance of the Y gyro
4. Input axis mass unbalance of the X gyro
5. Threshold of the Z accelerometer

The last-three errors sources in this group were not plotted. The first two were plotted (Figure 6-19 through 6-20) as there was some variation for changes in the tracking. These results will be discussed in a later section.

In Figures 6-4 through 6-6, the one curve which is shown is for the nominal model. In Figures 6-7 through 6-10, the curve labeled (1) pertains to the nominal model. In Figures 6-11 through 6-20 the nominal curve has been labeled as such.

The behavior of the guidance error standard deviations for nominal tracking may be summarized with the aid of Table 6-1. The initial and final values of the standard deviations are shown as well as the percentage decrease.

In general, the greatest improvement the standard deviations occurred for those error sources which caused the largest dispersion in the trajectory as determined in Table 5-1. An additional explanation for some specific component errors may be found in terms of the acceleration levels. As shown in Figure 4-3, the acceleration in the Z direction (CR) is very small. As a result the components that cause errors in this direction have less effect and therefore their standard deviations do not improve significantly.

TABLE 6-1

PERCENTAGE DECREASE IN GUIDANCE ERROR UNCERTAINTIES
FOR NOMINAL TRACKING

ERROR SOURCE*	INITIAL 3σ VALUE	FINAL 3σ VALUE	PERCENT CHANGE
17	0.174-3	0.869-4	50
18	0.873-4	0.492-4	44
2	0.739-4	0.52-4	30
3	0.739-4	0.688-4	7
16	0.873-4	0.594-4	32
21	0.242-6	0.132-6	45
4	0.739-4	0.474-4	36
6	0.739-4	0.579-4	22
20	0.242-6	0.158-6	35
11	0.5-6	0.418-6	16
10	0.5-6	0.334-6	33
12	0.5-6	0.448-6	10
1	0.36-4	0.203-4	43
5	0.36-4	0.198-4	45
19	0.242-6	0.229-6	5
27	0.371-4	0.371-4	No Change
30	0.202-2	0.202-2	No Change
23	0.148-4	0.148-4	No Change
22	0.148-4	0.148-4	No Change
15	0.2-7	0.2-7	No Change

*The numbers in this column are program numbers. See Table 5-1 for the corresponding error source.

For example, the improvement in the knowledge of the Z accelerometer misalignments in the X (No. 3), or Y (No. 6) direction is less than that of the X accelerometer misalignment in the Y direction (No. 4), or the Y accelerometer in the X direction (No. 2). Also the improvement in the Z accelerometer bias (No. 12) was smaller than the improvement in the X or Y accelerometer biases (Numbers 10 and 11). (See Table 6-1 for these comparisons.)

The results of simulating the combined platform-tracking system indicate that it would not be possible, at least for the values of the tracking accuracies that have been assumed, to significantly improve the uncertainty of the platform error sources. Therefore if the only objective is to update the guidance system during a flight, this method would not be feasible, assuming the guidance errors were equal or less than their 3σ values. However, if the objective is a postflight analysis, or if the tracking is improved, the conclusion may be considerably different.

6.2 ESTIMATION OF GUIDANCE ERRORS WITH ADDITIONAL KNOWLEDGE OF PLATFORM

In the previous section, the results were presented for the estimation of the guidance errors with nominal tracking. In succeeding sections, the estimation of these errors for improved tracking and degraded guidance errors will be presented. However, before discussing the results for parametric variations of the platform-tracking system, an important point concerning the correlation between the initial platform errors (errors in the accelerometer misalignments and the gyro misalignments) should be noted.

Preliminary results for estimating the guidance errors with improved tracking showed that there was no little improvement in the uncertainty of the gyro misalignments or the accelerometer misalignments regardless of how good the tracking was. This indicated that there was not enough information in the combined platform-tracking system to distinguish between

platform misalignments and accelerometer misalignments. The complete covariance matrix for the nominal simulation is included in Appendix A, and can be used to explain this result. It shows that the normalized correlations between (1) the Y accelerometer misalignment to the X axis and the platform misalignment about the Z axis ($C_{2/18}$), (2) Z accelerometer misalignment to the X axis and the platform misalignment about the Y axis ($C_{3/17}$), and (3) the Z accelerometer misalignment about the Y axis and the platform misalignment about the X axis, ($C_{6/16}$), are almost unity. As a result a large uncertainty in these three accelerometer misalignments prevents an improvement in the knowledge of the initial platform misalignments.

In order to see the effect of additional knowledge of the platform on the estimation of the initial gyro misalignments, an additional simulation was made assuming no errors in (1) the Z accelerometer misalignment about the Y axis, (2) the Z accelerometer misalignment about the X axis and (3) the misalignment of the Y accelerometer about the X axis. For the nominal tracking with these three errors omitted the uncertainties in the three initial gyro misalignments and the misalignment of the X accelerometer about the Y axis reduces as shown in Figure 6-7 through 6-10, curve (2).

There is additional justification for omitting these three platform error sources. As stated in Reference 1 the misalignments of the Z accelerometers would be eliminated before the flight by aligning the X-Y plane. In addition some calibration on either the X accelerometer or Y accelerometer would be necessary in order to be able to predict excessive variations in the initial gyro drift about the Z axis. This was evident from runs that were made with all five accelerometer misalignments. The result was that for very large values of the initial variances of the gyro misalignments, or very good tracking, no significant improvement was found in the uncertainty of the gyro misalignments at the end of the trajectory.

For the parametric results that are presented in the following sections, the following accelerometer errors were omitted from the model:

1. Z accelerometer misalignment in the direction of the X axis
2. Z accelerometer misalignment in the direction of the Y axis
3. Y accelerometer misalignment in the direction of the X axis.

6.3 ESTIMATION OF GUIDANCE ERRORS WITH IMPROVED TRACKING

Due to the fact that the ability to estimate the guidance errors with nominal tracking has been found to be somewhat marginal, a number of studies were made to investigate the system parametrically. The first parametric study involved the tracking accuracies. Runs were made with all the tracking error standard deviations (random and bias measurement errors, and station location errors) reduced by factors of 10, 100, 1000, and finally, with random errors reduced by a factor of 1000 and no bias errors. These results are shown in Figures 6-7 through 6-20. The purpose of this study was to determine if with good tracking, the knowledge of the guidance errors would improve. As discussed in the previous section, even with perfect tracking, it is not possible to estimate the errors in the initial gyro misalignments or the accelerometer misalignments any better than for the nominal tracking run. This is because of the high correlation between uncertainties in these platform error sources. As a result the improved tracking runs assumed a perfect knowledge of three accelerometer errors. As shown by Figures 6-7 through 6-20 all of the guidance error uncertainties in these figures can be improved significantly with better tracking. Again, in general, the amount by which the guidance errors improve depends on their relative effect on the trajectory. Of the total 17 guidance error sources, the three errors which have the least effect on the trajectory were not plotted. These errors are

- (1) The input mass unbalance of the Y gyro
- (2) The input mass unbalance of the X gyro
- (3) The Z accelerometer threshold error

The uncertainty in these error sources does not improve significantly even with good tracking.

From the results presented in this section it may be concluded that, in general, the feasibility of estimating the guidance errors does depend on the relative accuracies of the guidance errors and the tracking errors.

Approximately one order of magnitude improvement in the tracking accuracies would be required to obtain a significant improvement in the guidance error uncertainties during an actual flight. In addition this improvement would be contingent on a preflight calibration of three of the accelerometer misalignments.

6.4 ESTIMATION OF GUIDANCE ERRORS WITH PERFECT KNOWLEDGE OF THE TRAJECTORY END POINT

One method that was considered for improving the estimate of the guidance errors was to track the vehicle in a parking orbit. That is, the telemetry data and the tracking data would be combined in the same manner, only for a parking orbit rather than a powered flight ascent. The end result of this simulation would be an improvement in the knowledge of the end point of the powered flight trajectory.

Before simulating the system for a parking orbit, a check was made to determine the effect of perfect knowledge of the trajectory end point.

This would show the maximum decrease in the uncertainty of the guidance errors and would represent the results for perfect tracking. Six equivalent observations were made of the position and velocity states with zero error variance. The results are summarized in Table 6-2. As shown in the table there is very little improvement in the uncertainty of the guidance errors by a perfect knowledge of the trajectory end point. This indicates that there is even less knowledge that would be added to the guidance error uncertainties as a result of tracking the vehicle in a parking orbit. The parking orbit simulation was therefore not implemented.

6.5 ESTIMATION OF GUIDANCE ERROR WITH LARGE INITIAL UNCERTAINTIES

In addition to using the combined platform-tracking system to improve the knowledge of the vehicle state, or to update the guidance system during a flight, a third and perhaps more useful application would be in a post-flight analysis. For this latter objective it would be desirable to determine whether the guidance components performed normally, or whether there was a malfunction.

To evaluate the feasibility of estimating the guidance errors in a post-flight analysis, the combined platform-tracking system has been simulated for parametric variations in the guidance errors themselves. Large initial values of the guidance error standard deviations have been assumed to simulate a malfunction or a component error that was larger than predicted by the 3σ nominal value.

The time histories of the guidance error standard deviations are shown in Figures 6-21 through 6-32 for initial standard deviations of 10, and 100 times that of the nominal values. These results do not include curves for the three accelerometer errors Z to X, Z to Y, and Y to X. It was found that with these error sources in the model, the standard deviations of the gyro misalignments did not decrease, even for large initial values of guidance errors. However, with the assumption of a perfect knowledge of these errors, it is possible to reduce the uncertainty in the gyro misalignments.

TABLE 6-2

THE EFFECT OF A PERFECT KNOWLEDGE OF THE TRAJECTORY
END-POINT ON THE GUIDANCE ERROR UNCERTAINTIES

ITEM	NOMINAL @ t=9.5 MIN.	PERFECT OBSERVATION OF POSITION VELOCITY STATE @ t=9.5 MIN.
RMS P	0.938×10^{-2}	0.754×10^{-6}
RMS V	0.695×10^{-4}	0.697×10^{-8}
GUID. ERR. #17	0.874×10^{-4}	0.847×10^{-4}
18	0.489×10^{-4}	0.473×10^{-4}
16	0.599×10^{-4}	0.586×10^{-4}
21	0.100×10^{-6}	0.599×10^{-7}
4	0.478×10^{-4}	0.464×10^{-4}
20	0.146×10^{-6}	0.127×10^{-6}
11	0.423×10^{-6}	0.418×10^{-6}
10	0.350×10^{-6}	0.319×10^{-6}
12	0.457×10^{-6}	0.435×10^{-6}
1	0.211×10^{-4}	0.206×10^{-4}
5	0.221×10^{-4}	0.182×10^{-4}
19	0.228×10^{-6}	0.208×10^{-6}

The behavior of the 5 least important guidance errors, from Table 5-1, was not plotted. The uncertainty in these errors remain essentially constant at their initial values.

Of the twelve error sources which are plotted in Figures 6-21 through 6-32, it may be seen that the uncertainties in all these error sources decrease significantly for large initial values. It may therefore be concluded that it would be feasible to estimate these errors in a post-flight analysis.

That is, a malfunction in one of the guidance components that caused large deviation in the trajectory, could be identified by combining the telemetry and tracking data.

6.6 ESTIMATION OF GUIDANCE ERRORS WITH INCREASED OBSERVATION RATE

For the nominal tracking model an observation rate of one per second was used. One additional run was made to determine the effect of a reduced observation rate on the guidance error uncertainties. Table 6-3 shows a comparison of the guidance error uncertainties for 1 observation per second and 10 observations per second at 7 minutes along the trajectory. A decrease in the observation rate by an order of magnitude is seen to reduce the guidance error uncertainties by at most a factor of 2. The RMSP and RMSV are also shown in the table for the two observation rates.

TABLE 6-3

VARIATION OF GUIDANCE ERRORS, POSITION AND VELOCITY
WITH OBSERVATION RATE

	STATES AT 7 MIN.	
	NOMINAL CASE OBS ~ 1 SEC	OBS ~ 0.1 SEC
RMSP	0.193×10^{-1}	0.808×10^{-2}
RMSV	0.160×10^{-3}	0.775×10^{-4}
GUID. ER. #17	0.653×10^{-4}	0.439×10^{-4}
18	0.415×10^{-4}	0.287×10^{-4}
16	0.336×10^{-4}	0.245×10^{-4}
21	0.179×10^{-6}	0.130×10^{-6}
4	0.401×10^{-4}	0.250×10^{-4}
20	0.200×10^{-6}	0.156×10^{-6}
11	0.410×10^{-6}	0.337×10^{-6}
10	0.340×10^{-6}	0.233×10^{-6}
12	0.460×10^{-6}	0.366×10^{-6}
1	0.254×10^{-4}	0.189×10^{-4}
5	0.232×10^{-4}	0.175×10^{-4}
19	0.239×10^{-6}	0.237×10^{-6}
27	0.370×10^{-4}	0.371×10^{-4}
30	0.201×10^{-2}	0.202×10^{-2}
23	0.148×10^{-4}	0.148×10^{-4}
22	0.148×10^{-4}	0.148×10^{-4}
15	0.200×10^{-7}	0.200×10^{-4}

6.7 ESTIMATION OF GUIDANCE ERRORS WITH DIFFERENT KINDS OF TRACKING

In order to determine which type of tracking is the most effective for reducing the guidance error uncertainties, two runs were made; one with range observations only, and a second run with azimuth and elevation measurements only.

Position uncertainty (RMSP) and velocity uncertainty (RMSV) for these two cases are shown in Figures 6-33 and 6-34, respectively. The uncertainty in the guidance errors at the end of each of these runs is shown in Table 6-4.

The results of this study show very little difference between the effectiveness of range measurements and azimuth and elevation measurements.

TABLE 6-4

VARIATION OF GUIDANCE ERRORS FOR DIFFERENT TRACKING
@ t=9.5 MIN.

	RANGE ONLY	AZ&EL ONLY
RMS P	0.944×10^{-1}	0.853×10^{-1}
RMS V	0.485×10^{-3}	0.421×10^{-3}
GUID. ERR. #17	0.751×10^{-4}	0.705×10^{-4}
18	0.417×10^{-4}	0.480×10^{-4}
16	0.369×10^{-4}	0.414×10^{-4}
21	0.195×10^{-6}	0.178×10^{-6}
4	0.370×10^{-4}	0.486×10^{-4}
20	0.170×10^{-6}	0.210×10^{-6}
11	0.409×10^{-6}	0.432×10^{-6}
10	0.357×10^{-6}	0.459×10^{-6}
12	0.467×10^{-6}	0.475×10^{-6}
1	0.222×10^{-4}	0.336×10^{-4}
5	0.207×10^{-4}	0.300×10^{-4}
19	0.231×10^{-6}	0.239×10^{-6}
27	0.370×10^{-4}	0.371×10^{-4}
30	0.201×10^{-2}	0.201×10^{-2}
23	0.148×10^{-4}	0.148×10^{-4}
22	0.148×10^{-4}	0.148×10^{-4}
15	0.200×10^{-7}	0.200×10^{-7}

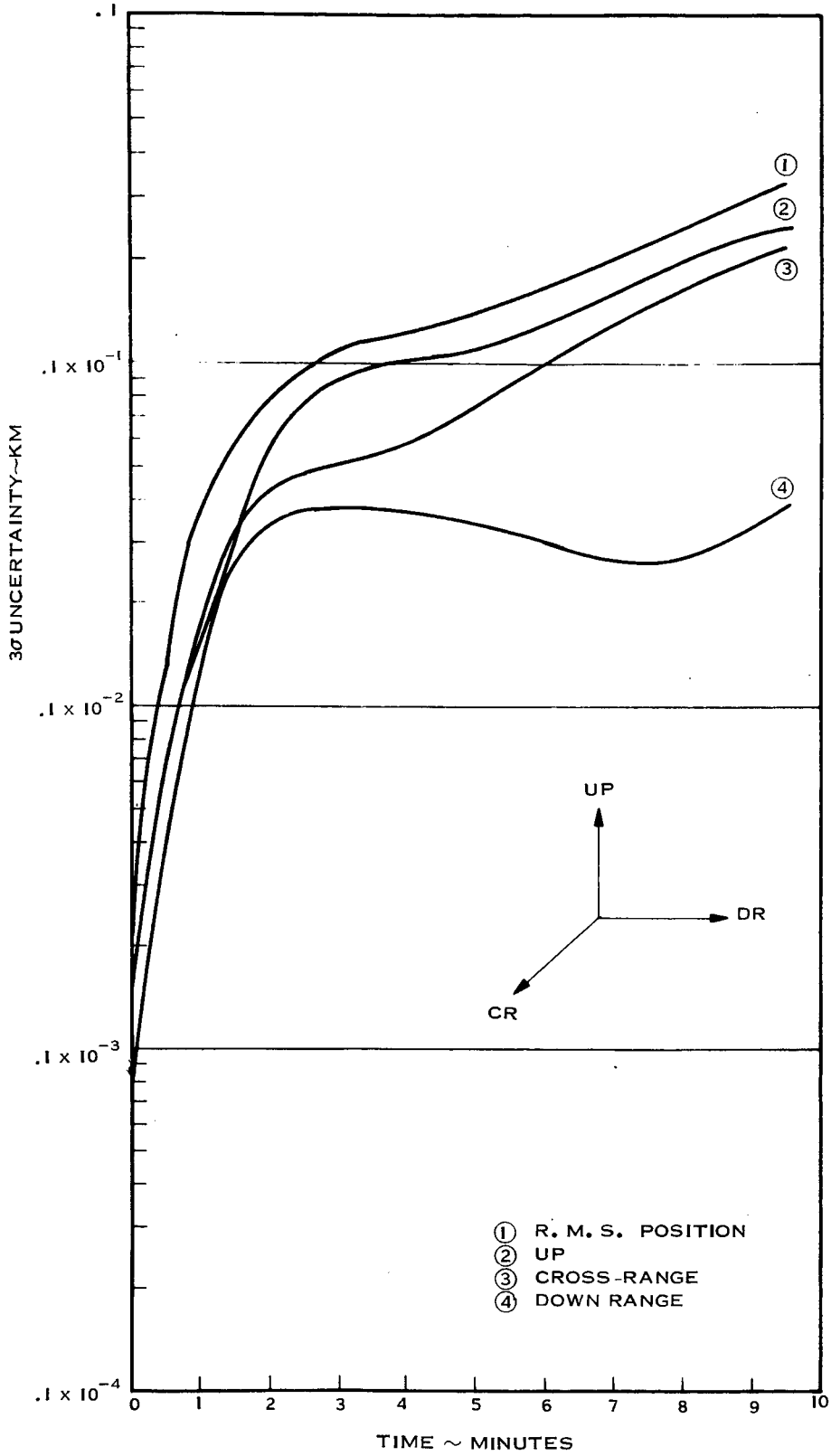


Figure 6-1 Variation in Position Uncertainties ~ Nominal Case

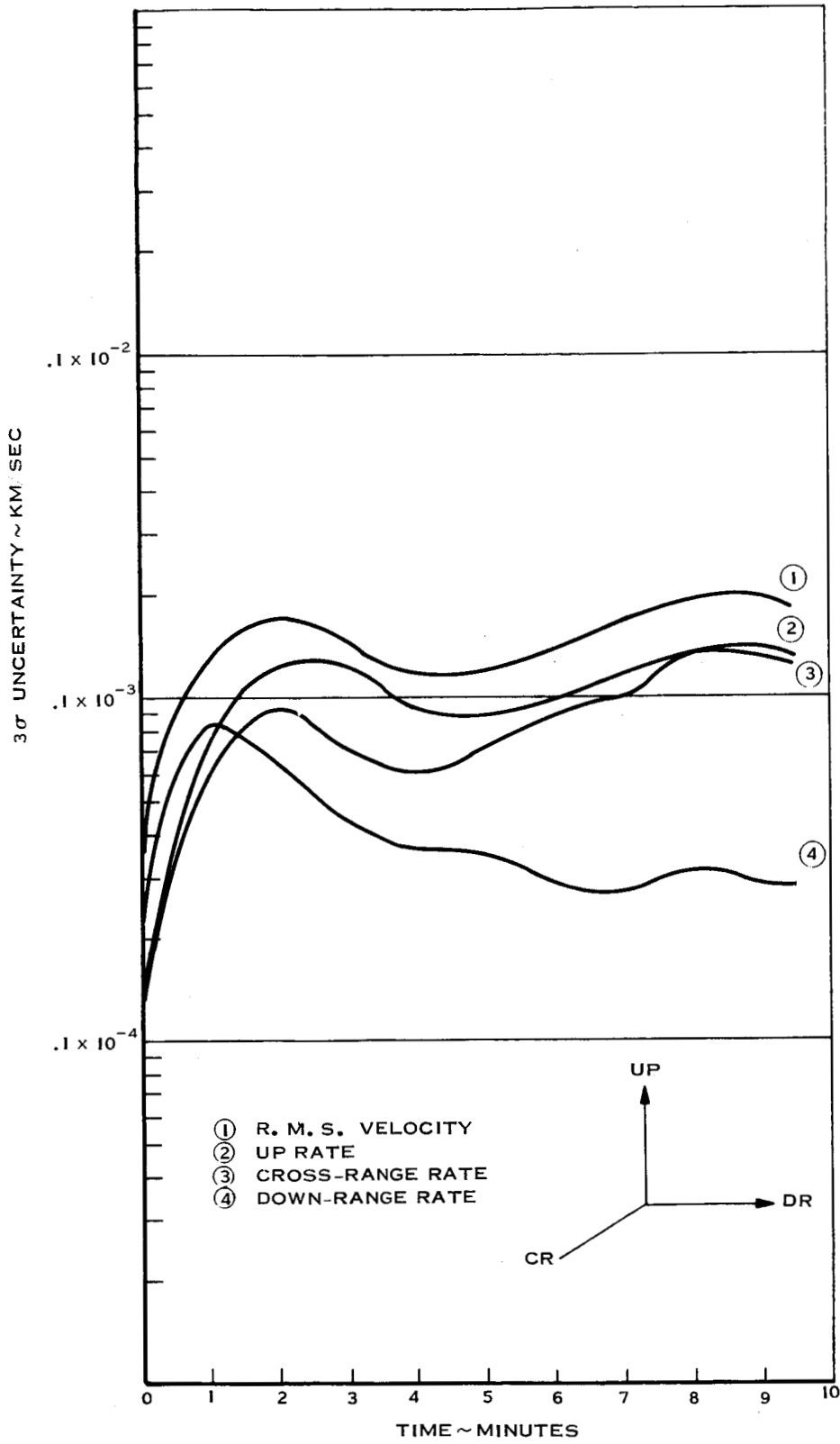


Figure 6-2 Variation in Velocity Uncertainties ~ Nominal Case

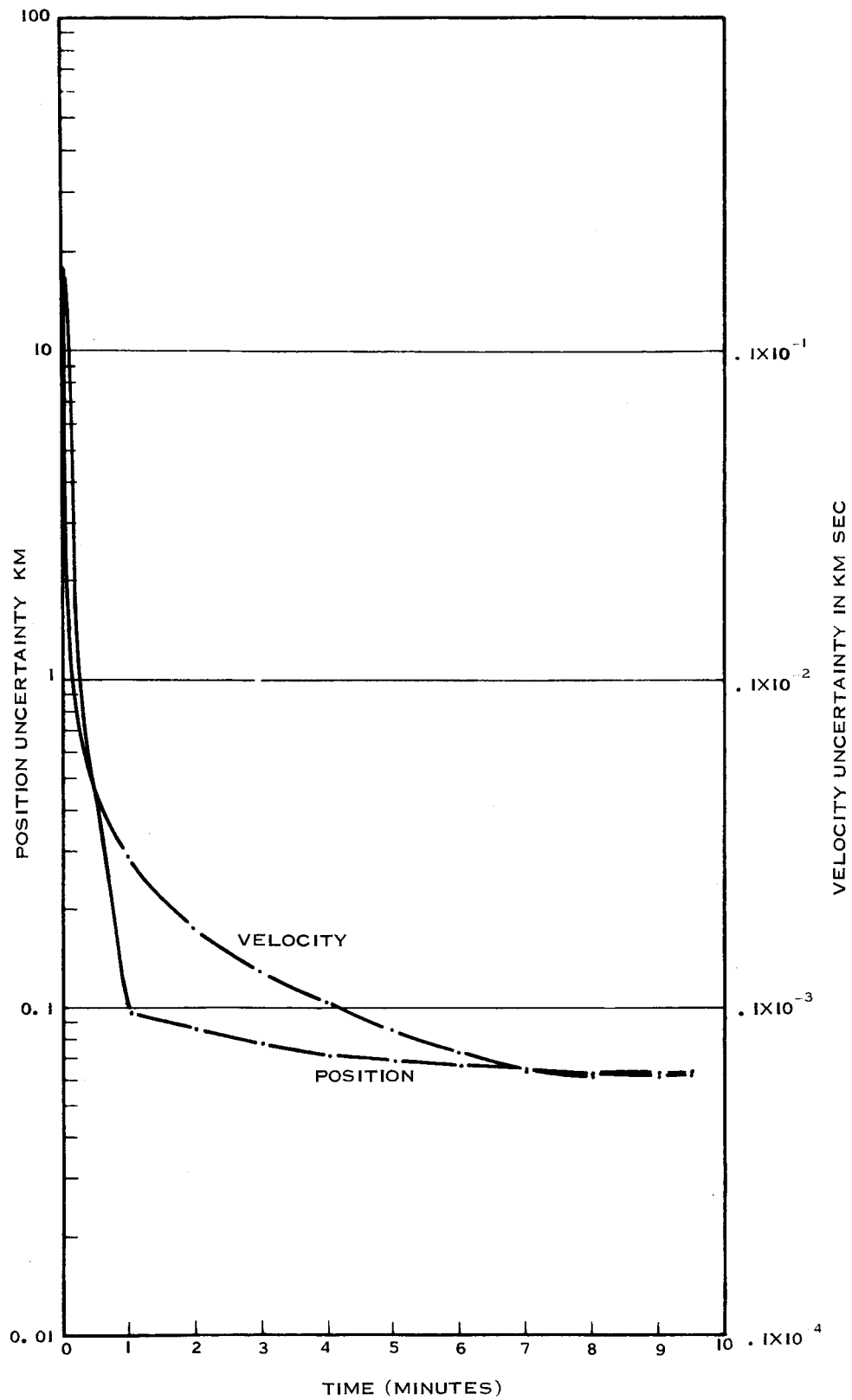


Figure 6-3 Position and Velocity Uncertainties with Tracking Only (No Telemetry Data)

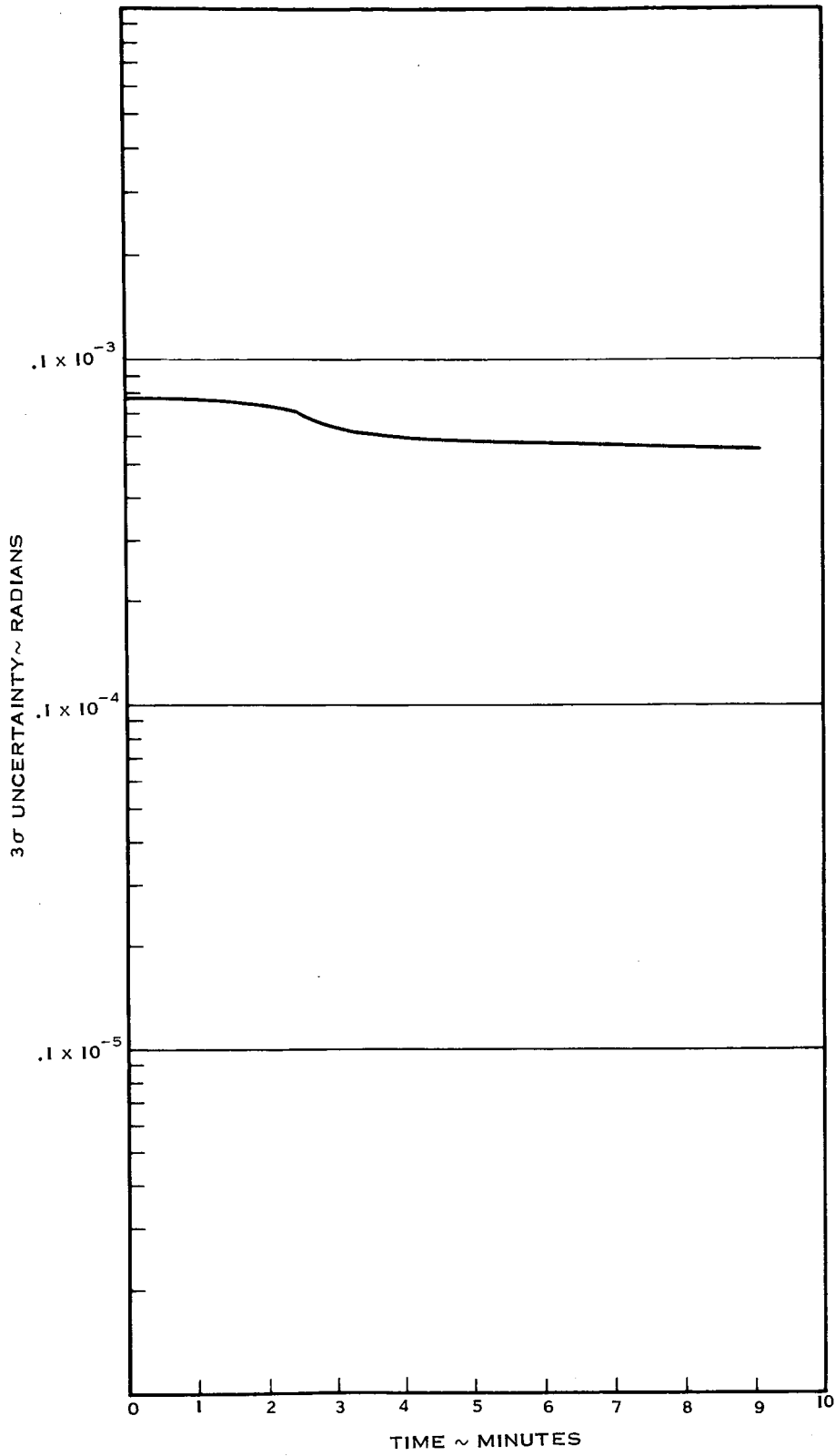


Figure 6-4 3σ Uncertainty in Y-Accelerometer Misalignment into X-Axis

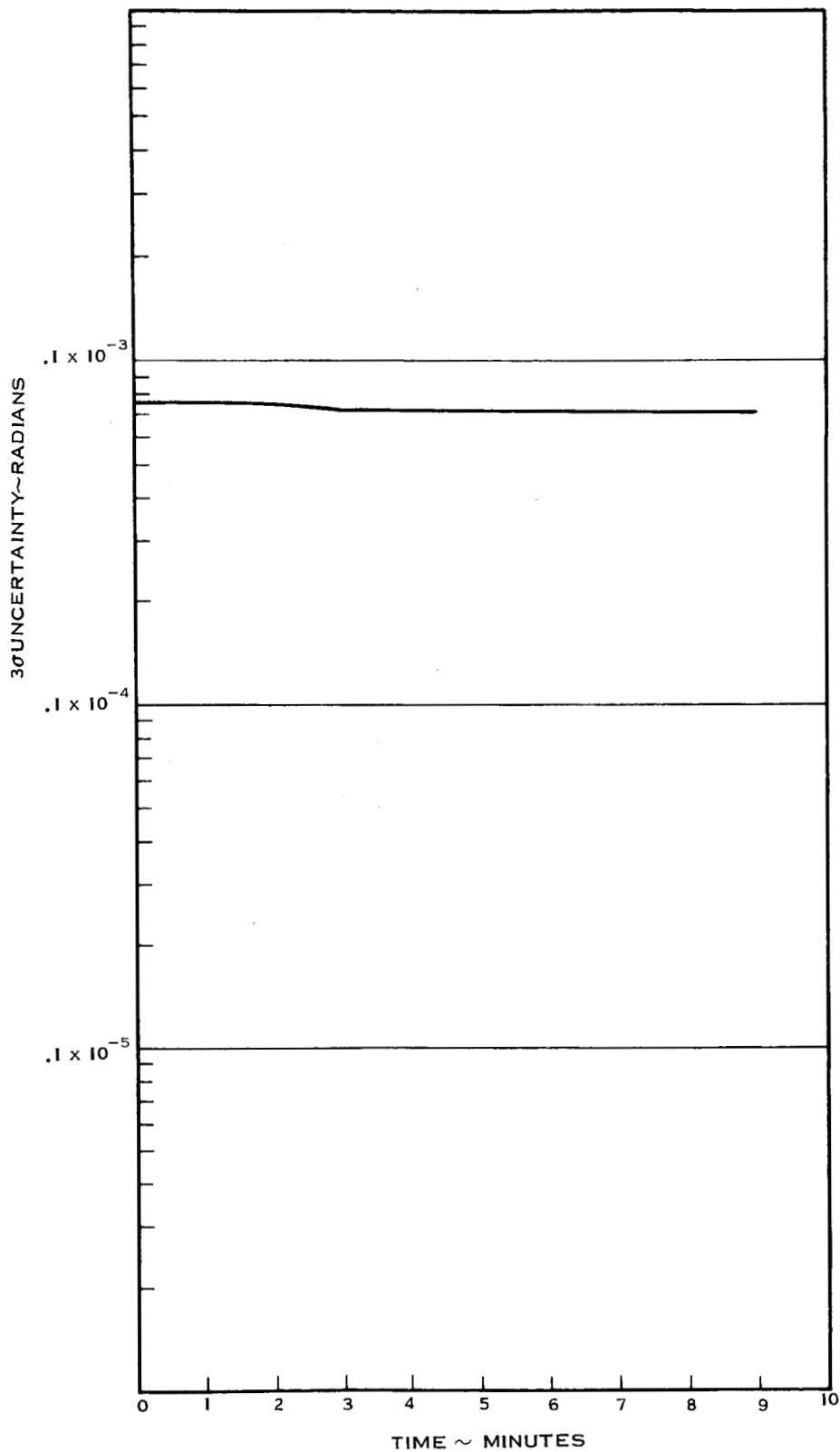


Figure 6-5 3 σ Uncertainty In Z-Accelerometer Misalignment Into X-Axis

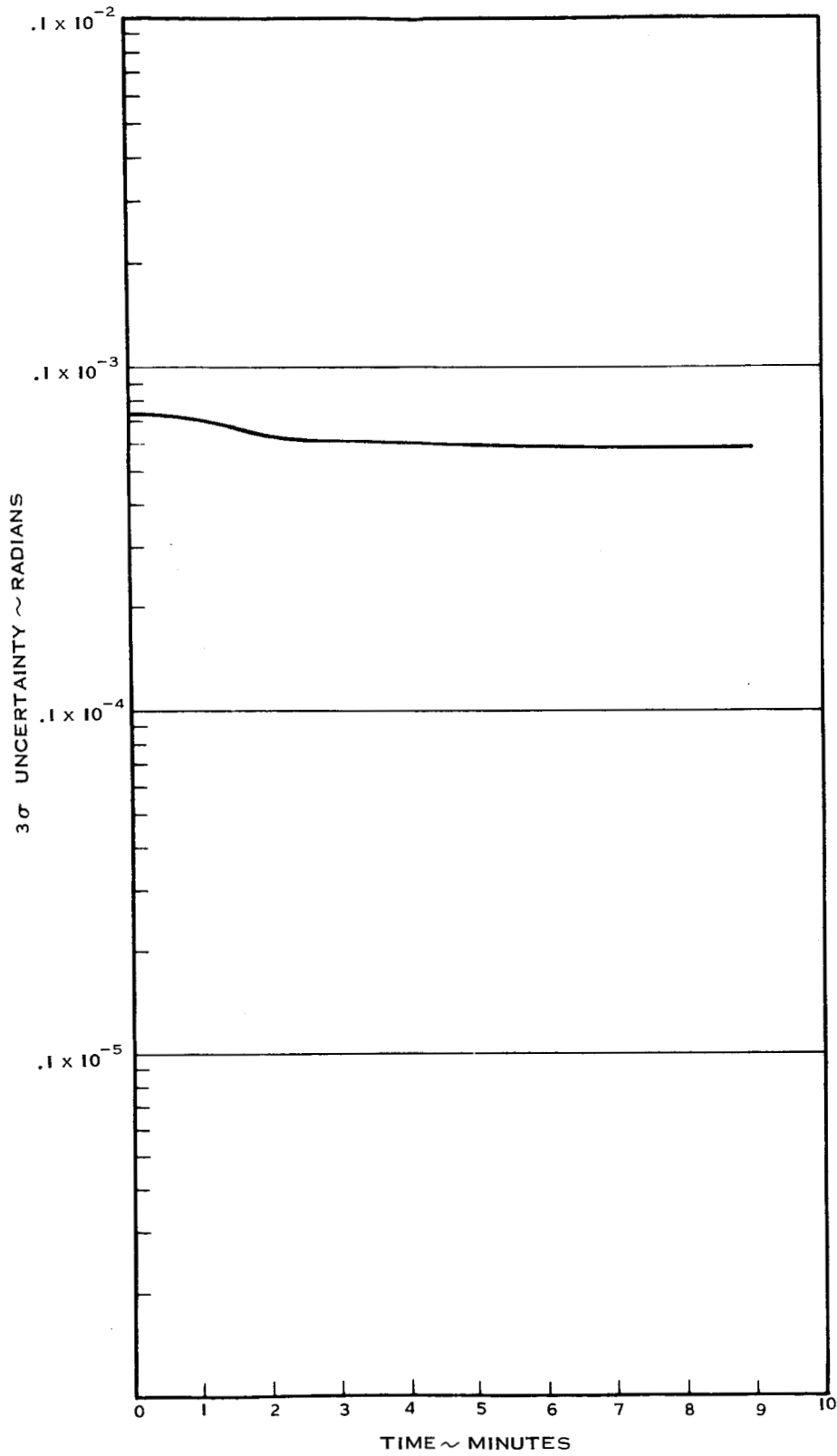


Figure 6-6 3σ Uncertainty in Z-Accelerometer Misalignment Into Y-Axis

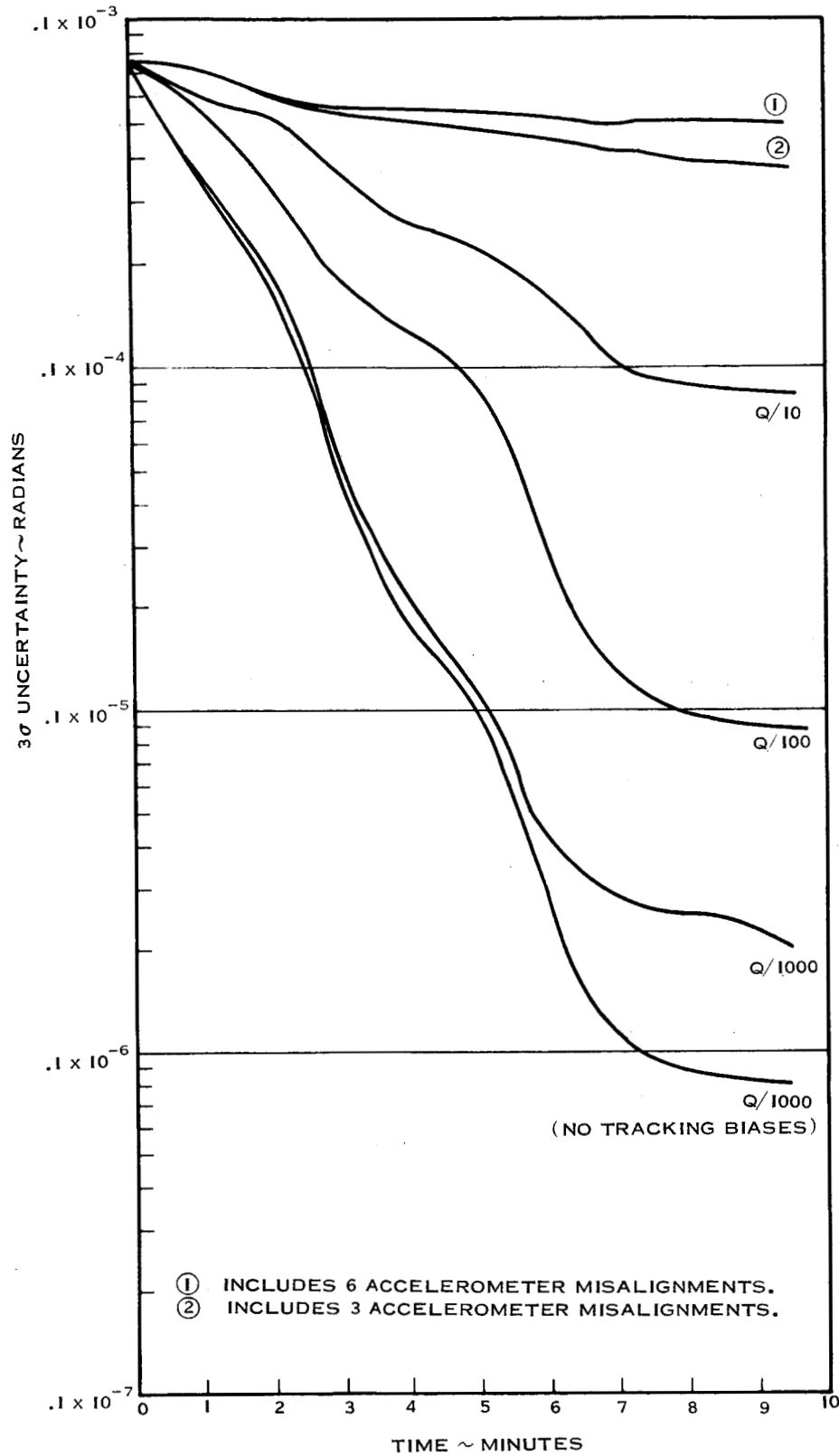


Figure 6-7 3σ Uncertainty in X-Accelerometer Misalignment Into Y-Axis

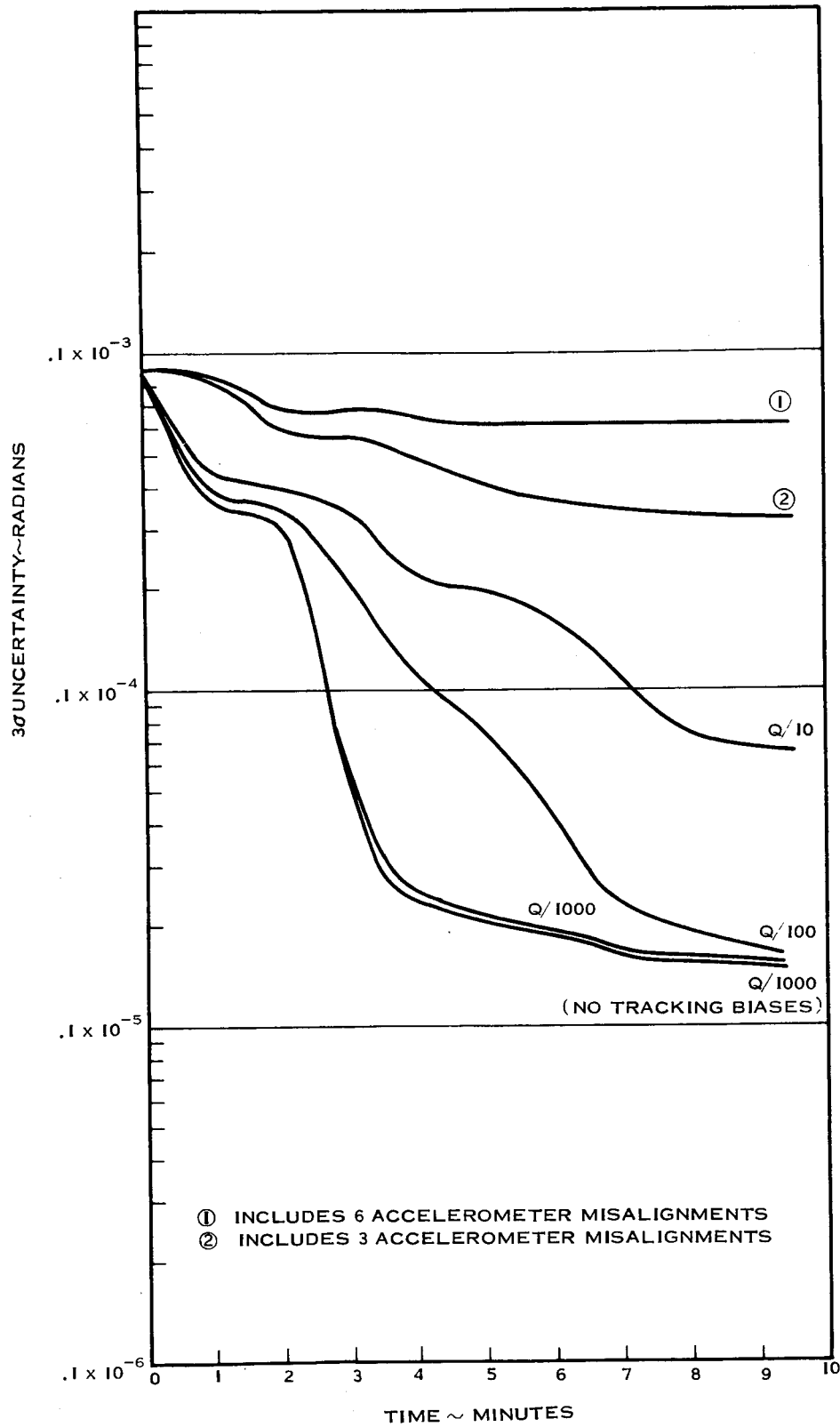


Figure 6-8 3σ Uncertainty in Initial Platform Misalignment About X-Axis

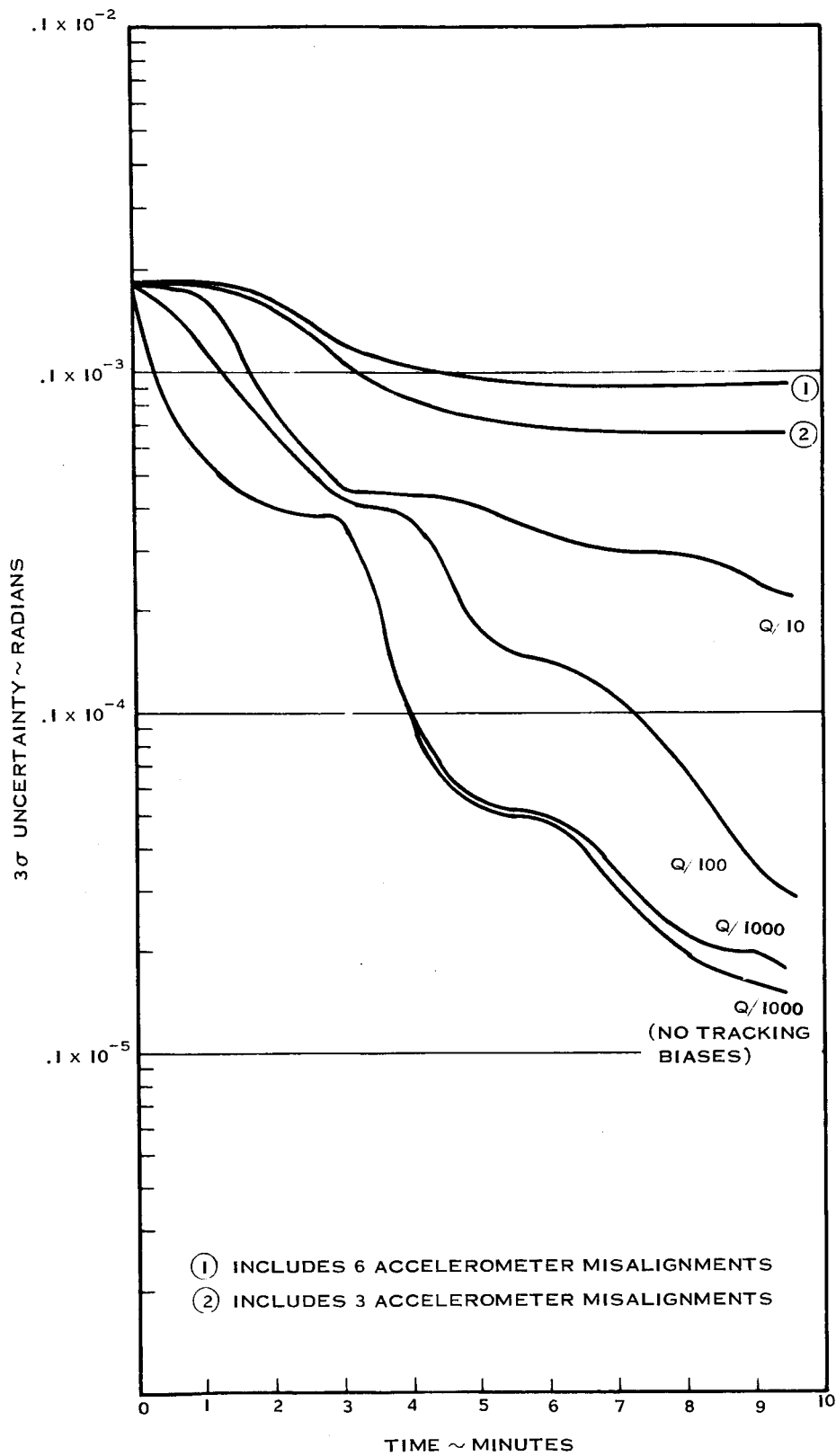


Figure 6-9 3σ Uncertainty in Initial Platform Misalignment About Y-Axis

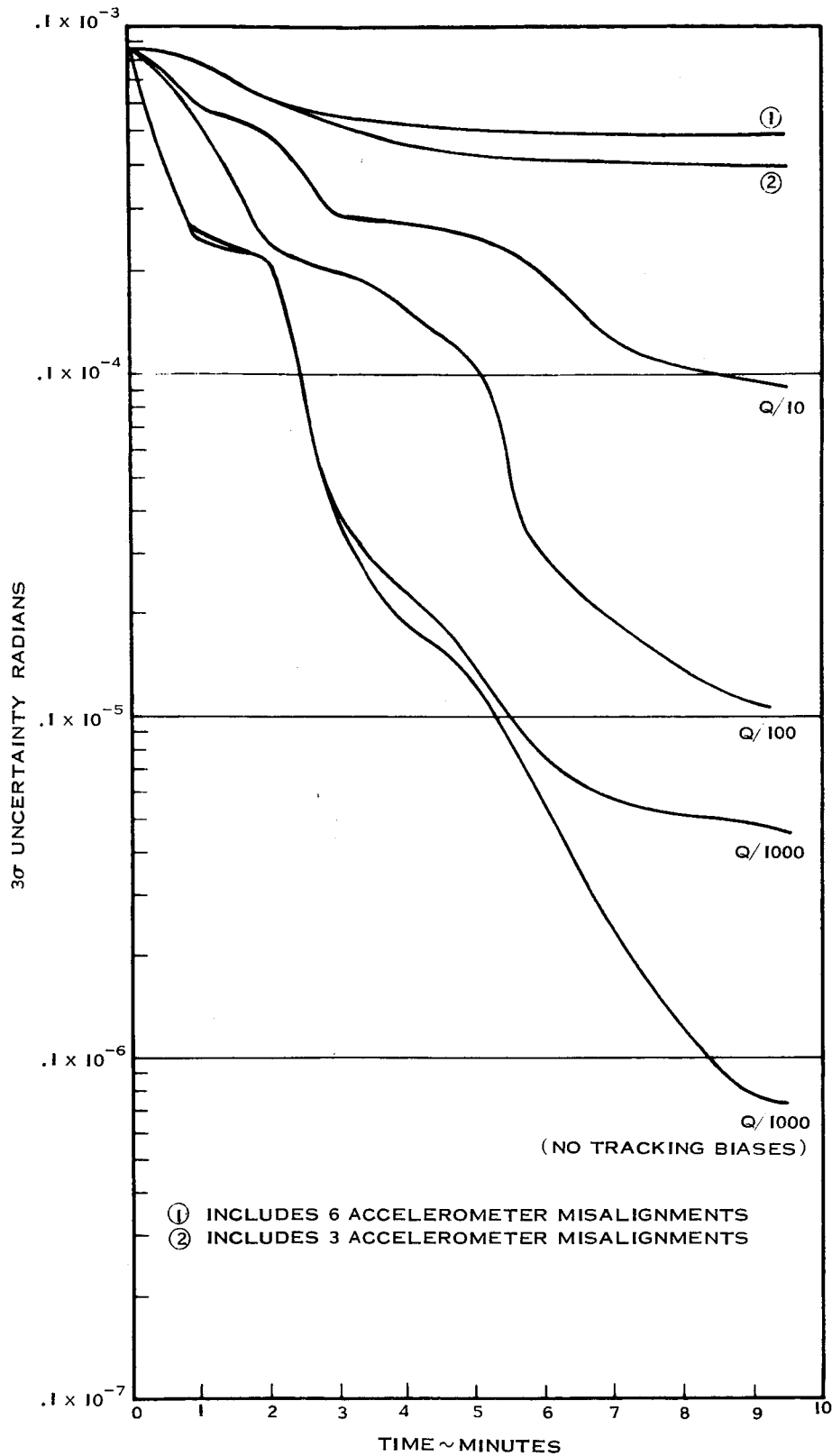


Figure 6-10 3σ Uncertainty in Initial Platform Misalignment About Z-Axis

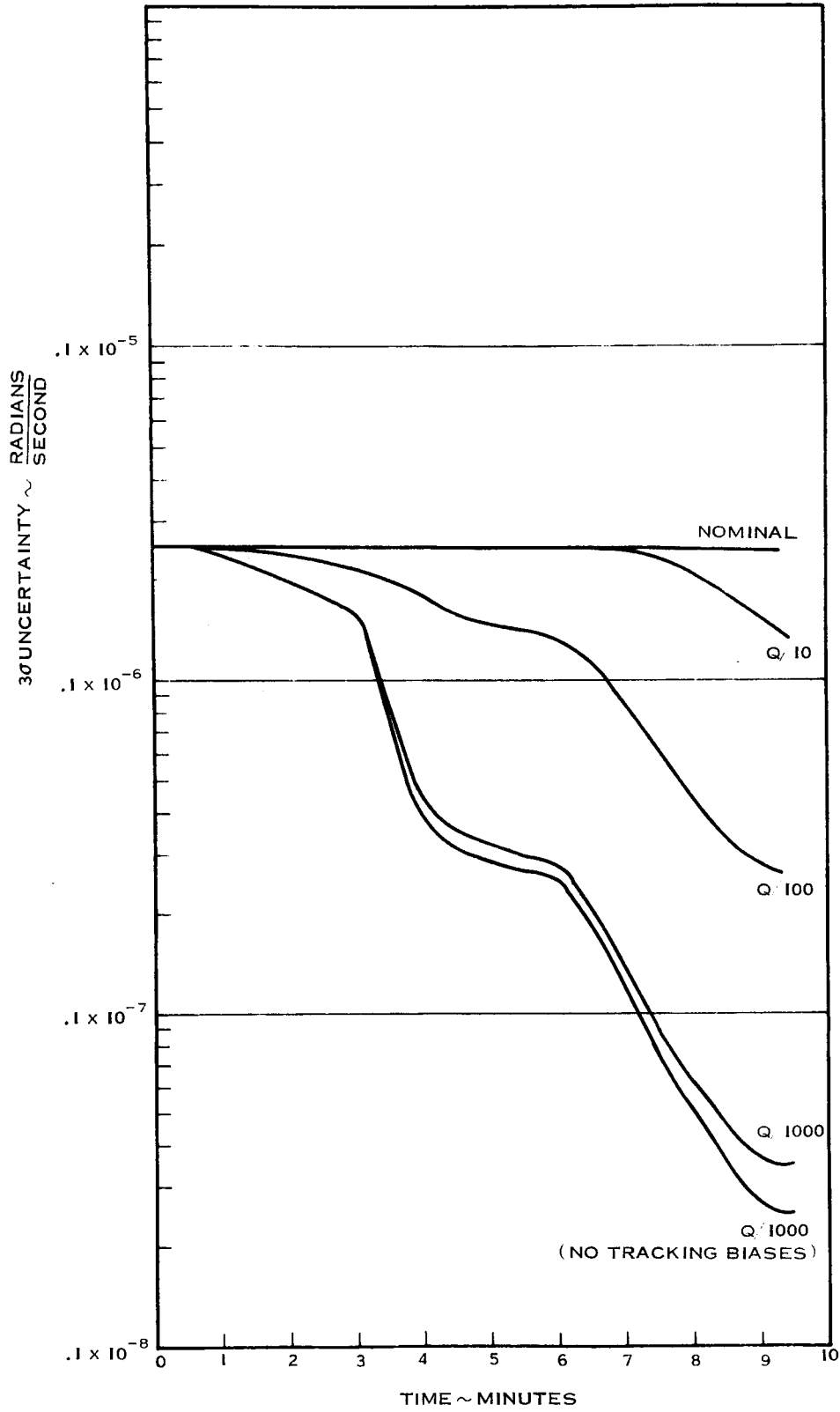


Figure 6-11 3σ Uncertainty in X-Axis Gyro Drift Rate

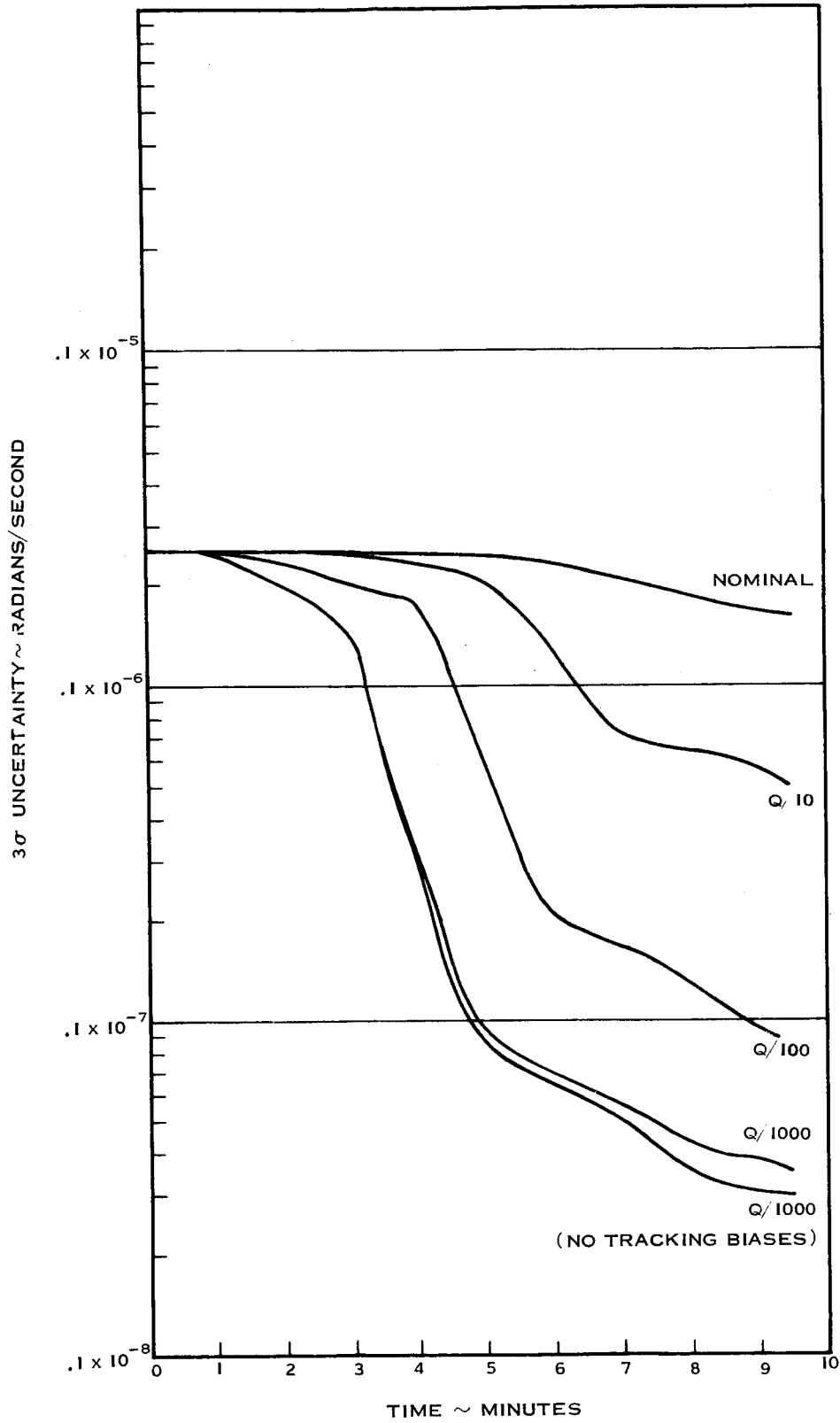


Figure 6-12 3σ Uncertainty in Y-Axis Gyro Drift Rate

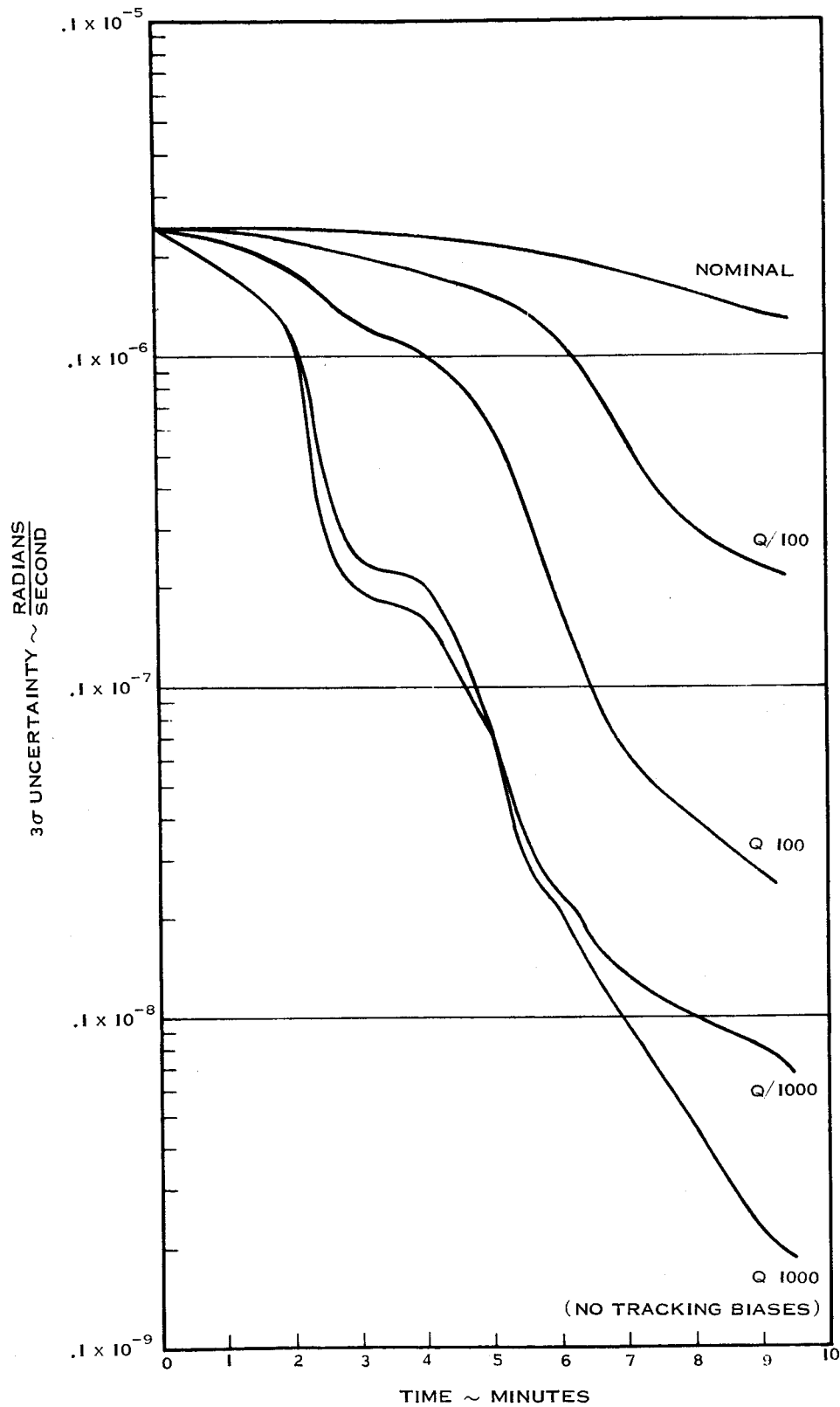


Figure 6-13 3σ Uncertainty in Z-Axis Gyro Drift Rate

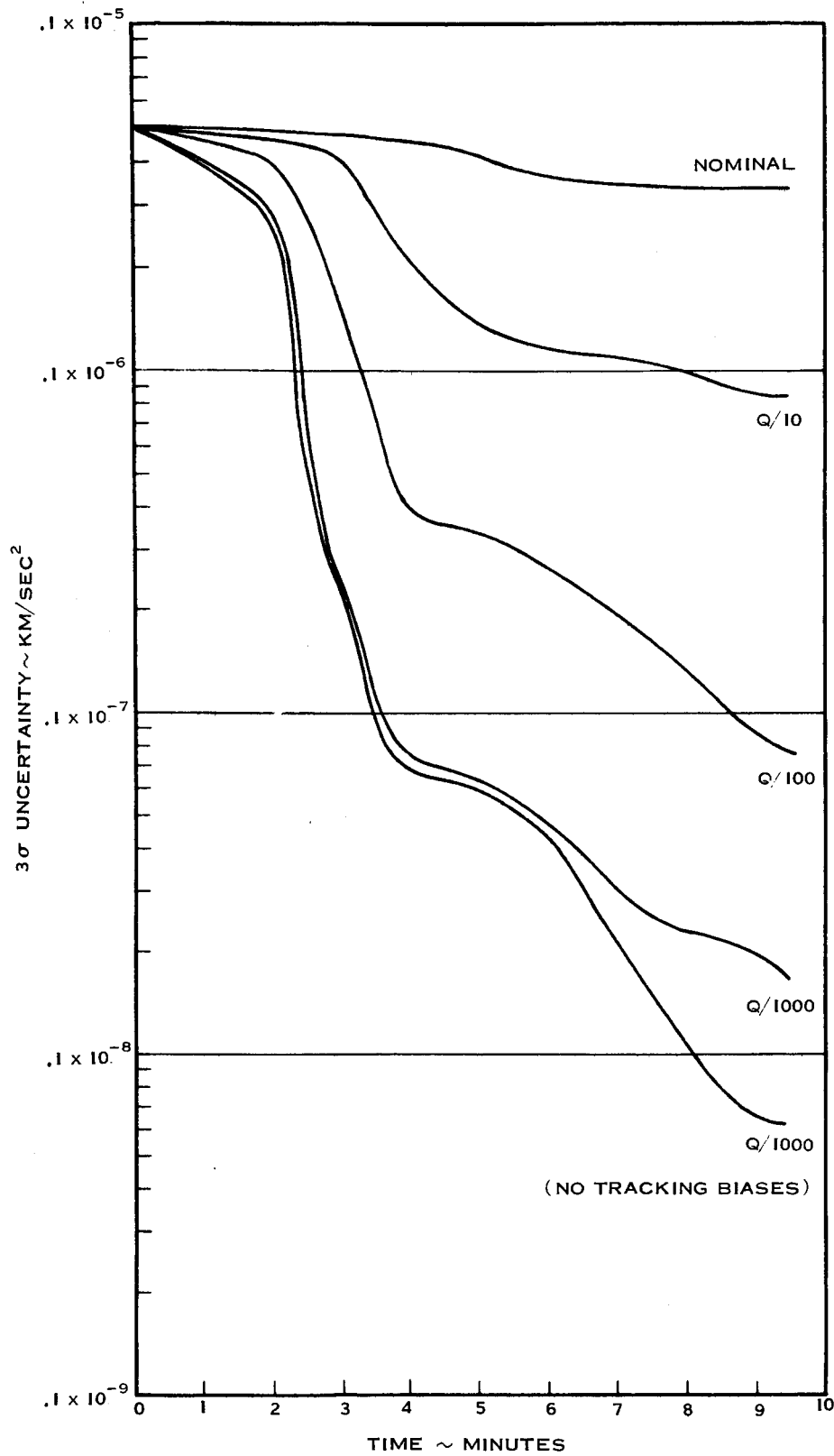


Figure 6-14 3 σ Uncertainty in X-Accelerometer Bias

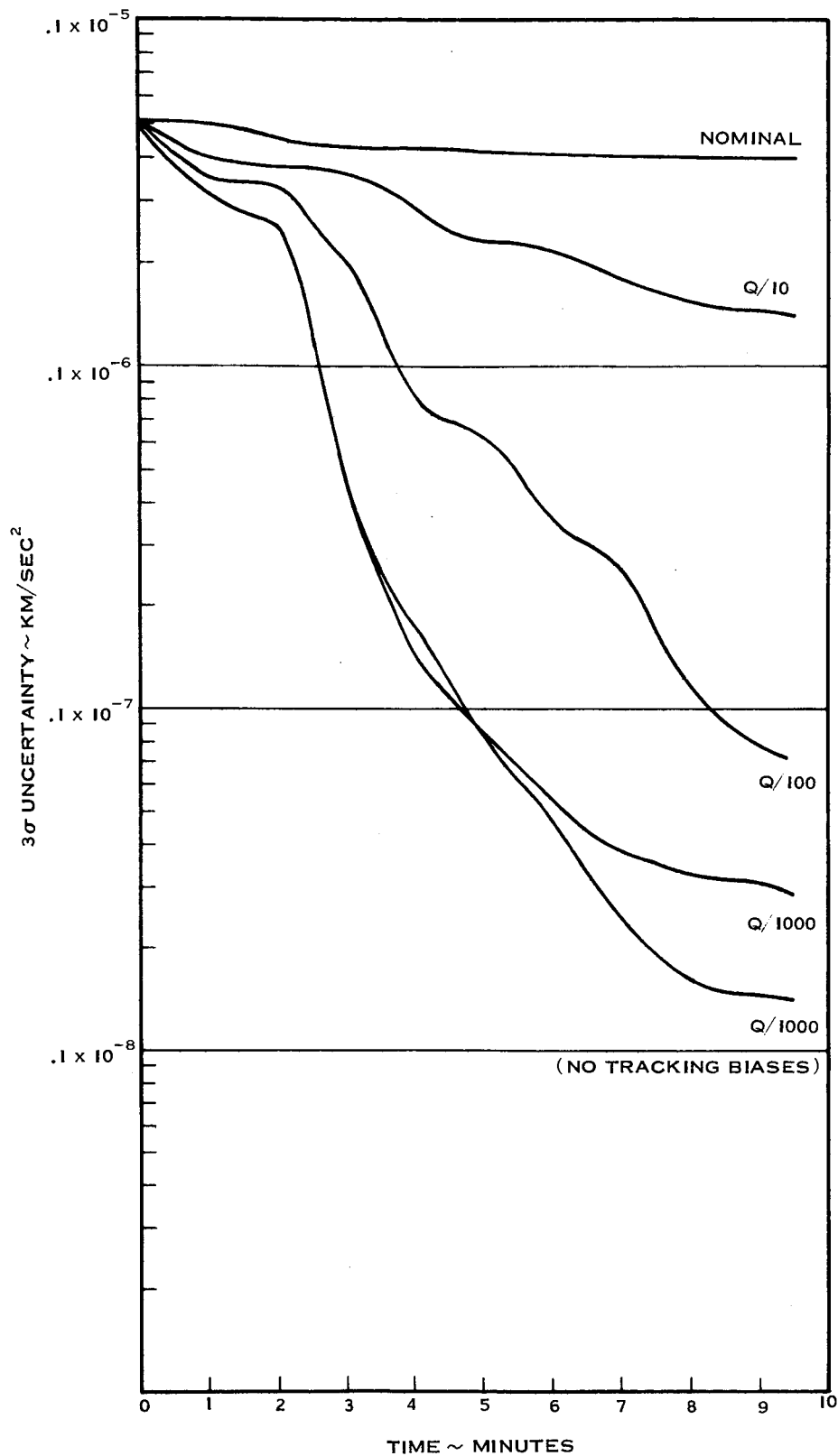


Figure 6-15 3σ Uncertainty in Y Accelerometer Bias

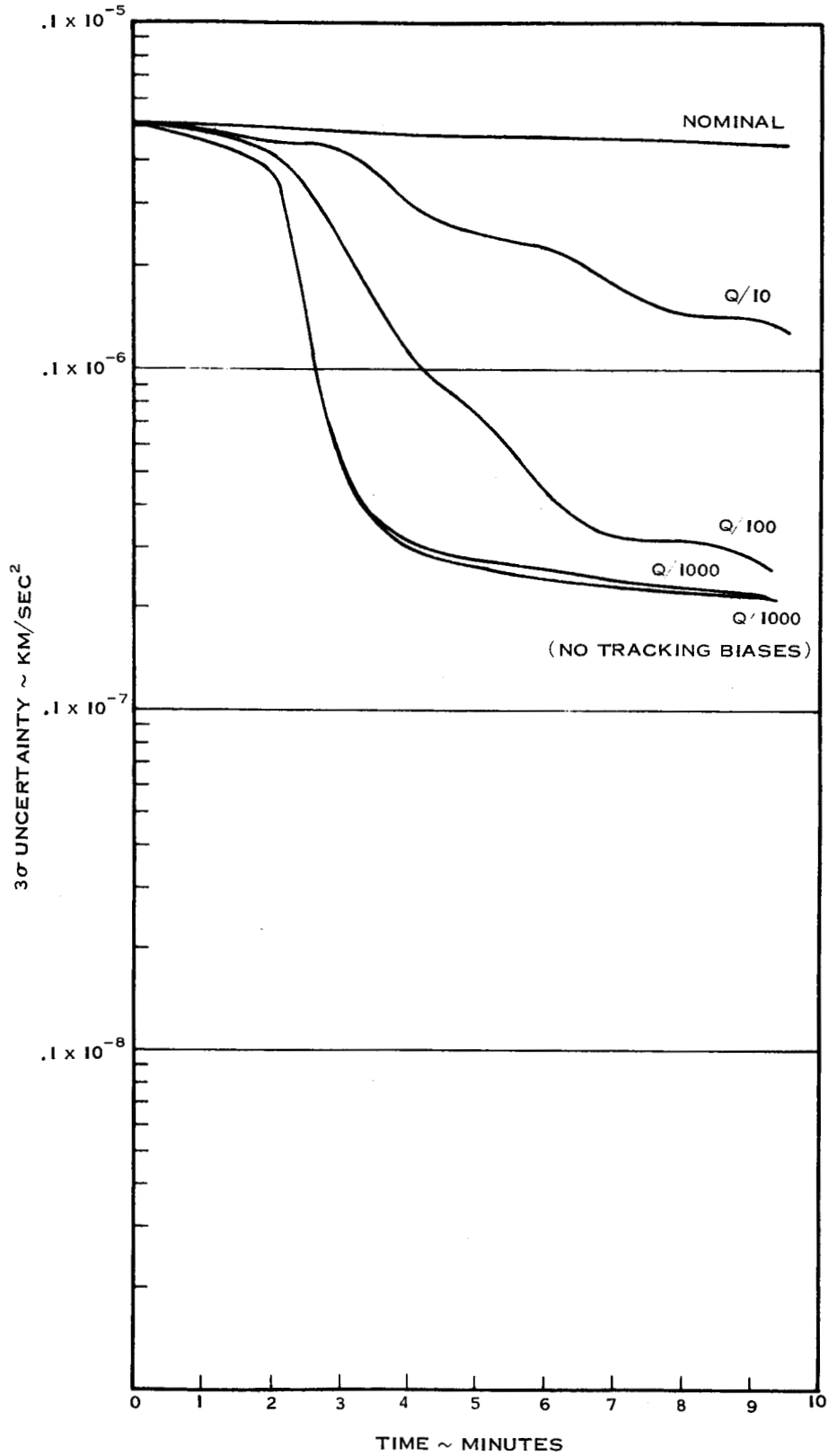


Figure 6-16 3σ Uncertainty in Z-Accelerometer Bias

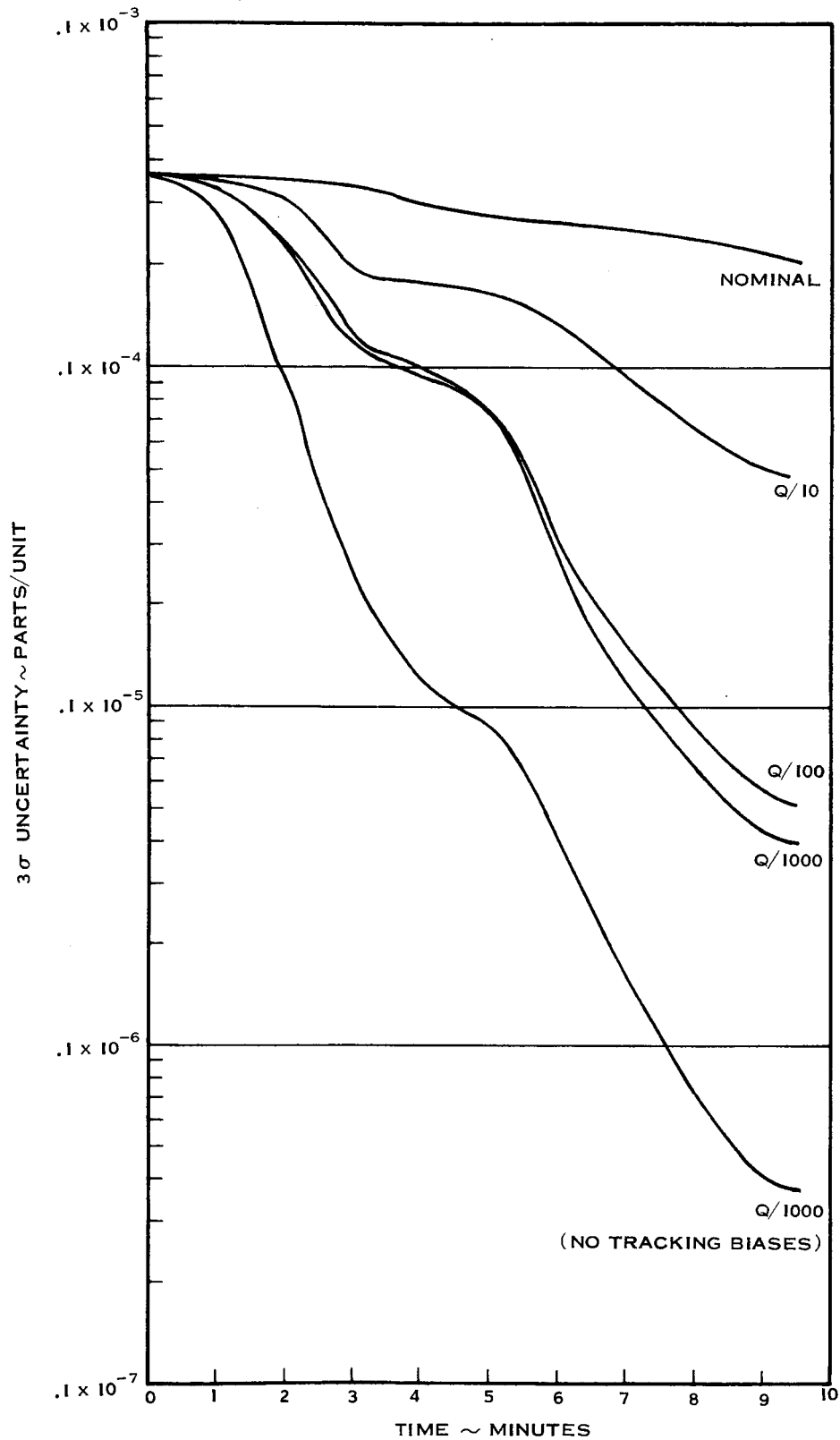


Figure 6-17 3σ Uncertainty in X-Accelerometer Scale Factor

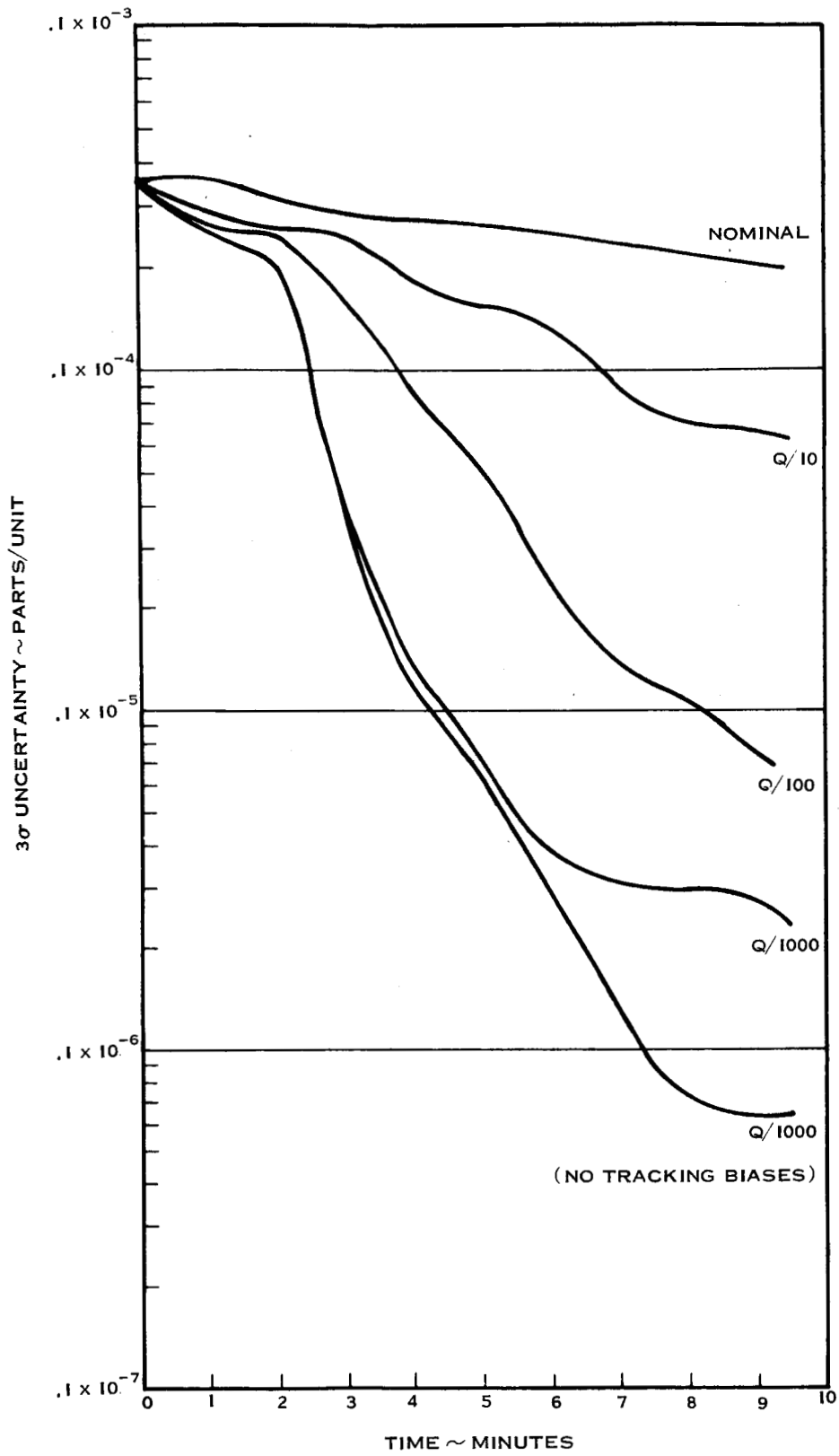


Figure 6-18 3σ Uncertainty in Y-Accelerometer Scale Factor

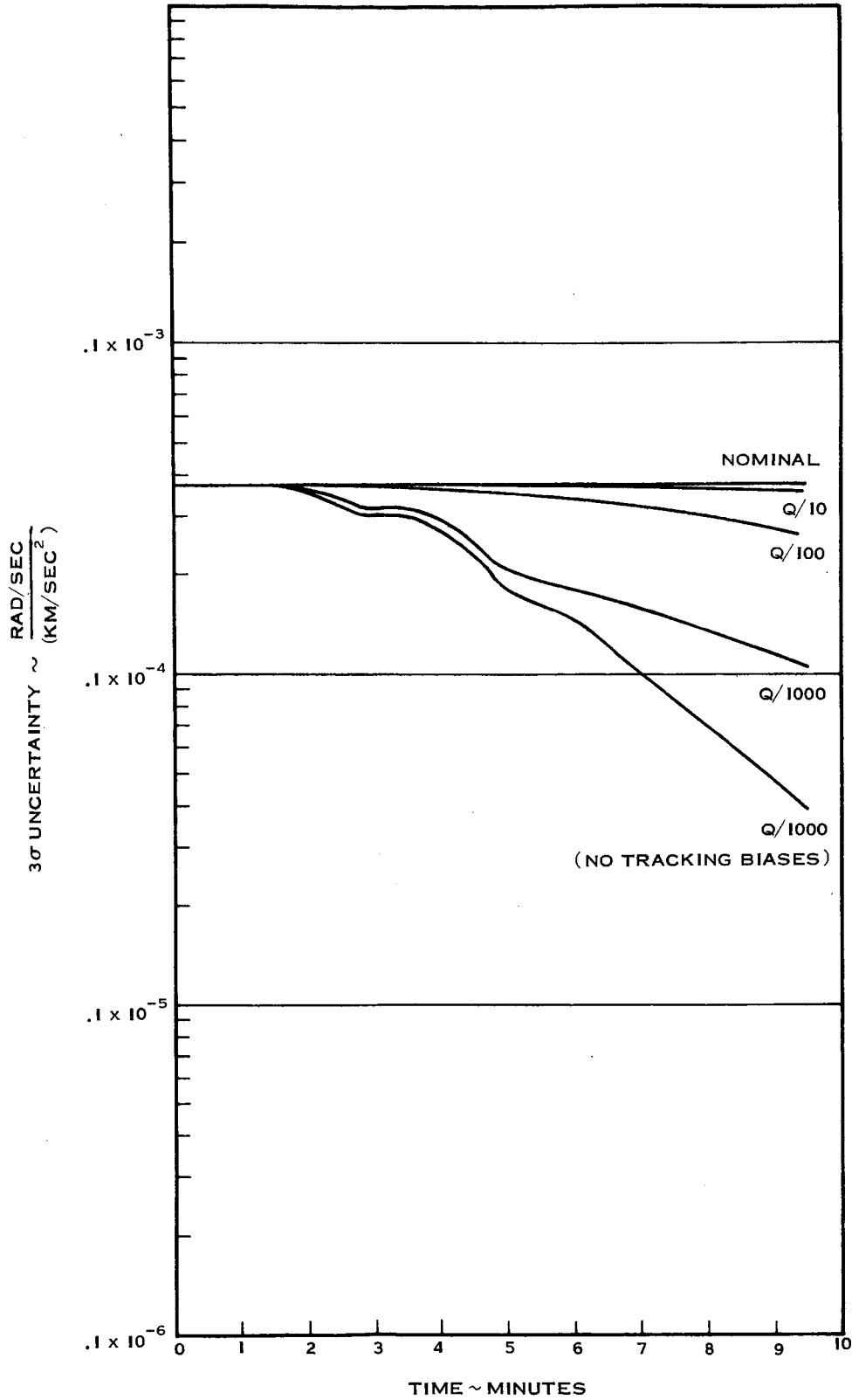


Figure 6-19 3σ Uncertainty in Z-Gyro Spin Axis Mass Unbalance

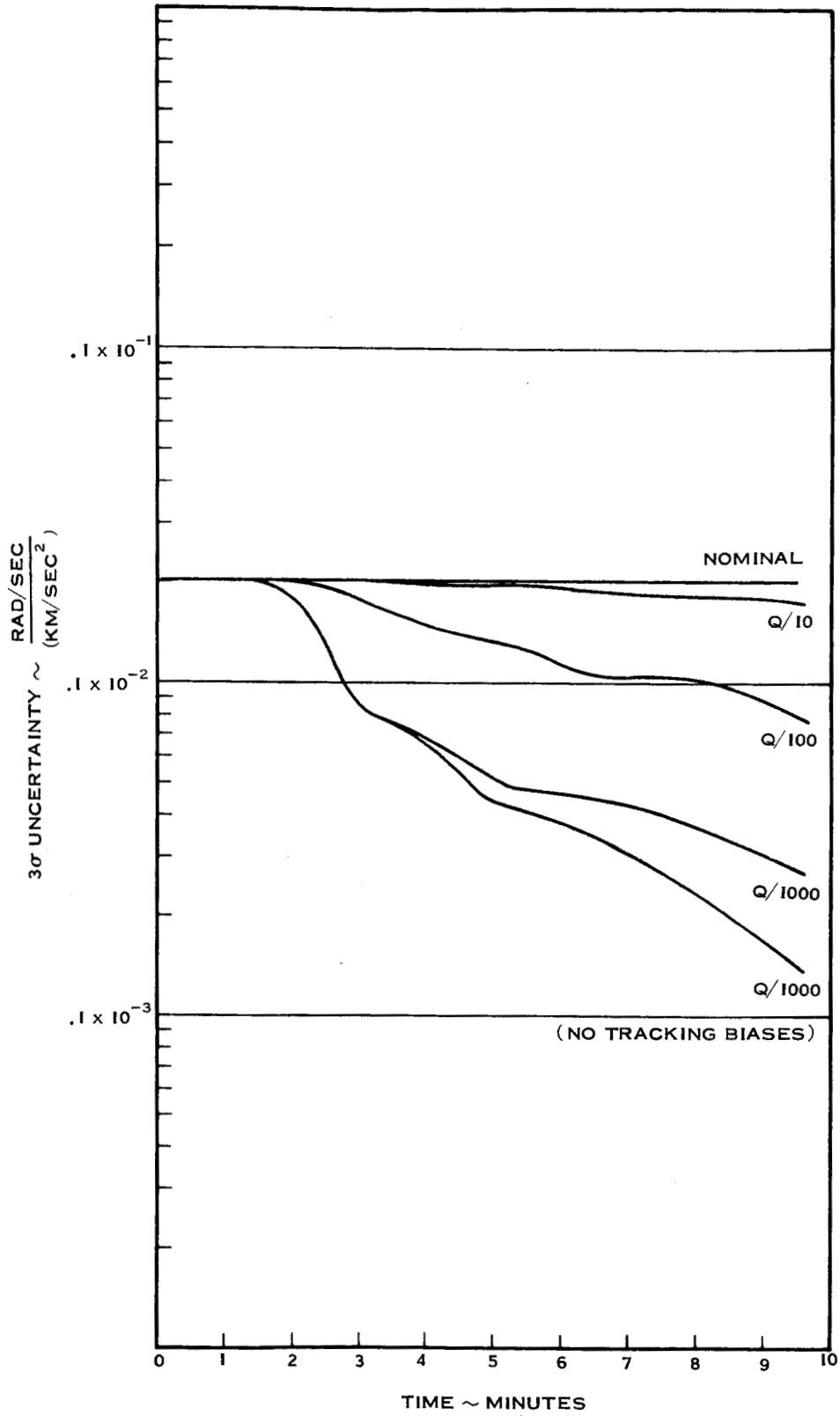


Figure 6-20 3σ Uncertainty in Z-Gyro Anisoelastic Drift

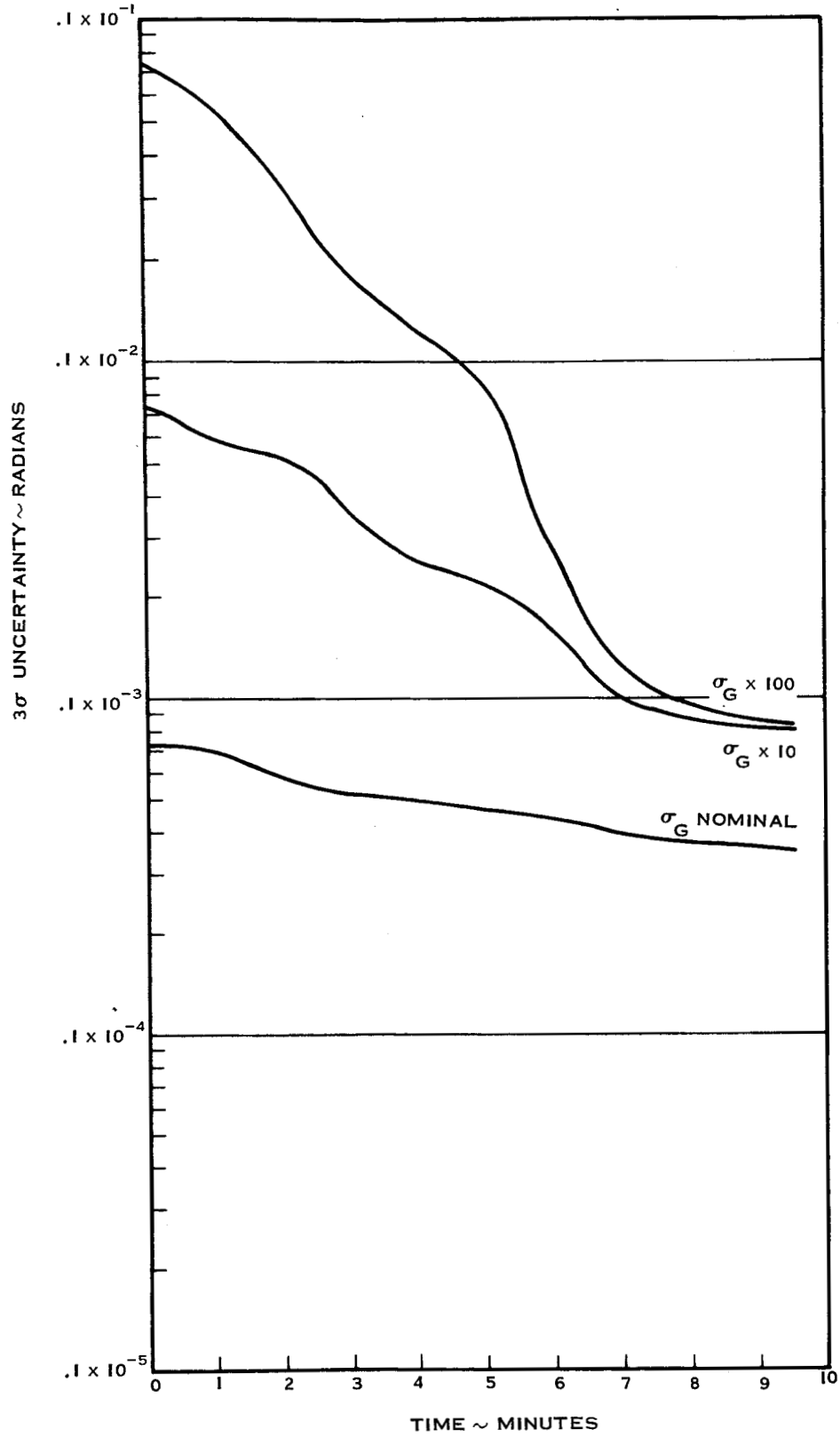


Figure 6-21 3σ Uncertainty in X-Accelerometer Misalignment Into Y-Axis for High Initial Uncertainties

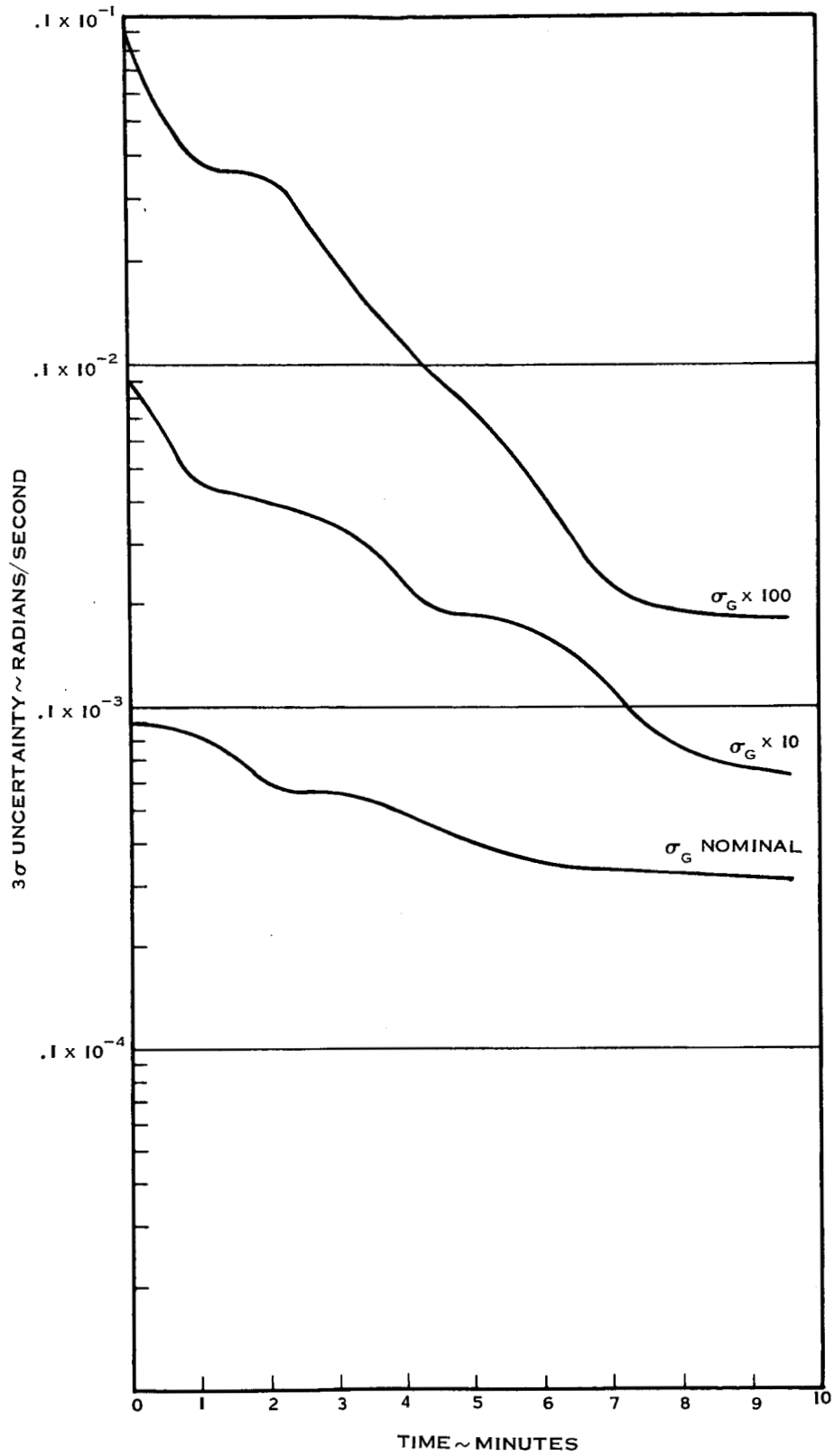


Figure 6-22 3σ Uncertainty in Initial Platform Misalignment About X-Axis for High Initial Uncertainties

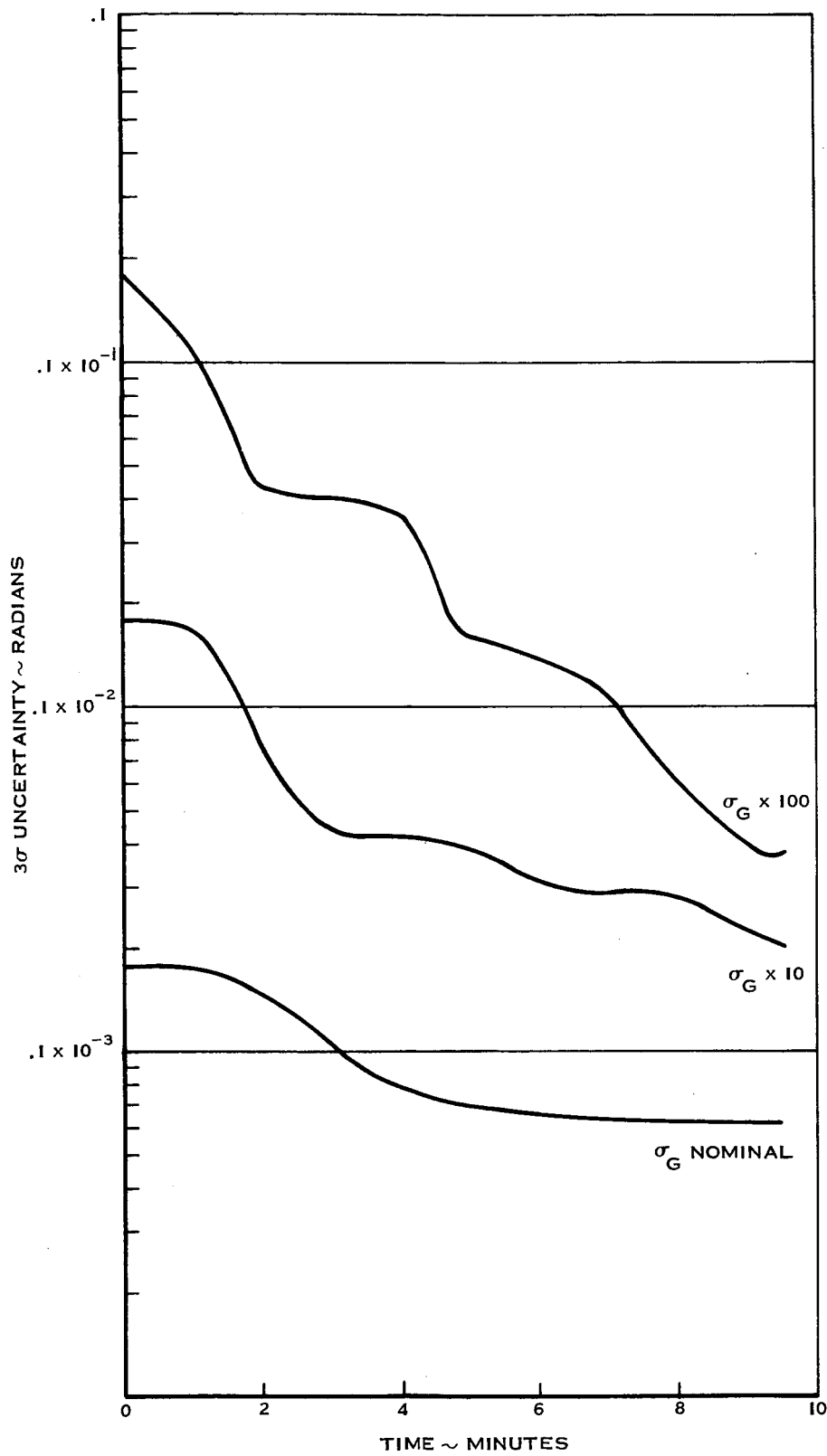


Figure 6-23 3σ Uncertainty in Initial Platform Misalignment About Y-Axis for High Initial Uncertainties

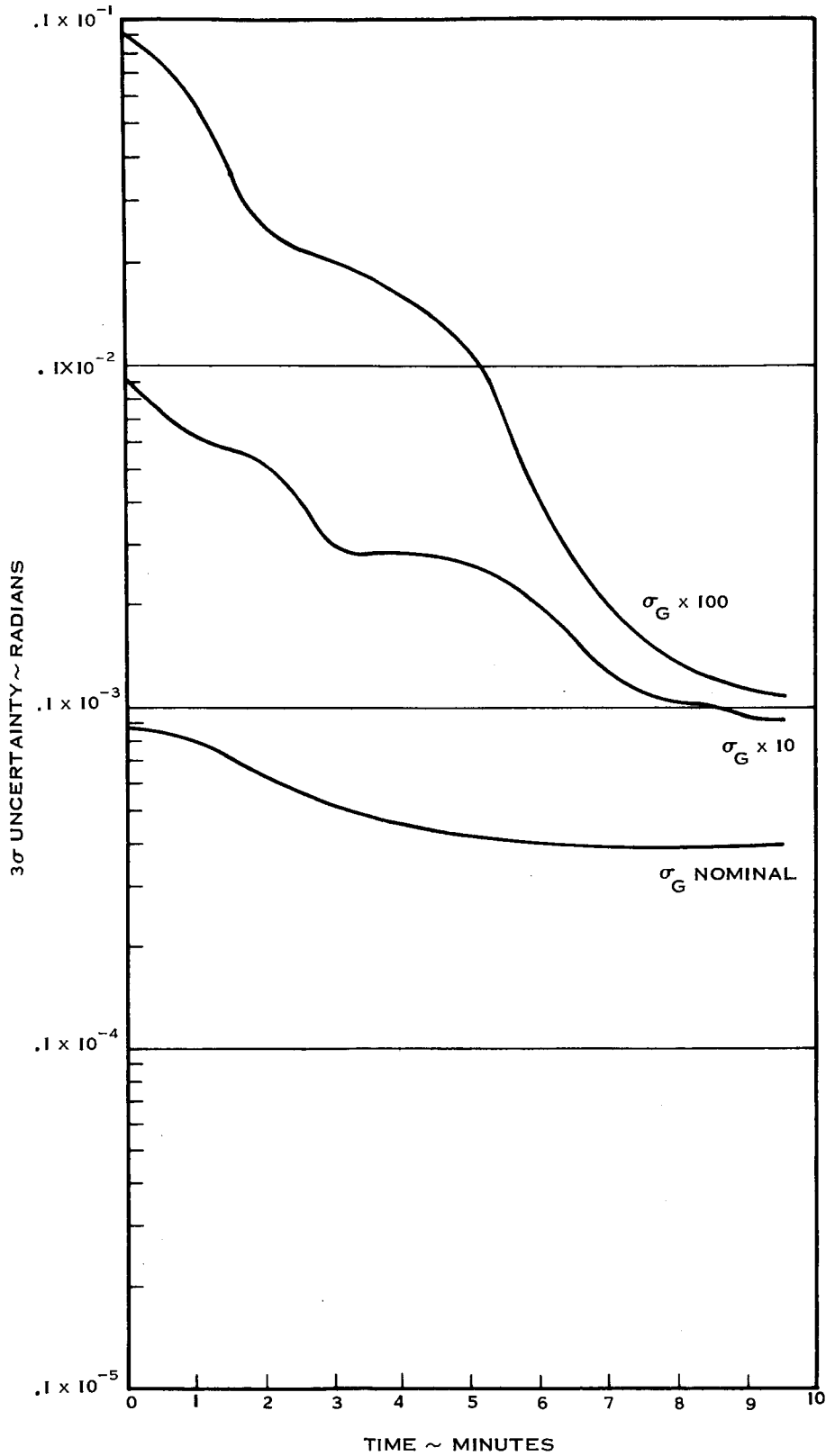


Figure 6-24 3σ Uncertainty in Initial Platform Misalignment About Z-Axis for High Initial Uncertainties

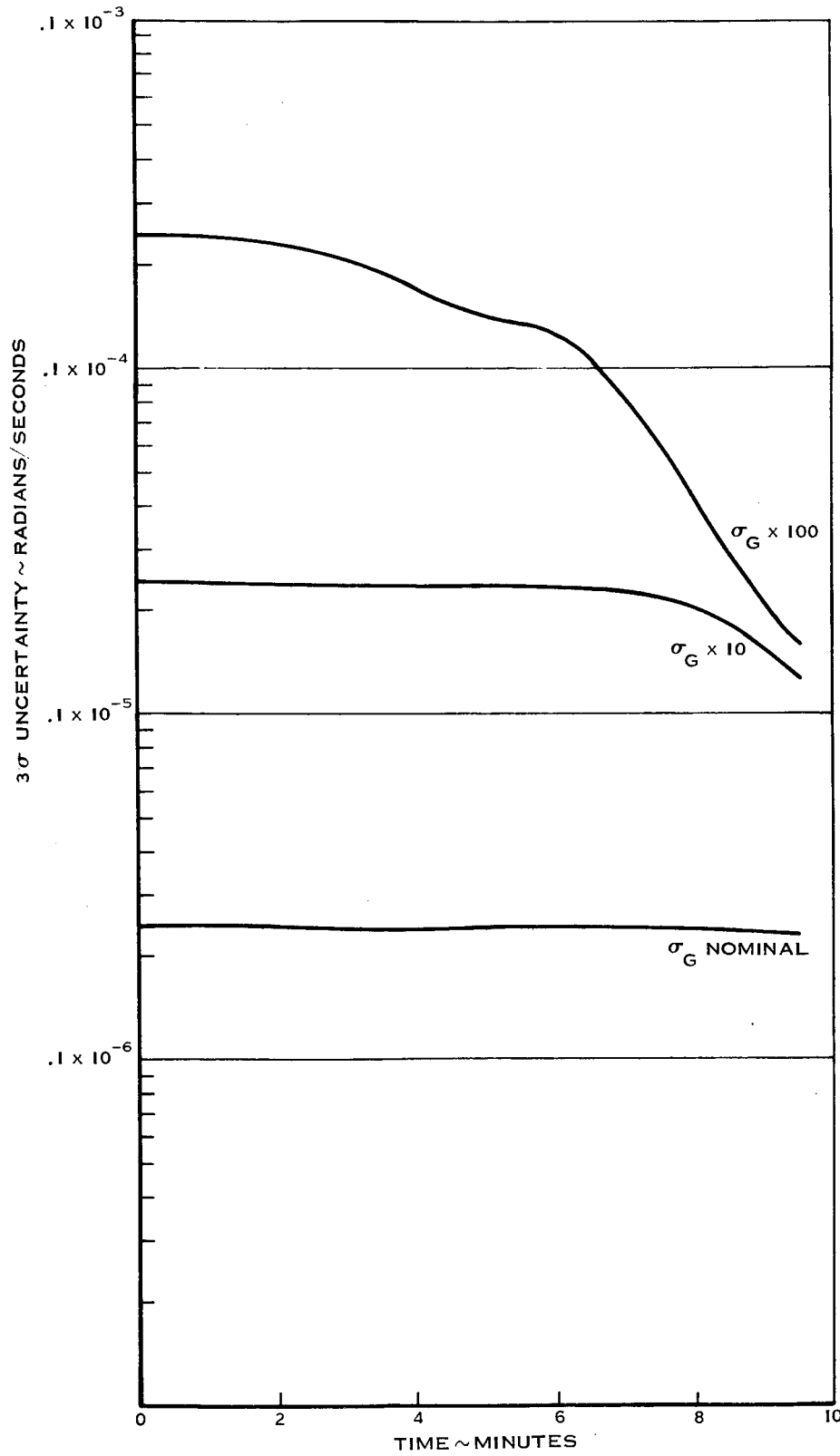


Figure 6-25 3σ Uncertainty in X-Axis Gyro Drift Rate for High Initial Uncertainties

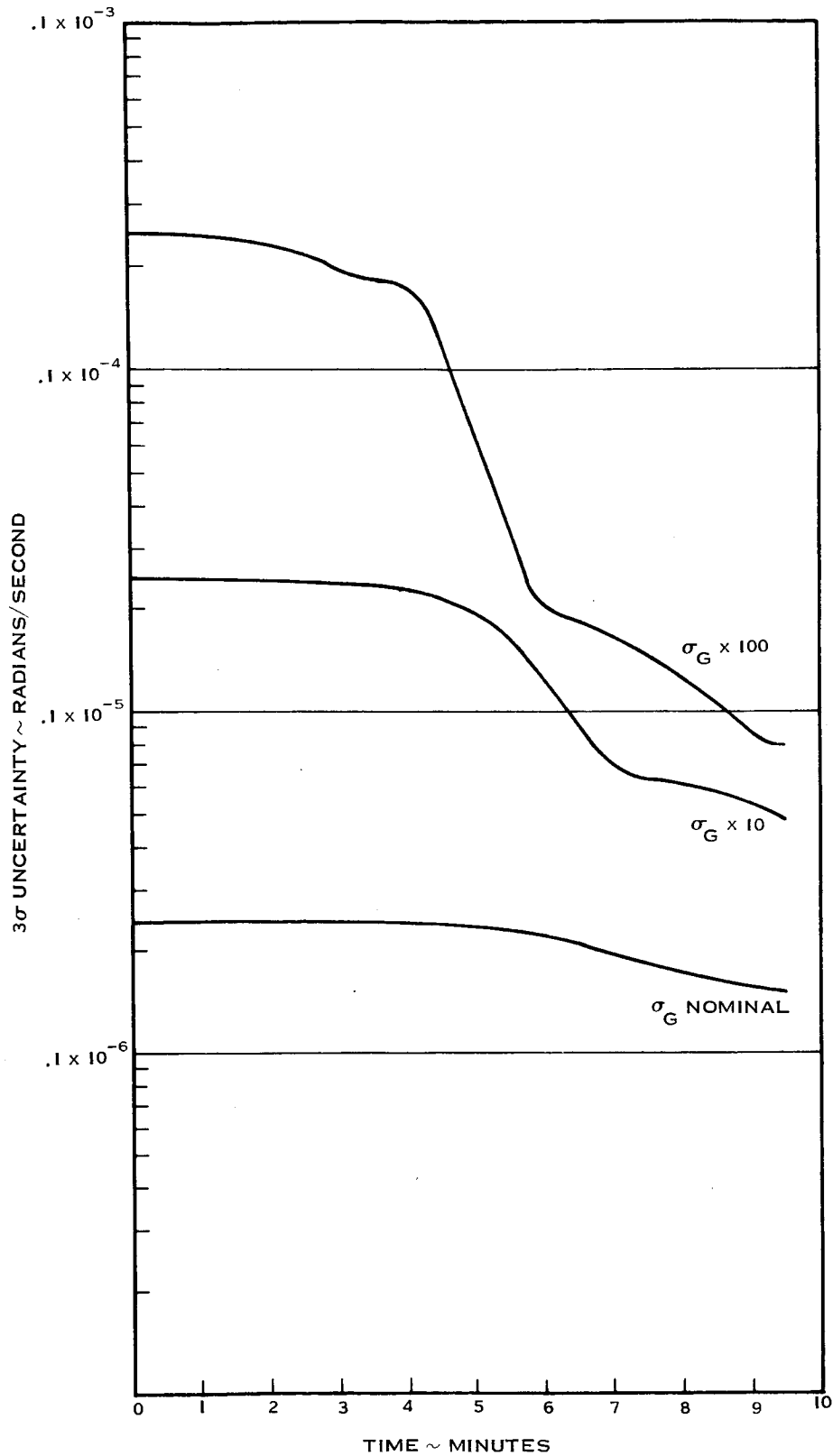


Figure 6-26 3σ Uncertainty in Y-Axis Gyro Drift Rate for High Initial Uncertainties

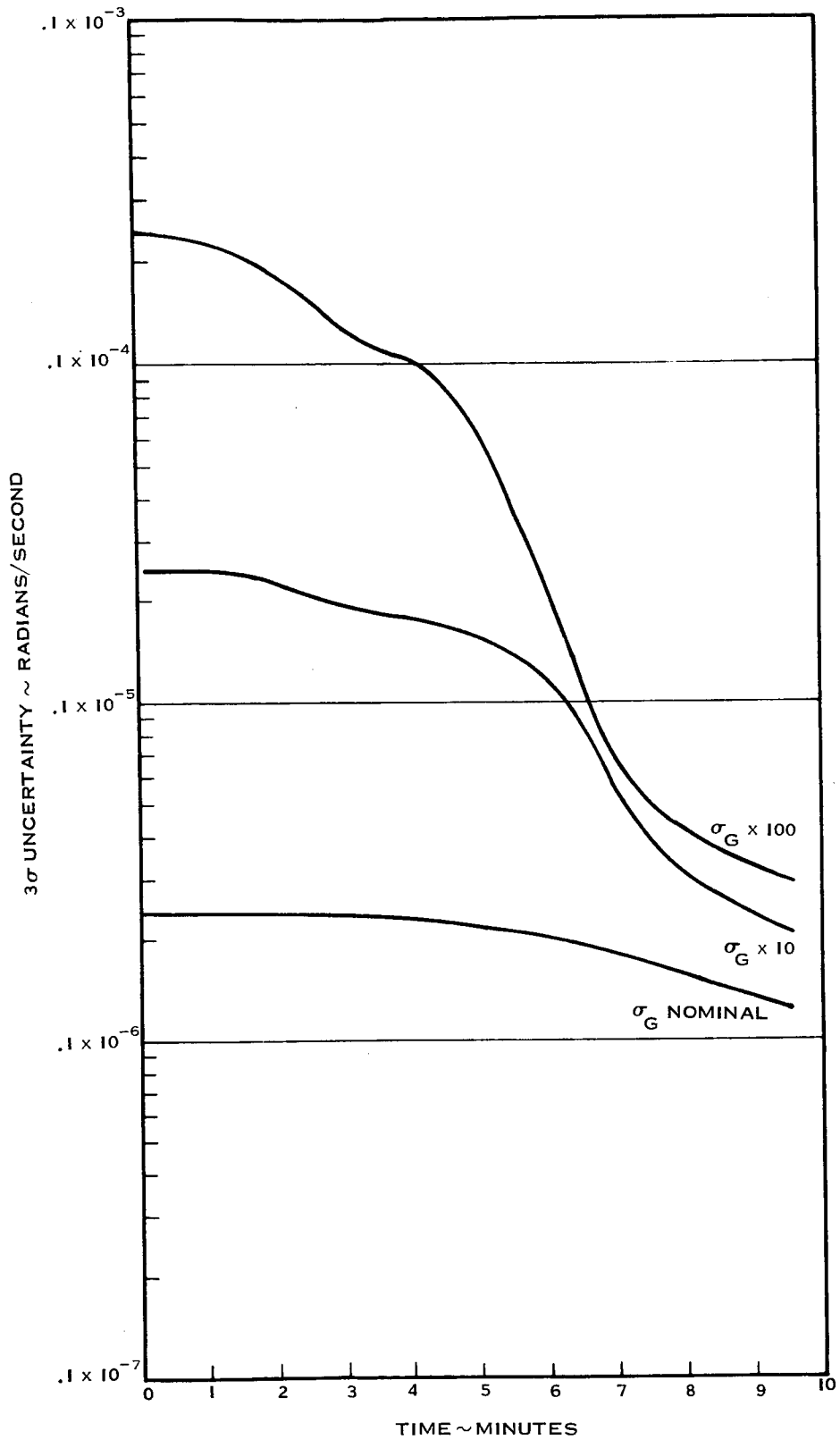


Figure 6-27 3σ Uncertainty in 2-Axis Gyro Drift Rate for High Initial Uncertainties

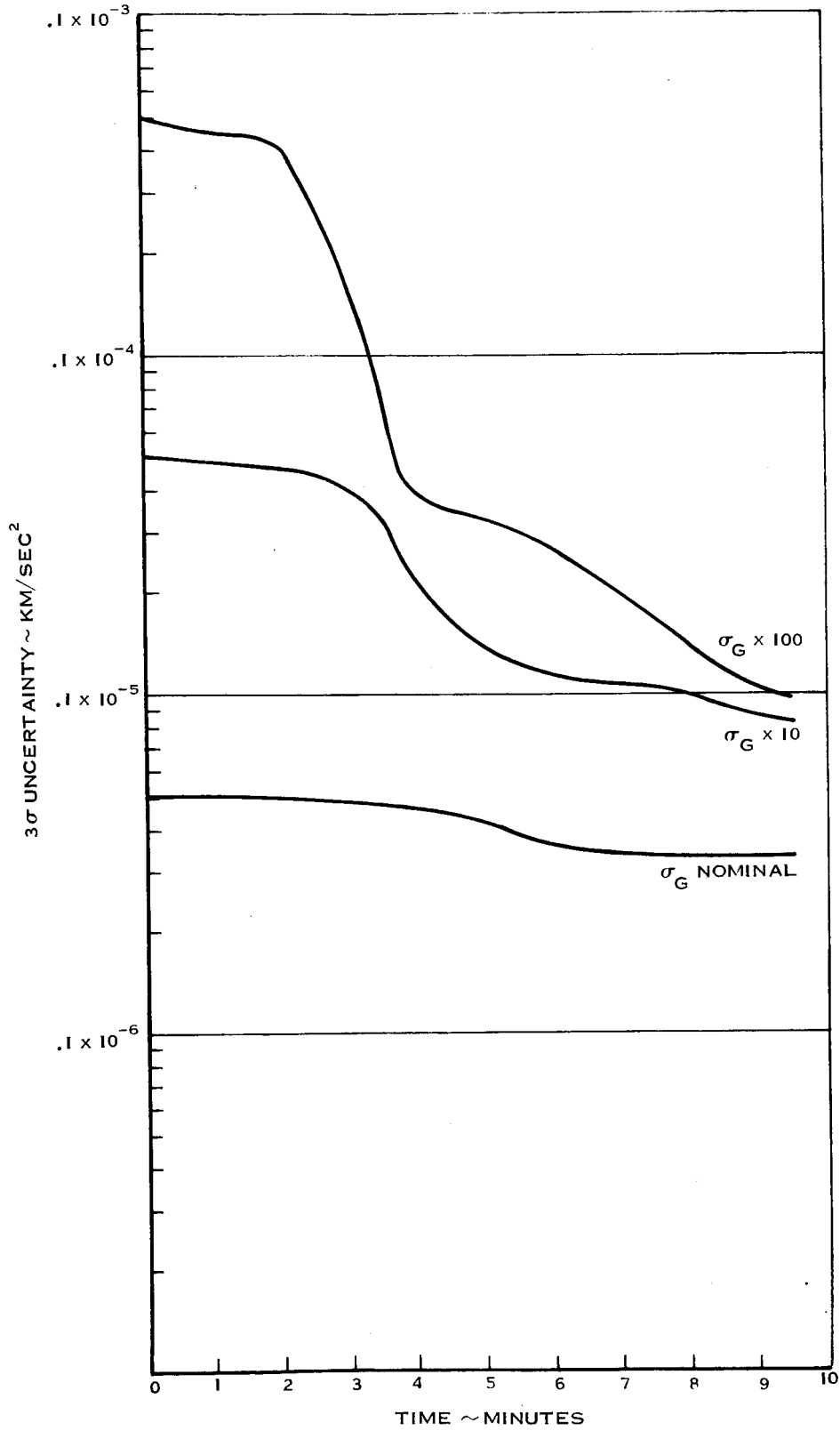


Figure 6-28 3σ Uncertainty in X-Accelerometer Bias for High Initial Uncertainties

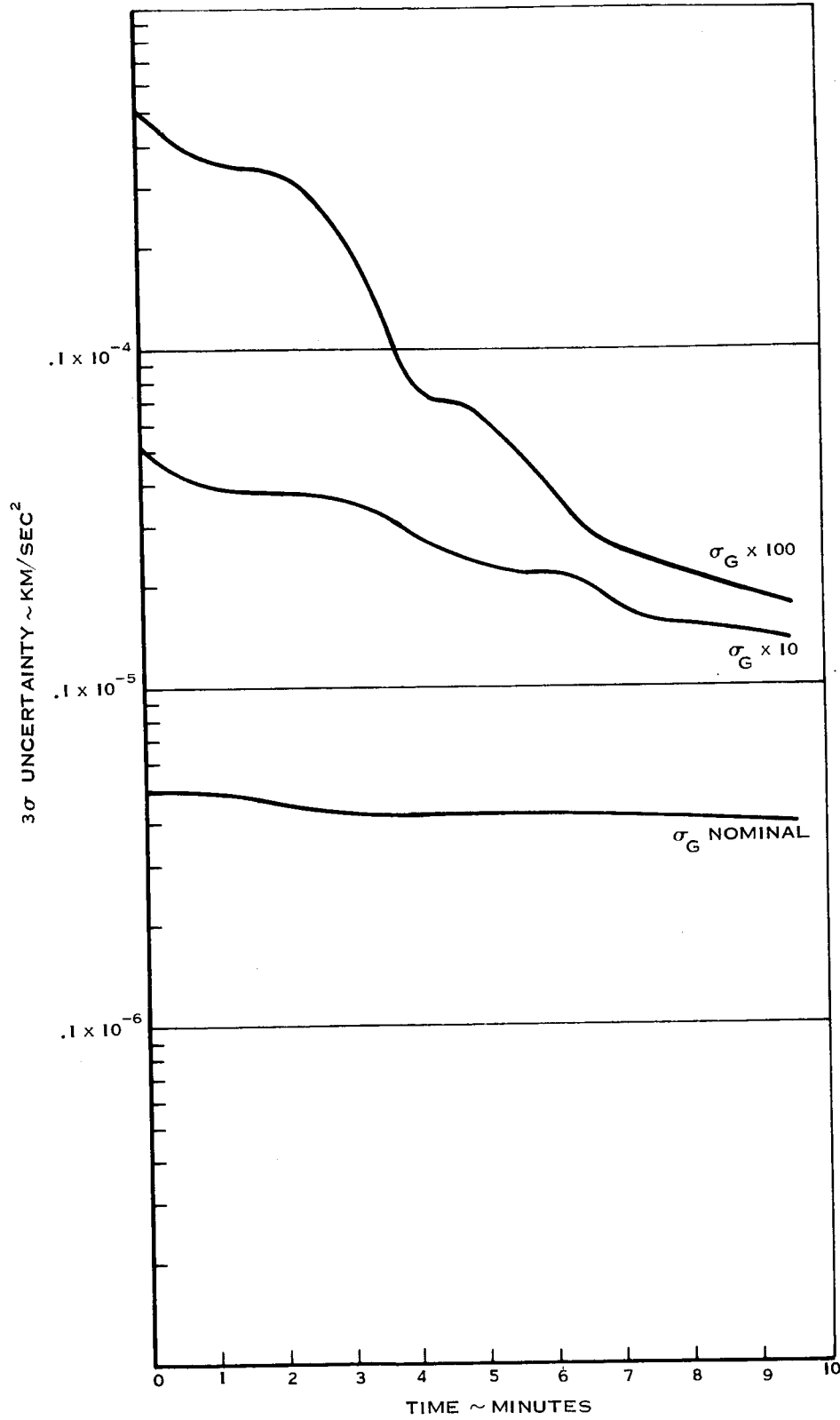


Figure 6-29 3σ Uncertainty in Y-Accelerometer Bias for High Initial Uncertainties

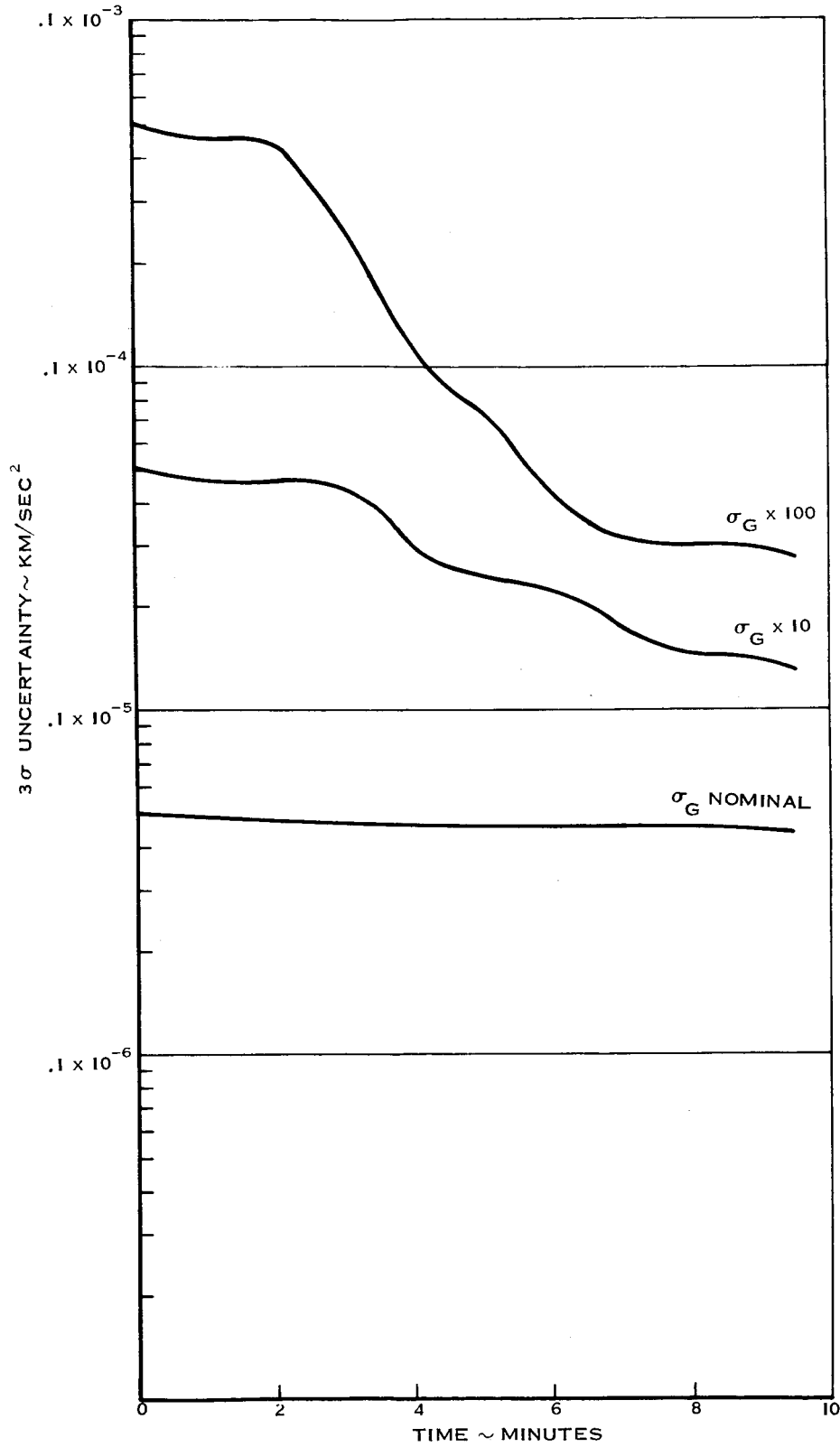


Figure 6-30 3σ Uncertainty in Z-Accelerometer Bias for High Initial Uncertainties

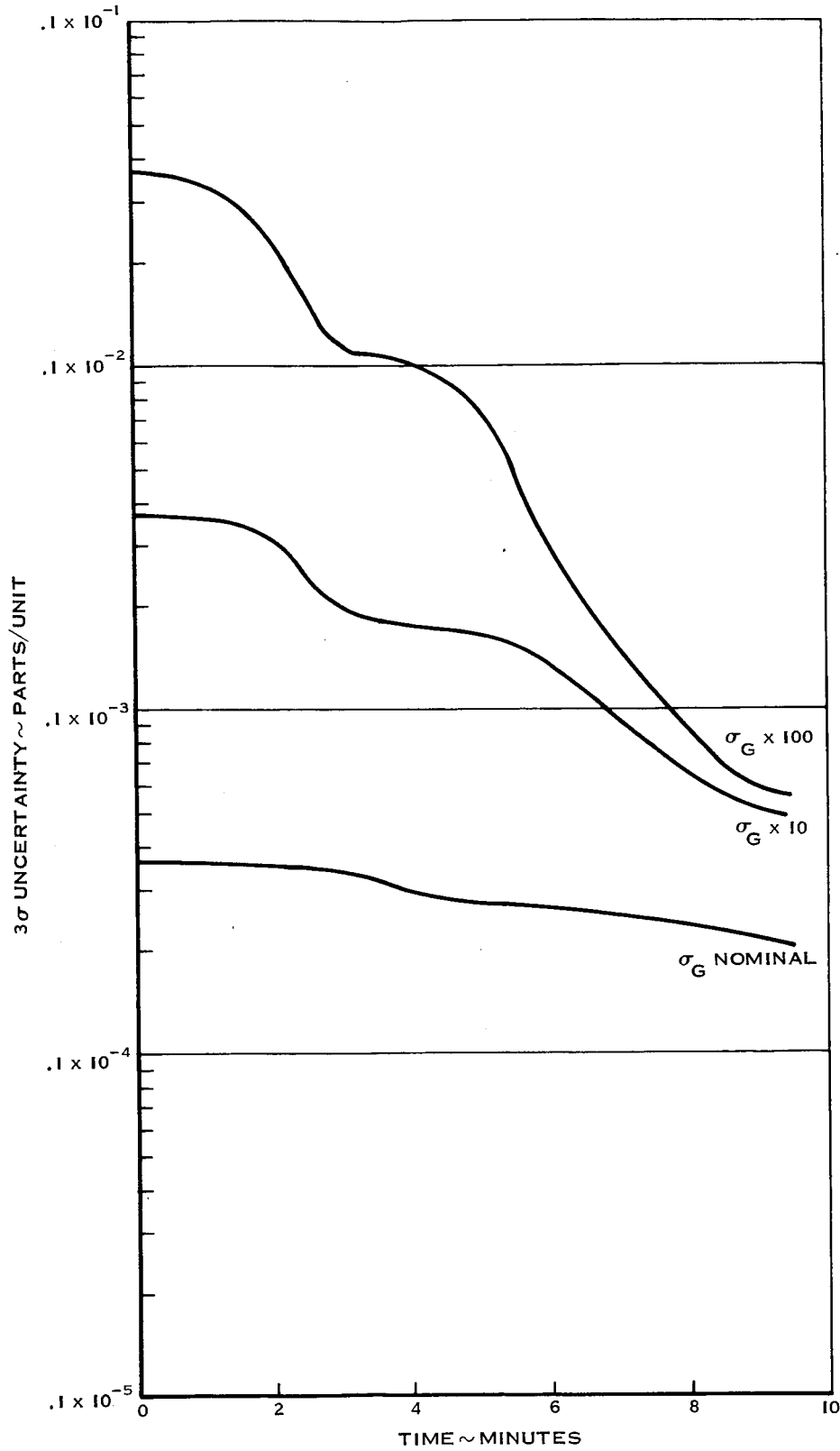


Figure 6-31 3σ Uncertainty in X-Accelerometer Scale Factor for High Initial Uncertainties

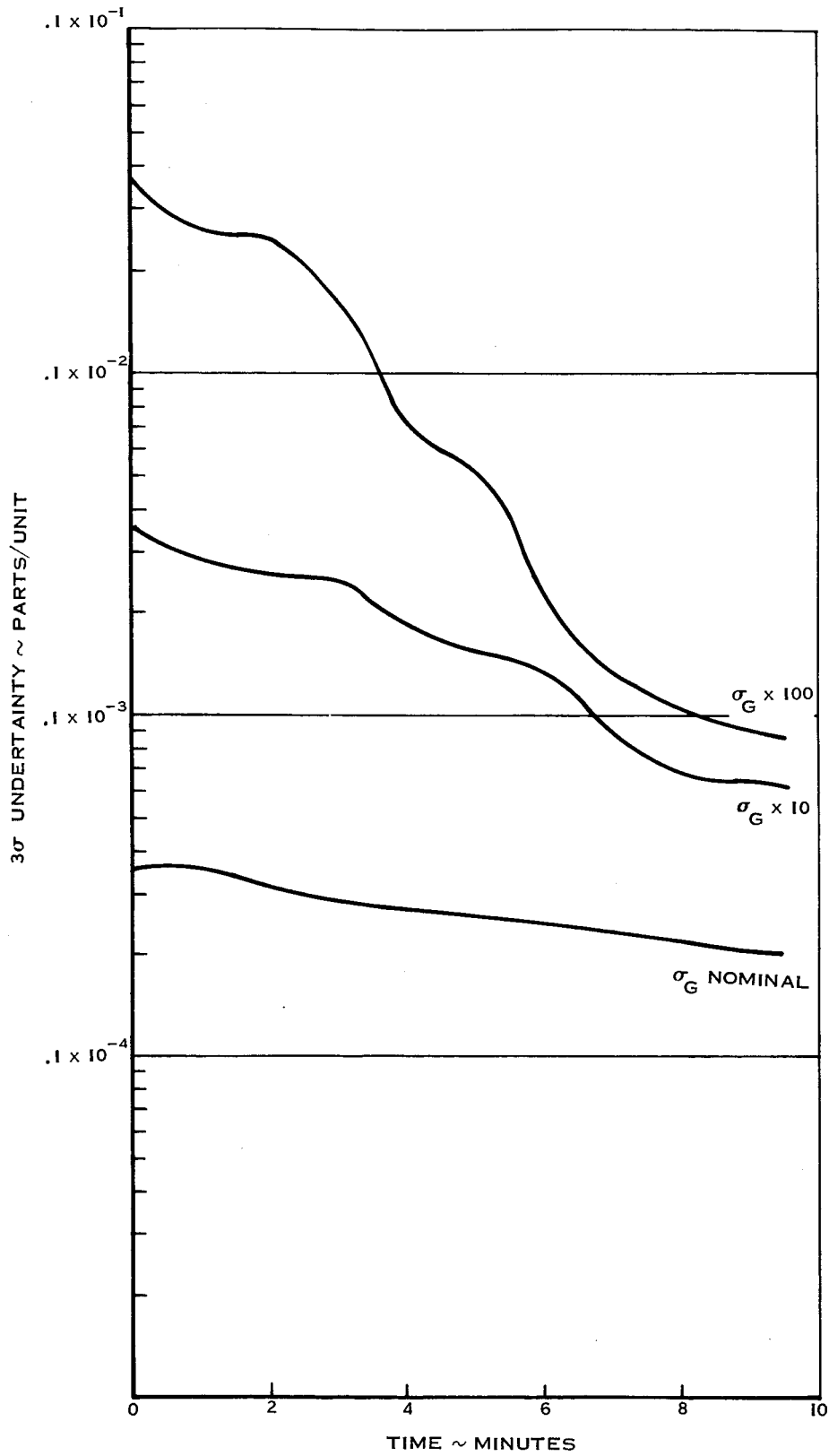


Figure 6-32 3σ Uncertainty in Y-Accelerometer Scale Factor for High Initial Uncertainties

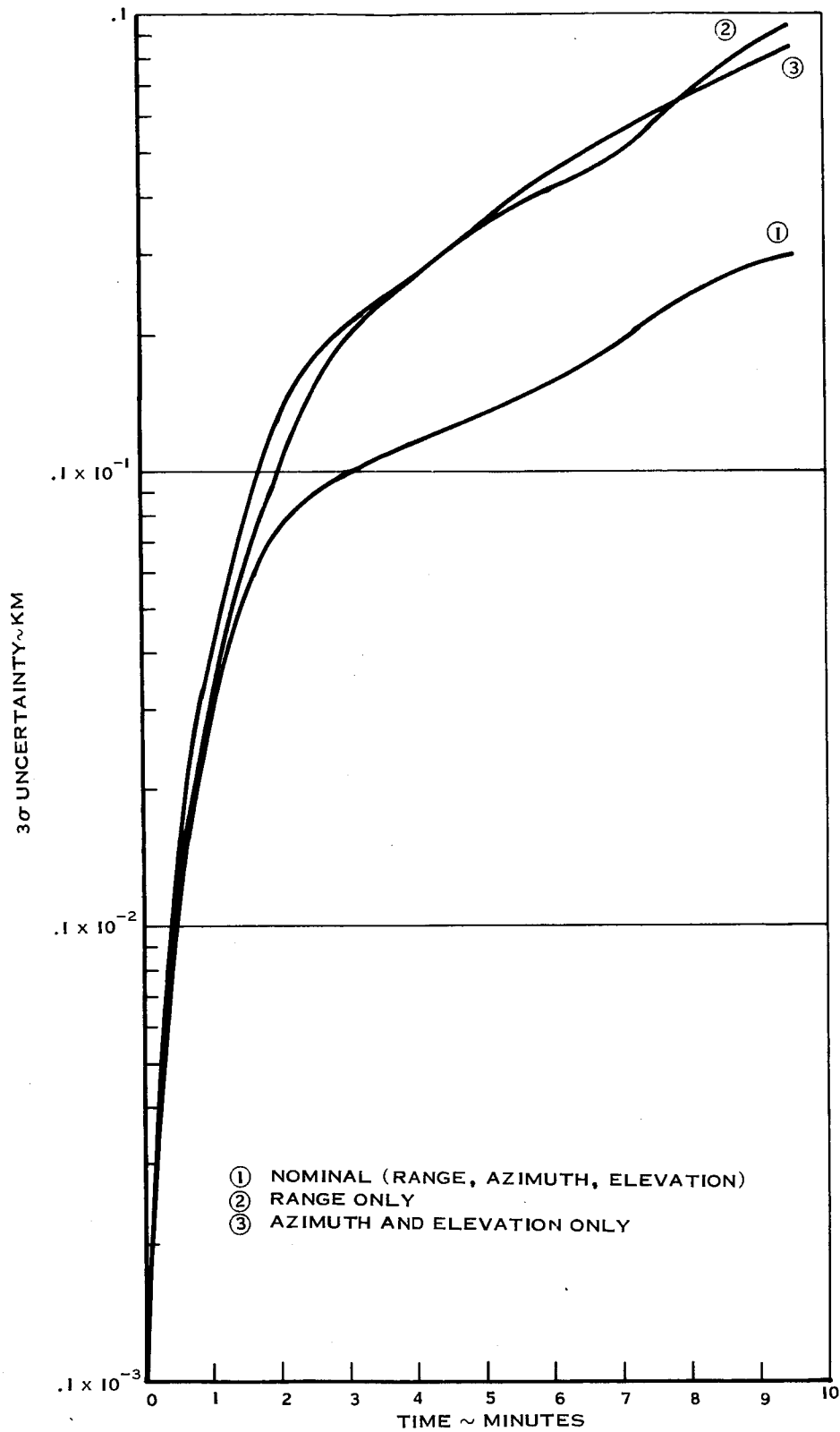


Figure 6-33 Variation in Position Uncertainty for Different Kinds of Tracking

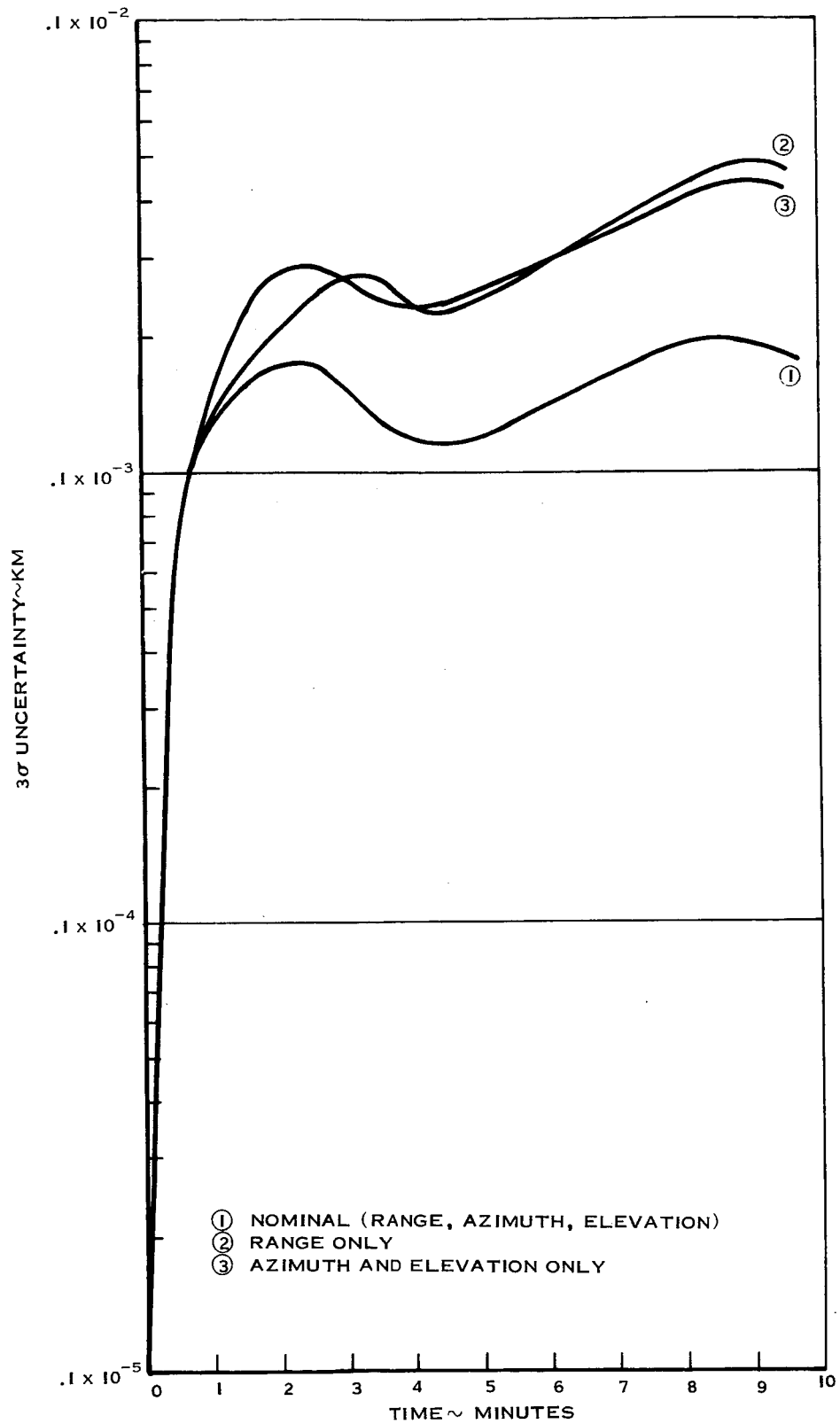


Figure 6-34 Variation in Velocity Uncertainty For Different Kinds of Tracking

SECTION 7

CONCLUSIONS

The over-all concept of combining telemetry and tracking data to estimate either the trajectory or error parameters that affect the trajectory has been found to be effective. However, the specific numerical results that can be obtained are highly dependent on the accuracy of the guidance system relative to that of the tracking system. As a result, the concept is, at the present time, more useful for some of the applications that were considered than it is for others.

The preliminary results presented in this report are mainly concerned with the importance of individual error sources in both the guidance and tracking systems. The effect of the guidance errors alone on the trajectory uncertainty is about 0.5 km in position and 2 meters/second in velocity. The most important error sources are the platform misalignments, the gyro drifts, the accelerometer biases, and some of the accelerometer misalignments and scale-factor errors. Some of the error sources, such as the Z accelerometer scale factor and the X and Y accelerometer misalignments in the Z direction, do not have a significant effect on the trajectory due to the low acceleration levels in the cross range direction. Other error sources, such as most of the mass unbalances, anisoelastic drifts, and accelerometer thresholds, do not cause any noticeable deviations in the trajectory. The final guidance model included twenty significant error sources.

The significant errors in the C-band radars included random and measurement bias errors in range, azimuth and elevation, as well as the station location errors. It was found that some of the station location errors and some of the azimuth and elevation biases could be omitted from the model. In addition to the random tracking errors, thirty-four bias errors were included in the final model.

The principal results of the report show the feasibility of estimating the platform error sources, both for the purpose of updating the guidance system during a flight and for a post-flight analysis. Although the primary interest for this investigation was in estimating the platform errors, results are also presented for estimating the trajectory.

With the combined platform-tracking model, the vehicle could be estimated to within 30 meters and 0.06 meters/second. This compared favorably to the 60 meters and 0.2 meters/second uncertainty with tracking only, i.e., no telemetry data.

For the tracking model used in this study, it may be concluded that the Saturn V type inertial platform errors are so small that it is not possible to significantly reduce the uncertainties in these error sources during a powered flight. The uncertainties in these error sources have been found to be reduced by about 20 to 50 percent. With an order of magnitude improvement in the present tracking accuracies, the significant guidance errors could be updated, i.e., these uncertainties could be reduced by about an order of magnitude. The general conclusion, therefore, is that the extent to which the guidance error uncertainties can be reduced does depend on the relative accuracies of the guidance components and the tracking system.

A notable exception to the above conclusions is that the ability to estimate the platform misalignments (orthogonal rotations), depends on a good **initial calibration of the accelerometer misalignments**. It was found that there is not enough information obtained from the telemetry-tracking system to distinguish between platform misalignments and accelerometer misalignments. However, if the Z accelerometer misalignments are eliminated, as well as either the X accelerometer misalignment in the Y direction, or the Y accelerometer misalignment in the X direction, then the three initial platform misalignments can be tied down.

The most effective use of the telemetry-tracking system is perhaps for a post-flight analysis. For this type of analysis, it would be possible to distinguish error sources that caused a malfunction, or more than normal error, from those components whose errors were less than the 3σ value. This result has been obtained by assuming large initial values for the guidance error standard deviations, and noting that there is a significant decrease in the uncertainty of these errors along the trajectory.

Additional results have been presented which show that:

- (1) a perfect knowledge of the trajectory end point has little effect on reducing the guidance error uncertainties,
- (2) the effectiveness of range tracking alone is about the same as the effectiveness of azimuth and elevation angle measurements, and
- (3) the effect of increasing the tracking rate by a factor of 10 decreases the guidance error uncertainties by, at most, a factor of 2.

APPENDIX A

COVARIANCE MATRIX DESCRIPTION

A complete covariance matrix as defined in (2-26) is presented in this section. It is taken from the Powered Flight Error Propagation Program (Reference 2) and lists values from the nominal tracking-guidance model at the end of an ascent trajectory. The off-diagonal numbers are normalized in UP, DR, CR coordinates with standard deviations on the diagonal, where

$$\text{Standard Deviation} = \sqrt{P_{ij}} \quad i=j$$

$$\text{Normalized Correlations} = \frac{P_{ij}}{\sqrt{P_{ii} P_{jj}}} \quad i \neq j$$

and P_{ij} is computed by equations (2-19) and (2-22).

The output format can be broken into three sections.

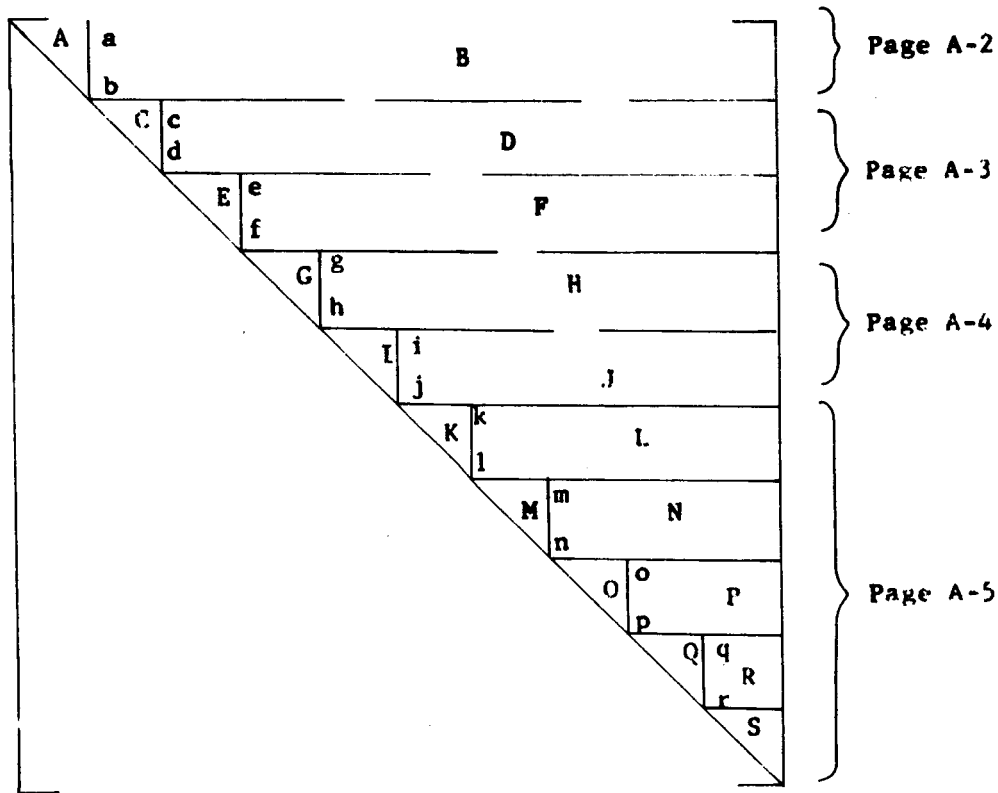
1. Time of printout. In this case time is that from launch until the end of the ascent trajectory
2. RMS position and velocity, where

$$\text{RMSP} = \sqrt{P_{11} + P_{22} + P_{33}}$$

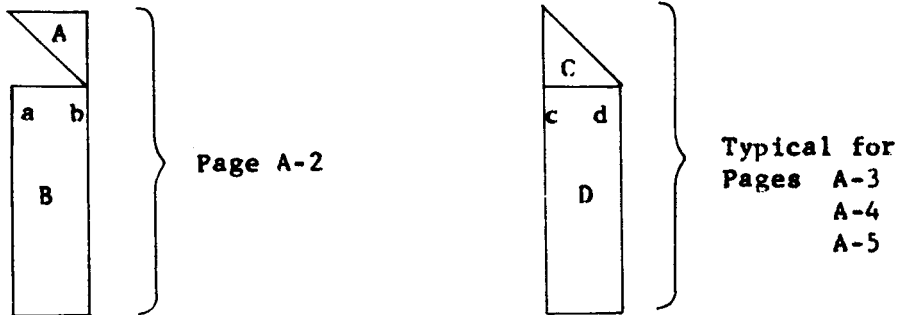
$$\text{RMSV} = \sqrt{P_{44} + P_{55} + P_{66}}$$

and standard deviations of bias errors being estimated.

3. Covariance Matrix. Since the covariance matrix is symmetrical only half of it is outputted. The format is as follows:



The format for the covariance matrix as defined above has been divided into pages as follows:



A-1a

To identify the standard deviation of specific error sources (diagonal terms) or the correlation between the bias error sources from the numbers printed out on the left and top of each page, the following code is used.

Guidance Errors ~ Numbers 1 through 30 .

Only 20 errors were included in the model.

The specific guidance errors defined by these numbers are shown in page 3-3 and Table 5-1.

Tracking Errors ~ The first digit denotes the station. The second and third digits specify the type of tracking error.

Stations:

1	Cape Kennedy	FPS-16
2	Merit Island	FPS-16
3	Patrick A.F.B.	FPS-16
4	G. Bahama	FPS-16
5	G. Bahama	TPQ-18
6	Bermuda	FPS-16
7	Bermuda	FPQ-16
8	G. Turk	FPS-16
9	Antigua	FPS-16

A-1b

Errors:

- 01 Range ~ meters
- 02 Range rate ~ meters/sec
- 03 Azimuth ~ millirad
- 04 Elevation ~ millirad
- 05 Azimuth rate ~ millirad/sec
- 06 Elevation rate ~ millirad/sec
- 07 Station latitude ~ degrees
- 08 Station longitude ~ degrees
- 09 Station altitude ~ meters
- 10 Station clock ~ seconds

The following examples illustrate the use of this numbering system:

1. 308 ~ Patrick AFB ~ longitude
10 ~ Accelerometer bias X-axis

The number in column 10 and row 308 (page A-3) is the correlation between Patrick AFB longitude error and accelerometer bias error in the X axis.
2. The value in the DR column and row 5 (page A-2) specifies the correlation between the Y-accelerometer scale factor error and the uncertainty in the downrange coordinate.
3. The number in column 3 and row 22 (page A-3) gives the correlation between Z accelerometer error into X-axis and X-gyro input axis mass unbalance.
4. The item at column 11 and row 11 is the standard deviation of accelerometer bias error on the Y-axis.

A-1c

END CONDITIONS

0 DAY 0 HRS 9 MIN 25.985 SEC

CASE 3 REC. 10 EVENT 8

CURRENT RMS VALUES
RMSP= 0.2856899E-01 RMSV= 0.1747118E-03 1= 0.2033137E-04 2= 0.5203584E-04 3= 0.6876384E-04 4= 0.4735066E-04

5= 0.1983611E-04 6= 0.5794824E-04 10= 0.3340303E-06 11= 0.4181578E-06 12= 0.4485762E-06 15= 0.1999510E-07
16= 0.5936066E-04 17= 0.8694120E-04 18= 0.4917875E-04 19= 0.2294555E-06 20= 0.1577291E-06 21= 0.1315124E-06
22= 0.1482978E-04 23= 0.1482969E-04 27= 0.3701221E-04 30= 0.2006918E-02 101= 0.1293153E-02 104= 0.2660293E-04
201= 0.1290303E-02 203= 0.2203202E-04 204= 0.2064433E-04 301= 0.4830693E-02 303= 0.2261715E-04 304= 0.2158076E-04
308= 0.4959798E-02 401= 0.3155088E-02 407= 0.4882960E-02 408= 0.2713148E-02 501= 0.3007574E-02 507= 0.4666228E-02
508= 0.2639081E-02 601= 0.1197393E-01 607= 0.2311298E-01 608= 0.1061544E-01 609= 0.2156260E-01 701= 0.1239769E-01
704= 0.4026404E-04 707= 0.2460006E-01 708= 0.1059291E-01 709= 0.2821349E-01 801= 0.1204296E-01 804= 0.3909360E-04
807= 0.2049557E-01 808= 0.9650091E-02 809= 0.2542227E-01 901= 0.3463467E-01 904= 0.4252512E-04 907= 0.3890744E-01
908= 0.2497937E-01 909= 0.4055488E-01

P MATRIX. STD DEV. ON DIAGONAL

Table with columns for matrix elements (UP, DR, CR, UPD, DRD, CRD) and rows for various parameters (1-909). Each row contains numerical values for different matrix components.



DETERMINISTIC ERRORS

Table with 6 columns (1-6) and 100 rows of numerical data. Each row contains a sequence of values, some with leading zeros and some with negative signs, representing deterministic errors.

DETERMINISTIC ERRORS

Table with 6 columns (10-17) and 100 rows of numerical data. Each row contains a sequence of values, some with leading zeros and some with negative signs, representing deterministic errors.



Table with columns 18, 19, 20, 21, 22, 23. Header: DETERMINISTIC ERRORS. Data rows include values like 0.49178747E-04, 0.22945548E-06, etc.

Table with columns 27, 30, 101, 104, 201, 203. Header: DETERMINISTIC ERRORS. Data rows include values like 0.37012210E-04, 0.20069184E-02, etc.



REFERENCES

1. Neighbors, A. K., Cole, J.W., and Daniel, F., "Error Analysis of Saturn Guidance Hardware as Applied to a Lunar Mission, MTP-ASTR-A-63-4, March 1963, Marshall Space Flight Center, Huntsville, Alabama.
2. "Users Manual for Powered Flight Optimization and Error Analysis Programs", Philco WDL-TR2759, Palo Alto, California, 15 February 1966.
3. Schmidt, S. F., "The Application of State Space Methods to Navigation Problems", Philco WDL-TR4, Guidance and Control System Engineering Department, July 1964.
4. Tyler, J. S., Jr., "Improved Techniques for Statistical Error Analysis and Parametric Studies of Space Systems", Philco WDL-TR2892, 1 May 1966, Palo Alto, California.
5. AF ETR Instrumentation Handbook, ETR-TR-65-9, Pan American World Airways, Inc., Guided Missiles Range Division Development Planning, August 1965.
6. Junkin, Bobby G., "A Tracking System Error Model Regression Analysis for Systematic Error Evaluation of Apollo - Saturn Radar Flight Test Data", NASA TMX-53487, July 5, Marshall Space Flight Center, Huntsville, Alabama.